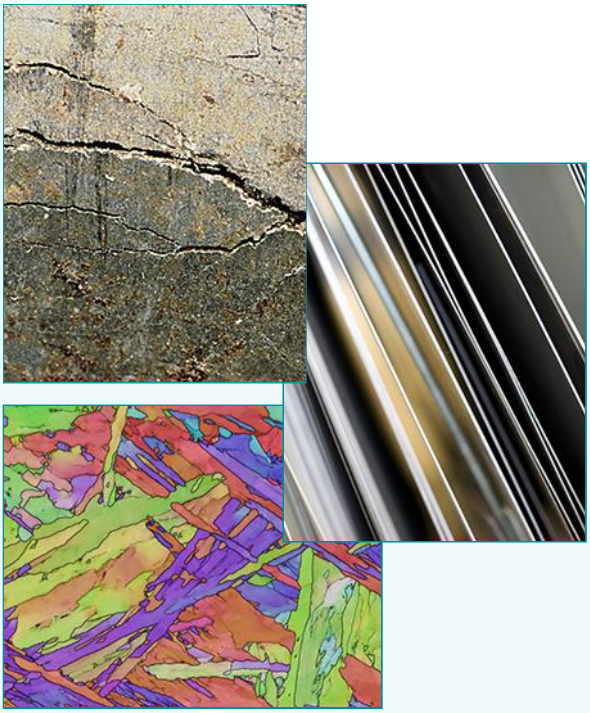

Research report
[Open]

In-situ Reduction by Incorporating H2-Filled Hollow Glass Microspheres in PM HIP Capsules

Pelle Mellin, Emil Strandh, Irma Heikkilä, Christer Eggertsson

Report number. KIMAB-2018-168

swerea|KIMAB

Title	In-situ Reduction by Incorporating H2-Filled Hollow Glass Microspheres in PM HIP Capsules
Authors	Pelle Mellin, Emil Strandh, Irma Heikkilä, Christer Eggertsson
Publication date	20180925
Report number	KIMAB-2018-168
Status	Open
Project number	14246
Department	Material & Process Development
Research Area	Powder materials
Member Research Consortium (MRC)	Powder Materials
Financing	The Åforsk Foundation

Approved by

2018-09-27

X

Signerat av: Jesper Vang

Business Leader, Jesper Vang

ISSN 1403—848X

In-situ Reduction by Incorporating H2-Filled Hollow Glass Microspheres in PM HIP Capsules

Pelle Mellin, Emil Strandh, Irma Heikkilä, Christer Eggertsson
Report number KIMAB-2018-168

Abstract

For many metal components the presence of hard, non-metallic inclusions such as oxides lowers the impact toughness by acting as fracture initiation points and easing crack propagation. In components produced by powder metallurgy hot isostatic pressing (PM HIP), oxides often form a continuous network of small, spherical inclusions after consolidation at the prior particle boundaries (PPB). It is therefore of great importance to reduce surface oxides before consolidation in order to improve mechanical properties.

In this work, oxides were attempted to be reduced directly prior to the consolidation of one tool steel and one low-alloy steel by introducing H_2 into sealed PM HIP capsules. The two H_2-carriers were hollow glass microspheres and the compound ammonia borane (H_3NBH_3). The H_2-carriers were placed separately from the metal powder. Microspheres were filled at 300 °C with a gas mixture at 675 bar resulting in a storage capacity of 0.16 wt%. Gaseous species released from the H_2-carriers during heating were analysed by mass spectrometry. Results showed that the microspheres only release H_2 while ammonia borane in addition releases other nitrogen and boron containing species.

Impact testing as well as chemical and microstructural analysis was performed on the two consolidated materials with samples retrieved from different vertical and radial positions. Both H_2-carriers had leaked into the material resulting in decreased impact toughness compared to the reference. Further from the source of the contaminants, oxygen content was reduced and impact toughness was improved. Microspheres showed overall better reduction ability even though they release less hydrogen compared to ammonia borane. Impact toughness was not improved as much with ammonia borane even though similar oxygen levels were achieved. Ammonia borane's decomposition products likely obstruct the oxide reduction or introduce new inclusions lowering the impact toughness.

swerea KIMAB

Box 7047, 164 40 Kista, Sweden
+ 46 8 440 48 00, www.swereakimab.se

Table of contents

1 Introduction

1.1 Background and literature study

In this work, an attempt to reduce oxides in a tool steel and a low-alloy steel by incorporating H_2 inside sealed inside PM HIP-capsules was made. Hollow glass microspheres were filled with hydrogen by a high pressure gas mix consisting of argon and hydrogen at an elevated temperature. At room temperature, the hydrogen is locked inside the microsphere and can be loaded into the PM HIP-capsules. The capsules were then sealed and heated to a temperature where hydrogen was released from the microspheres and could reduce surface oxides. Then a further increase in temperature and pressure fully consolidate the metal powder.

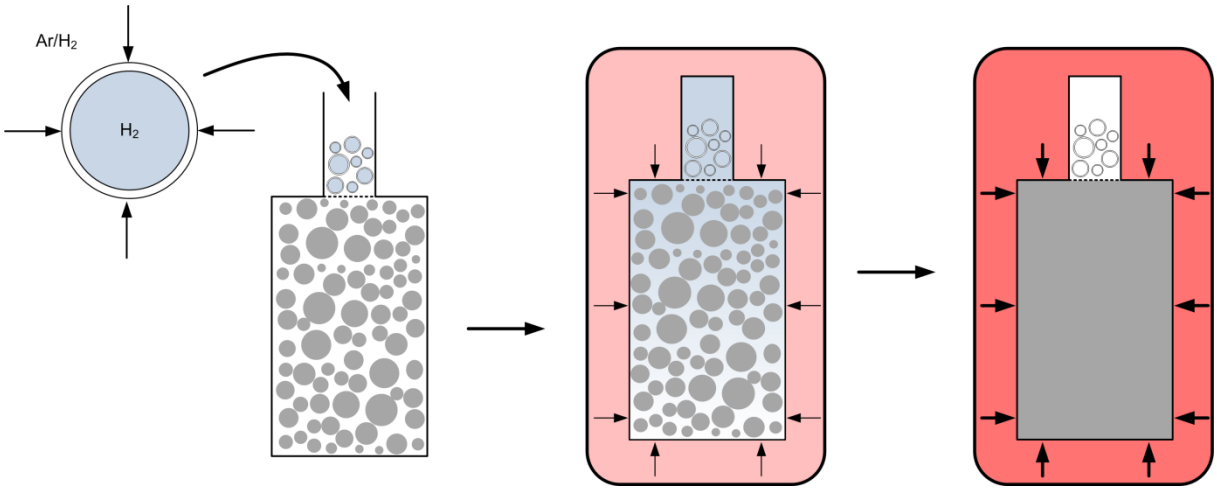

Figure 1 – Overview of the microspheres being filled with hydrogen, loaded into PM HIP-capsules and subsequent oxide reduction and powder consolidation.

Tool steels produced by powder metallurgy (PM) is only a small part of the tool steels manufactured worldwide. However, they are also the best performing grades because of the very fine and isotropic microstructure that PM enables. Furthermore, unworkable compositions that would disintegrate during hot working if conventionally casted into ingots can be manufactured through PM. [1] Low-alloy steels produced by PM are used in for example metal injection moulding (MIM), plasma and thermal spray. [2] Future applications of components produced by PM HIP in nuclear power plants are investigated, one example is reactor pressure vessel components. PM HIP enables better inspectability and the production of large, near-net-shape components. [3]

For many metal components the presence of hard, non-metallic inclusions such as oxides, nitrides or sulphides can be detrimental for the components performance. Components produced by metal powder are susceptible to embrittlement if it contains an excessive amount of oxides. Oxides can exist as exogenous, endogenous or surface oxides. Exogenous oxides are the result of refractory wear, slag mixing into the melt or improper melting practice resulting in large inclusions, directly harmful to the mechanical properties. Endogenous oxides are deoxidation products which because of the high solidification rate during gas atomization, i.e. melt stream disintegrated and quenched by high velocity inert gas [4], are small and evenly distributed. Therefore, they have no major influence on the final mechanical properties. [5] Furthermore, the particle surface is often oxidized during production, handling and storage especially for easily oxidized materials. This poses a problem since the oxides

creates a continuous network of small, spherical inclusions after consolidation at the prior particle boundaries (PPB). [6]

Oxides as well as other non-metallic inclusion lower the impact toughness by acting as fracture initiation points as well as easing crack propagation. The crack propagates along inclusions and pores due to localized stress concentrations which cause the material to reach its fracture strength at the crack tip. [7] This is why the continuous network of oxides, the PPB, are a problem for components produced by PM HIP. Therefore, it is of great importance to reduce the surface oxides in order to improve the mechanical properties. Generally, this can be done by using a reducing gas that reacts with the oxygen in the surface of the particles and transporting the gaseous products away. The reducing gas can be for example H_2 or CO. [8]

1.1.1 Hot isostatic pressing

Hot isostatic pressing (HIP) is a process using high pressures, between 1000-2000 bar, and temperatures between 900 to 1250 °C to densify powders, cast and sintered parts. The uniform gas pressure ensures isotropic properties in the consolidated material. HIP is complementary to other Powder Metallurgy (PM) processes such as pressing and sintering, Metal Injection Moulding (MIM) and Additive Manufacturing (AM) and can be used to further densify parts produced by these processes. Large HIP units can reach 220 cm in diameter and more than 400 cm in height with a capacity of 30 tonnes. [9] The HIP process is effective only if the pressure medium cannot penetrate the open pore structure and it is therefore crucial to seal the pores from direct contact with the pressure gas. This can be achieved in two ways: encapsulated HIP or containerless HIP. Containerless HIP is the hot isostatic compaction of preforms which were first sintered in order to close the surface porosity, thus achieving a gas tight surface. Encapsulated HIP instead utilizes a capsule often made of carbon steel or austenitic stainless steel sheets which are formed and welded into a specific shape. The welds are then helium leak tested and if the capsule is approved it is then filled with the metal powder, degassed and sealed. [10] Gas atomized powders are most suitable because of their spherical shape which together with their size distribution ensure a high fill density and consistent and predictable deformation behaviour. [9]

During the HIP process itself the temperature, gas pressure and holding time varies depending on the material. Temperatures are often less than 80% of the melting temperature to avoid any liquid phase, pressure gas is often argon or mixes thereof. For many steels HIP parameters of around 1100 °C and 1000 bar are often used, more process parameters are shown in Table 1. [11] After the chamber has been evacuated it is filled with a calculated gas pressure using a compressor. The temperature in the furnace is increased resulting in an increase in pressure by thermal expansion. After a certain dwell time the furnace is cooled and subsequently degassed. The part is then removed from the capsule by machining or acid pickling. [9] The powder is thus densified due by pressure assisted sintering.

Table 1 – HIP parameter from literature.

Material	Gas atomized D7 tool steel [12]	Nitrogen atomized 316L powder [13]	Low-alloy steel castings [14]
Temperature [°C]	1000	950 - 1120	1250
Heating rate [°C/min]	10	5.5	8.6
Pressure [bar]	300 - 500	1030	1000
Dwell time [min]	240	0	70

Generally, sintering occurs in three stages. Firstly, the pressure rearranges and plastically deforms the particles. Then, necks are formed where the particles are in contact because of the increased diffusion at elevated temperatures. Lastly, the necks grow and the centres of the particles are brought closer together. Once the porosity changes to a closed structure a further densification is achieved by the external pressure which aids the solution of gas into the metal matrix as well as diffusional creep, i.e. diffusion of vacancies through the crystal lattice. After a sufficiently long time a consolidated material is achieved with low porosity. [11] HIP'd components typically display increased yield strength, ultimate tensile strength and ductility compared to forged components of the same alloy. This is because of the smaller and more isotropic grain structures displaying no grain directionality as that of for example rolled components. [15] During consolidation, surface oxides are partly transformed. For instance, HIP'd gas atomized martensitic stainless steel powder has been shown to have reduced amounts of Fe oxides and to a large extent also Cr and Mn oxides as HIP temperature increase. Silicon segregates to the PPBs and form oxide particles. [16]

1.1.2 Microspheres

Microspheres are microscopic spheres made of glass or polymer. Glass microspheres are used in a wide range of industries as a filler or additive in order to achieve weight reduction, density control and in other ways enhance product properties. The glass microspheres can be solid or hollow with a varying wall thickness. The particle sizes of hollow glass microspheres can vary between 5 – 200 µm with modern day applications at around 15 – 65 µm. [17, 18]

The most used manufacturing process starts with the production of amorphous glass particles. A mixture of glass-forming constituents, with a relatively broad possible composition range as shown by Table 2, is heated to the fusion or melting temperature, with subsequent cooling and crushing into frit, i.e. small particles. The frit then undergoes a flame spray pyrolysis process. Glass frit is sprayed into an oxy-fuel flame heating the glass to 1000 – 1200 °C where the reduced viscosity and large surface tension shapes the irregular glass frit into a sphere. At these temperatures, sulphates present in the glass undergo thermal decomposition releasing gases such as SO_2 and O_2. The gaseous compounds inflate the glass particles creating a void inside which is permanent upon cooling thus producing a spherical hollow glass microsphere. By selecting appropriate sulphate contents, size and shape of the glass frit a desired density and wall thickness can be selected. [19] Some sulphur-oxygen compounds are contained in its gaseous phase inside the microsphere, preferably no more than 0.01 – 0.2 wt%. Other gases such as H_2O, CO_2, air (N_2 and O_2) could also be present inside the void. The hollow microspheres are then separated from the non-expanded particles via e.g. flotation on water. [17, 20]

Table 2 - Constituents and their range in common hollow glass microspheres. [21]

Component	SiO_2	B_2O_3	Al_2O_3	Na_2O	K_2O	CaO
Range [wt%]	30-96	1-25	0.5-20	0-20	0-20	0-15

1.1.3 Ammonia borane

Ammonia borane, also known as borazane, is a chemical compound with the formula H_3NBH_3. It is a suggested storage medium for hydrogen in fuel cells. Ammonia borane is also used to form hexagonal boron nitride monolayer, a substrate for growing graphene. [22] Ammonia borane can be produced by for example a reaction between sodium borohydride and ammonia chloride in diethyl ether at room temperature: [23]

$$NaBH_4 + NH_4Cl \rightarrow H_3NBH_3 + NaCl + H_2 \quad (1)$$

Ammonia borane is a stable solid at room temperature in air and water in addition to having a higher hydrogen storage capacity than other chemical systems. It contains 2.9 mol H_2 per mol H_3NBH_3 and releases 2.2 mol H_2 per mol H_3NBH_3 together with other thermal decomposition products during heating, resulting in a hydrogen storage density of 14.3 mass%. [24, 23]

A comprehensive study by Baitalow et al. [24] of the thermal decomposition of ammonia borane has been performed using combined thermoanalytical methods. The study found two decomposition steps when heating the material in a nitrogen atmosphere up to 227 °C at 0.5 °C/min. But the two steps could not be distinguished at 5 °C/min. The first step releases 1.1 mol H_2 per mol H_3NBH_3, half the total amount of released H_2. Furthermore, the amount released hydrogen up to 200 °C is independent of the heating rate. However, the release of volatile decomposition products increases with increasing heating rate. The study found that except hydrogen gas, three other gaseous elements are released; aminoborane (BH_2NH_2), borazine $(BHNH)_3$ and diborane (B_2H_6). The product yield at different heating rates is presented in Table 3. Borazine is released only in considerable amounts at the second decomposition step while aminoborane is released at both step but mostly at the second step between 147 – 227 °C. Below 147 °C, the major decomposition product is most likely the non-volatile polymeric aminoborane $(BH_2NH_2)_x$. [24]

Table 3 – Product yield of gaseous elements from the thermal decomposition of H_3NBH_3 up to 227 °C at different heating rates. [24]

Heating rate	mol product per mol H_3NBH_3			
	H_2	BH_2NH_2	Borazine	Diborane
0.5 K min^{-1}	2.2	0.12	0.035	0.02
1.5 K min^{-1}	2.2	0.16	0.05	0.025
5 K min^{-1}	2.2	0.21	0.065	0.04

A more recent study [25] evaluated ammonia borane at higher temperatures as well as determined the reaction temperatures of the two first decomposition steps to occur at 108 °C

and 125 °C respectively. At temperatures between 1170 and 1500 °C, polyiminoborane form a semi-crystalline hexagonal boron nitride (BN). However, the kinetics of the mass loss at these temperatures is much slower than for the first two steps and therefore limits the available amount of hydrogen released at these temperatures. [25] The reaction steps and its products are shown in Figure 2.

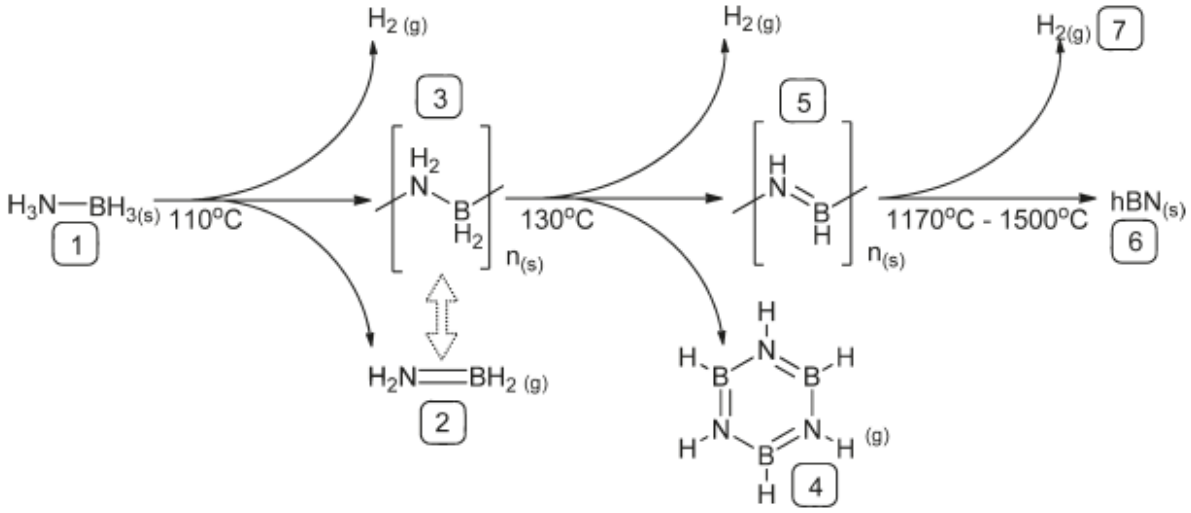

Figure 2 - Thermal decomposition of ammonia borane. (1) Ammonia borane, (2) aminoborane, (3) polyaminoborane (PAB), (4) borazine, (5) polyiminoborane, (6) semi-crystalline hexagonal boron nitride, (7) hydrogen gas. [25]

The reaction between aminoborane and polyaminoborane (PAB) is reversible and dependent on temperature, chain length and the degree of branching of the solid PAB. Low temperatures favour PAB, while PAB decomposes at increasing temperatures according to Figure 2 into aminoborane, borazine, polyiminoborane and hydrogen. [25]

A third study by Babenko et al. [26] identified ammonia (NH_3) and borane (BH_3) in addition to the previously mentioned species when heating ammonia borane at 100 °C. They are formed by a symmetrical splitting of ammonia borane where the borane then rapidly reacts to form diborane, as shown by the reactions below. The heating in a H_2/NH_3 atmosphere shifts the chemical equilibrium from diborane towards $B_xN_yH_z$ containing species.

$$H_3NBH_3 \rightarrow NH_3 + BH_3 \quad (2)$$

$$BH_3 + BH_3 \rightarrow B_2H_6 \quad (3)$$

1.1.4 Oxide reduction

Whether it is possible to reduce the surface oxides with hydrogen gas is determined by the equilibrium of the reduction reaction and the H_2/H_2O -ratio:

$$Me_yO_x + xH_2(g) = yMe + xH_2O\ (g) \quad (4)$$

A higher content of the reducing hydrogen gas naturally increase the ability to reduce oxides. Another factor is temperature (T), with higher reduction ability at higher temperatures. This can be summarized by the equation for Gibbs standard energy, assuming the activity of the solids is 1:

$$\Delta G° = -RTln\left(\frac{p_{H_2O}^x}{p_{H_2}^x}\right) \quad (5)$$

This can be written in terms of the partial pressure ratio:

$$\frac{p_{H_2}}{p_{H_2O}} = \exp\frac{\Delta G^0}{xRT} \quad (6)$$

The reduction of iron oxides by hydrogen occurs in two or three steps. Firstly, Fe_2O_3 transform into Fe_3O_4, then into FeO if the temperature is above 570 °C and lastly into metallic iron. Below 570 °C, FeO is not thermodynamically stable and Fe_3O_4 is instead directly transformed into iron. The reduction of iron oxides by hydrogen is endothermic and thermodynamically favourable compared to carbon monoxide above 800 °C. [27]

Iron based powders containing Cr, Mn, and Si form a thin, heterogeneous oxide layer over the entire particle. The strong oxide formers exist as small "islands" on the particle which are covered by ferrous oxides. Between these particulate oxides and ferrous oxides, spinels such as iron chromate ($FeCr_2O_3$) can form. [28, 29] Below 1100 °C, iron chromate is reduced by hydrogen in two steps. Firstly, it is reduced to iron and chromium oxide before a subsequent reduction of the chromium oxide to chromium. Above 1100 °C, the reactions co-occur. [30] Pure chromium oxides are reduced above approximately 1050 °C in pure hydrogen with water vapour continuously removed from the reaction zone. [31] Similar spinels exist for Fe-Mn-Cr systems with the stability of the spinels between the monolithic oxides. The stability and therefore the reduction difficulty in an increasing order is $Fe_2O_3 \rightarrow FeO \rightarrow MnFe_2O_4 \rightarrow FeCrO_4 \rightarrow Cr_2O_3 \rightarrow MnCr_2O_4 \rightarrow MnO$. [29] Heterogeneous surface oxide layers are reduced in two stages; removing iron oxides at lower temperatures and reduction of Cr, Mn and Si particulate oxides at higher temperatures. The majority (90%) of a low-alloy steel powder's surface oxides are iron oxides with a thickness between 6-7 µm. [29] For steels containing nickel, nickel oxide (NiO) can be reduced between 275 – 455 °C when heated at a rate of 5 °C/min in a hydrogen atmosphere. [32]

By using equation 6 and thermodynamic data from the National Institute of Standards and Technology [33] the temperature dependence of the equilibrium partial pressure ratio for a number of oxides can be calculated. Above each curve in Figure 3, oxides are reduced while the metal is oxidized below the curve. Again, the spinels of the Fe-Mn-Cr system described in the previous paragraph will be reduced by partial pressure ratios between the monolithic oxides.

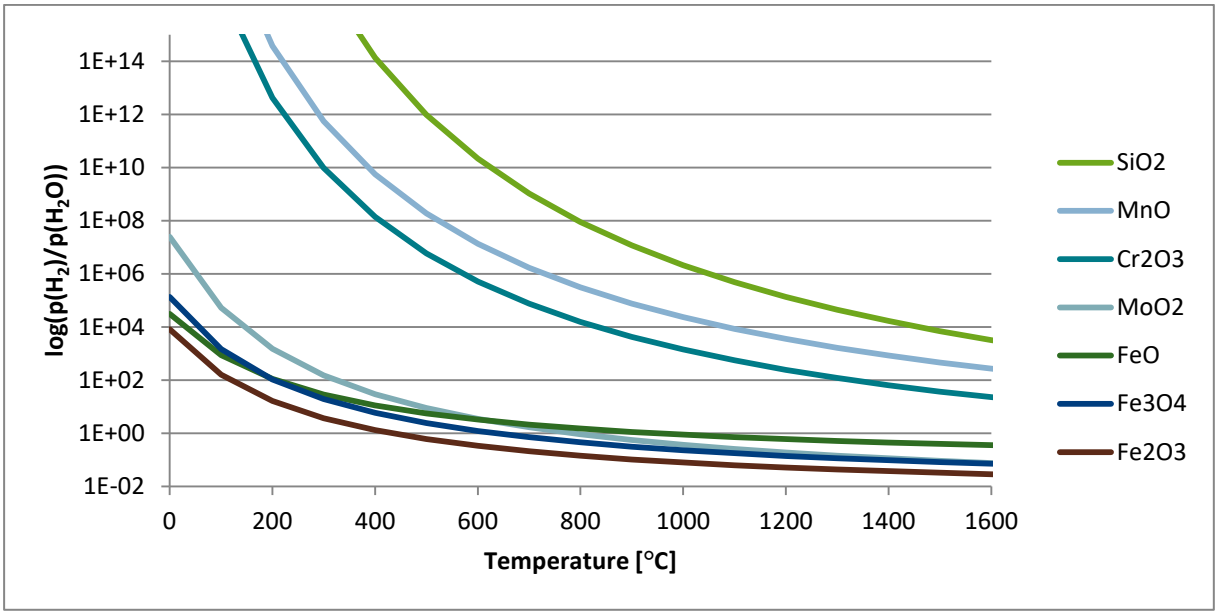

Figure 3 - Temperature dependence of equilibrium partial pressure ratio.

1.2 Materials

1.2.1 Low-alloy steel

The low-alloy steel powder was received as fraction of -500 µm. HIP, cut-out and impact testing was performed at Swerea KIMAB while oxygen analysis was performed by Carpenter Powder Products AB.

1.2.2 Tool steel

The tool steel was received sieved to a fraction of 53-150 µm. HIP and cut-out of chemical analysis samples were done at Swerea KIMAB. Sample for chemical analysis were sent to Carpenter Powder Products AB.

1.2.3 Microspheres

Microspheres, also called glass bubbles by the producer and supplier 3M are a hollow glass spheres made of soda-lime borosilicate glass. 3M's product information document state the isostatic crush strength of different microsphere grades which was the basis for the product selection. The grade S60HS has a 90% survivability at 1241 bar and is selected for the tests. It was delivered with a size span between 12 – 48 µm. S indicates that the material is silicate, 60 indicate its true density, and HS indicates that the microspheres were produced for high strength. The high strength made this grade suitable for this work where the microspheres were subjected to high pressures. [18]

1.2.4 Ammonia borane

Because of technical limitations in the HIP-furnace's pumps, the intended high fill pressure for the microspheres was not achieved. Instead, ammonia borane was used to simulate the high filling pressure in the application. With the formula H_3NBH_3, ammonia borane has a high hydrogen content (about 20 wt%). It was therefore chosen as the second hydrogen bearer for this work, 20 g of the compound was acquired from the manufacturer Sigma-Aldrich. [23] This new hydrogen carrier decomposed into a range of unwanted compounds that may be problematic in the application; in this sense the microspheres are a much better solution. But

the ammonia borane will at least show the reduction ability of high-pressured filled microspheres.

1.3 Previous work

A low oxygen and oxide content is often an important aspect of metallic materials in order to yield adequate mechanical properties. This is especially true for components made through powder metallurgy. Therefore, a great deal of research on the area has been done and below follows a summary of research related to this work.

1.3.1 Oxygen reduction in HIP-capsules

There has been extensive research by Swerea KIMAB on the reduction of oxides inside PM HIP-capsules which this research is based on. The exact method is confidential and can therefore not be discussed in this work.

It is well known that the oxygen content influence the impact strength of a hot isostatically pressed material. Surface oxides on the powder particles negatively influence the impact strength by preventing complete particle interaction during HIP. [34, 15] Higher oxygen contents correlates with the increased amount of non-metallic oxide inclusions in the material. For example, a reduction of the oxygen content from 190 ppm to 100 ppm for a 316L stainless steel increased the impact strength at room temperature from 120 J to 200 J. [15] Lind et al. [34] reduced the oxygen content prior to HIP and compared it to a non-reduced 316LN stainless steel powder. The material was HIP'd at two different temperatures, 1020 °C and 1060 °C. For the lower temperature, impact strength was increased from 112 J/cm^2 to 199 J/cm^2 when decreasing the oxygen content from 154 ppm to 69 ppm. At 1060 °C, an increase from 120 J/cm^2 to 214 J/cm^2 was measured when the oxygen content was reduced from 143 ppm to 76 ppm. [34]

1.3.2 Hydrogen storage in microspheres

Filling hollow glass microspheres with hydrogen gas have been tested before by Shelby et al. Samples were filled with 1 - 345 bar at 400 °C with a resulting storage capacity, defined as the mass of hydrogen over the mass of microspheres, of up to 2.2 wt%. [35] Microspheres were filled into a Pyrex tube that was flame sealed at one end and a glass wool plug was used to secure the microspheres during evacuation of the fill system. The open Pyrex tube was placed into a silica tube and a tube furnace was then raised around it. When the system reached the desired temperature it was flushed and evacuated before increasing the pressure. After a certain time has passed the tube furnace was lowered and the system is evacuated while a fan blows air onto the silica tube to cool the samples quickly to prevent loss of gas. The release of hydrogen was performed in a furnace at 150 or 300 °C as well as by using an IR lamp. The outgassing of hydrogen was shown to depend on the filling pressure with higher outgassing pressure resulting from a higher fill pressure. Microspheres were also divided into three fractions where, as expected, the largest fraction could store more hydrogen. However, the largest fraction of microspheres (>100 µm) filled with the highest pressures fractured when heated because of the rapid expansion of the gas, resulting in an erratic release of hydrogen gas. This was because of a low average aspect ratio of 0.029, i.e. wall thickness to diameter. Even though increases in diameter tend to increase the wall thickness, it was not sufficient for the largest fraction and instead the aspect ratio decreased causing the microspheres to burst during heating. Furthermore, it was found that a significant hydrogen loss had occurred during storage for 35 days at 50 °C. [35]

Another study by Tajmar and Reissner [36] were able to fill microspheres (S38 from 3M) with up to 700 bar of hydrogen. Microspheres were filled in a high pressure autoclave at 250 °C for 350 hours at peak pressure. Microspheres filled at 350 bar released similar amounts of hydrogen as the ones filled at 700 bar. This was due to that half of the microspheres filled at 700 bar were broken, which is expected as S38's isostatic crush strength with 90% survivability is 275 bar.

A recent theoretical study stated that gravimetric hydrogen storage densities of 14.1 – 25.2 wt% can be achieved depending on the aspect ratio of the microspheres, i.e. wall thickness to diameter. Microspheres can be filled in a high pressure autoclave at 250 °C and 850 bar. The limiting factor is the isostatic crush strength of the microspheres which the fill pressure should be below. A safety factor of 1-4 should also be considered to allow for some variance in wall thickness. [37]

1.4 Objective

The objective of this work is to test the effectiveness of introducing hydrogen carriers into sealed PM HIP-capsules for reducing surface oxides by an additional step before the complete consolidation into a fully dense part. The objective is to avoid forming strings of oxides lined at the prior particle boundaries thus improving impact toughness. This would enable more applications to use the near-net shape capabilities of PM HIP thus minimizing overall material waste and improving the sustainability of metal component production.

2 Preliminary calculations

In order to determine the feasibility of this work, preliminary calculations of critical parameters were performed:

1. Minimum amount of H_2 needed to reduce a certain amount of oxygen.
2. Optimal parameters to fill microspheres with H_2.
3. Amount of microspheres required for the calculated amount of H_2.
4. Amount of ammonia borane required for the calculated amount of H_2.
5. Loss of hydrogen through the HIP-capsule wall.

2.1.1 Minimum amount of H_2

Firstly, an assumption of the oxygen content to be reduced is required. 200 ppm oxygen is assumed to be common levels for nitrogen gas atomized powders. [38] Then, the total amount of oxygen in metal powders is calculated using the internal volume of the HIP-capsules and an estimation of the apparent density of the powders. The mass of the powder is calculated as:

$$m_{powder} = V_{capsule} * 0.7\rho_{th} \qquad (7)$$

No information existed for the packing density of the tested powders and it was therefore assumed to be 70% of the theoretical density. [38] Where, ρ_t, is the theoretical density of a fully dense material of the two powders, assumed to be 7800 kg/m^3, $V_{capsule} = 816.8\ cm^3$ and $320.1\ cm^3$ respectively for the two capsules used in this work. Now, the amount of oxygen can be calculated as:

$$n_O = c_O \frac{m_{powder}}{M_O} \quad (8)$$

With, $M_O = 16 \frac{g}{mole}$. The oxygen is bonded to common oxides that are likely to dominate because of the materials' composition, for example FeO, Fe_2O_3, Fe_3O_4 and Cr_2O_3. From the reduction reaction of a metal oxide, equation 4, the ratio of H_2 to oxygen is 1:1. This yields the total amount of hydrogen to reduce all the oxygen present in the two materials to approximately $0.056\ mol$ and $0.022\ mol$ for the tool steel and the low-alloy steel, respectively.

2.1.2 Filling microspheres with H_2

The ability to store hydrogen in microspheres is dependent on the diffusion of hydrogen through the thin wall and the compressive strength during loading. A minimal loss of hydrogen is furthermore preferred at room temperature to maximize long term storage ability. The optimal release conditions for this work are that the hydrogen is released and spread out evenly at temperatures suitable to reduce the oxides. Ideally, the pressure gas used to fill the microspheres is pure hydrogen. However, microspheres have also been shown by Shelby [39] to selectively separate hydrogen from mixed gases containing argon, nitrogen and carbon dioxide up to 93% purity. It is not 100% because some adsorption of these gases on the surface of the microspheres occurs. However, none of these gases were stored in the microspheres since they were released at low temperatures (~50 °C) before any release of hydrogen occurred. This is commonly associated with adsorbed gases. [39] Pure silica glass for instance exhibit a hydrogen to argon selectivity of 6.69 x 10^6. [40]

In order to determine suitable fill pressures and temperatures one first has to estimate which pressures the microspheres can withstand during filling. Furthermore, during the release of hydrogen the microspheres can burst due to the rapidly increasing internal pressure during heating, especially if the temperature exceeds the temperature used during filling. However, in this work the microspheres are already loaded into the sealed HIP-capsule and bursting with subsequent rapid release of hydrogen is not devastating. Therefore, only the buckling pressure during loading is considered. The external pressure should be controlled in order to prevent a collapse when the difference in internal and external pressures exceeds the buckling pressure. The theoretical critical buckling pressure (P_{cr}) under isostatic pressures can be calculated by: [19]

$$P_{cr} = \frac{2Et^2}{\left(\frac{d}{2}\right)^2 \sqrt{3(1-\nu^2)}} \quad (9)$$

Where, E and ν are the Young's modulus and Poisson's ratio of the glass, respectively. With $E = 62\ GPa$ and $\nu = 0.22$ from Rambach and Hendricks [41] and $d = 29\ \mu m$ with its respective wall thickness, $t = 1.19\ \mu m$, a critical buckling pressure of 4936 bar is obtained. This is the same for all three diameters in the size span (D10, D50 and D90) in Figure 5 because they are assumed to have the same aspect ratio (t/d=0.041). However, defects in the glass influence the buckling strength heavily. The manufacturer's product sheet states a critical buckling pressure with 90% survivability at 1241 bar thus establishing the maximum fill pressure for the experiment. [18] An additional safety factor is also needed accounting for

possible wall thickness variations. This together with the softening point of the glass at 600 °C set the limiting fill conditions.

Hydrogen diffuses as a molecule in glass and its permeability (K) is the product of the hydrogen's diffusivity and solubility in the glass. Glass can consist of two kinds of components which affect the permeability. Firstly, network formers such as SiO_2 and B_2O_3 hold the glass together and have a high permeability. Secondly, the non-network formers such as Na_2O and CaO break up the lattice, affecting the permeability. How the fraction of non-network formers (M) affect the permeability can be calculated as:

$$K = [3.4 + (8 * 10^{-4})M^3] * 10^{-17}T * exp\left(\frac{-(3600 + 165M)}{T}\right) \left[\frac{mol}{s\ Pa\ m}\right] \quad (10)$$

$$J = \frac{K}{t}\Delta P_{H_2} \left[\frac{mol}{m^2 s}\right] \quad (11)$$

It is valid when silica is the major ingredient and M<30%. [42] Equation 11 describes the flux (J) of hydrogen in the wall of one microsphere, where K is the permeability, t is the wall thickness and ΔP_{H_2} is the hydrogen partial pressure difference between the outside and inside of the microsphere. The gas mixture used in the experiments is 5% H_2 and 95% Ar and is assumed to be an ideal gas. Thus, the partial pressure of hydrogen is 5% of the total external pressure.

The time required to fill the microspheres at elevated temperatures could then be calculated by numerical iteration implementing equations 10 and 11 into Matlab. The fraction of non-network formers was assumed to be 20%, as used by Duret and Saudin [43] for a similar microsphere grade, S60 from 3M. It was also assumed that the inside of the microspheres initially don't contain any hydrogen. The amount in mol that permeates into the void at each timestep is inserted into the ideal gas law to calculate the new internal pressure. At first, the pressure difference (ΔP_{H_2}) is equal to the external partial pressure of hydrogen but decreases as hydrogen permeates and equalise the pressure. Thus, the flux is large at first but decreases with time. Figure 4 show the resulting internal pressure in one microsphere of a specific diameter and wall thickness calculated using the supplier's specification and equations 10 and 11. The external pressure is 1000 bar with a hydrogen partial pressure of 50 bar. It is clear that the temperature's influence on the fill time is large at lower temperatures.

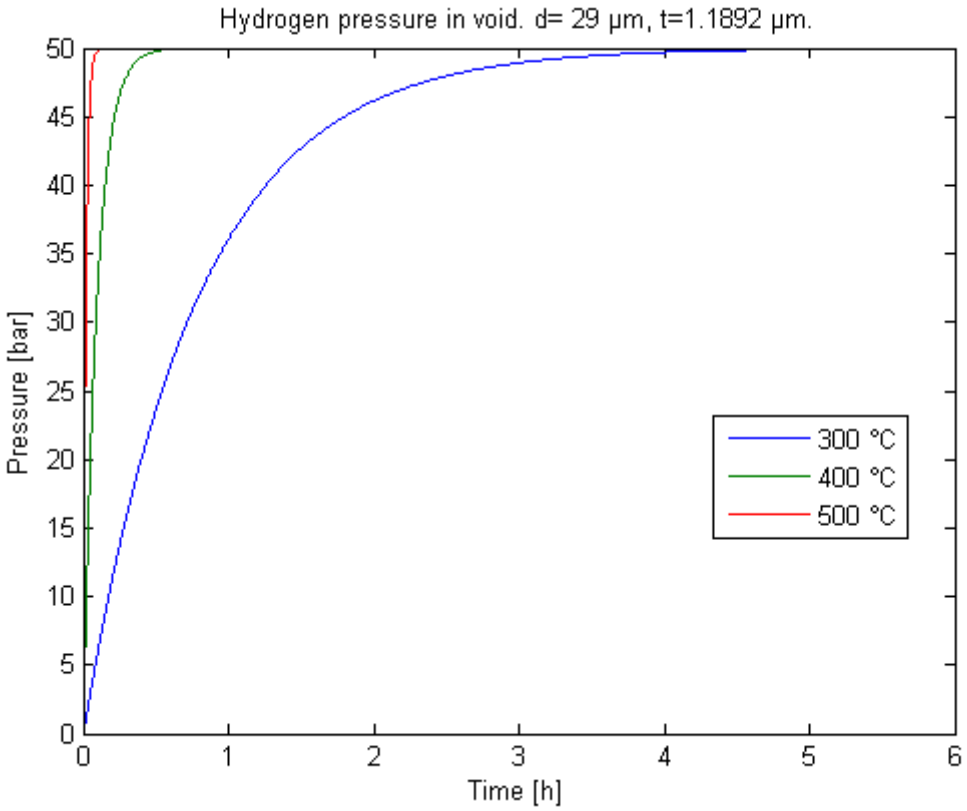

Figure 4 – Temperature's influence on the required time to fill a microsphere with an Ar/H_2 gas mixture at 1000 bar. Where d is the diameter of the microsphere and t is the wall thickness.

The investigated microspheres have according to the supplier a size distribution between 12 – 48 µm (D10-D90). [18] Figure 5 show the internal pressure for three sizes of the investigated microspheres: D10, D50 and D90. These two calculations show that at lower temperatures, such as 300 °C, the size of the microspheres and therefore their wall thickness influence the fill time drastically, spanning from 1-12 hours depending on the microsphere's diameter. By raising the temperature to 400 °C, the largest microspheres are instead filled in less than 2 hours. Therefore, the microspheres' size span is less important to achieve reasonable fill times at higher temperatures. It should also be noted that the fill pressure does not affect the fill time since an increased partial pressure difference also increases the flux proportionally according to equation 11, thus keeping the fill time constant. The fill pressure only affects the final internal pressure which is equal to the partial pressure of hydrogen, i.e. 5% of the total pressure.

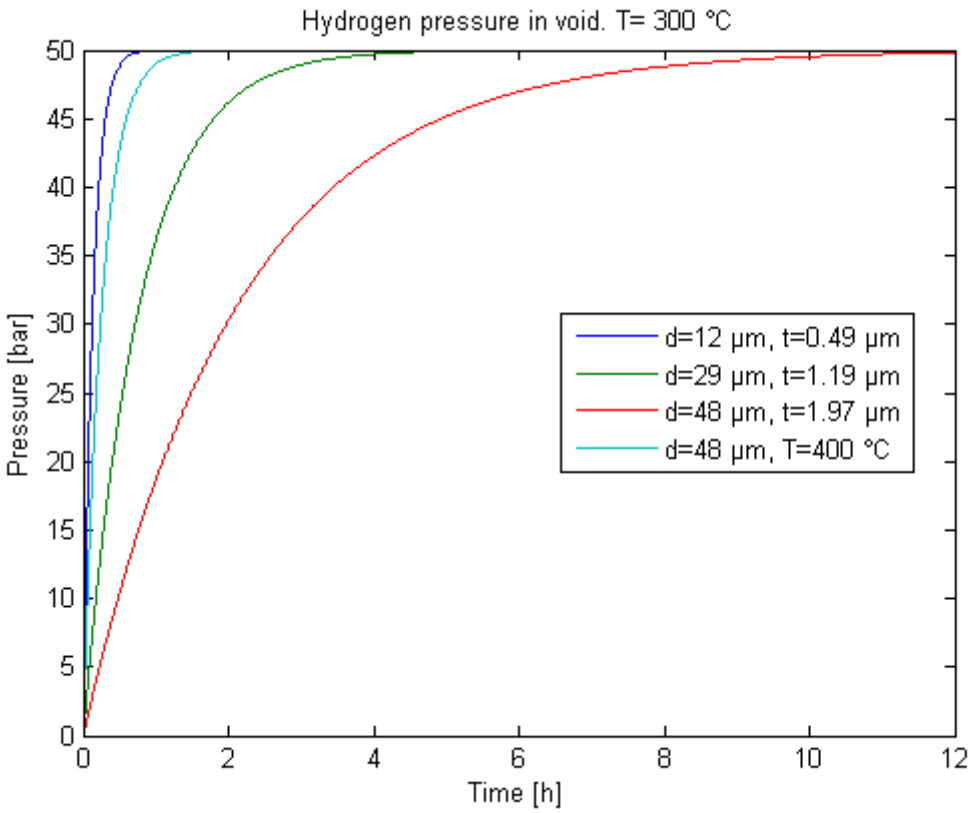

Figure 5 – Particle size's influence on the required time to fill a microsphere with 1000 bar Ar/H_2 gas mixture at 300 °C. Where d is the diameter of the microsphere and t is the wall thickness. The fill time for the largest microsphere at 400 °C is also shown.

Figure 4 showed that the temperature is a big factor on the fill time. However, the stored amount of hydrogen is influenced by the fill temperature as the gas exhibit a larger volume at higher temperatures. Hence, a lower amount of hydrogen gas is stored once cooled down to room temperature. Thus, a higher temperature increases the permeability but at the same time decrease the storage capacity.

Figure 6 summarize how the temperature affects the theoretical storage capacity and fill time at the target fill pressure of 1000 bar. Storage capacity is defined as the mass of hydrogen over the mass of microspheres and is independent on the microsphere's diameter since it is based on the aspect ratio and true density which is assumed to be the same for all diameters. Fill time is here defined as the time to reach 99.9% of the equilibrium hydrogen partial pressure, i.e. 49.95 bar. Fill time is dependent on particle diameter assuming constant aspect ratio. Microspheres should therefore be filled at as low temperatures as possible in order to minimize the volume of the gas. Moreover, the temperature should also be high enough for a sufficiently high permeability, enabling reasonable fill times. Thus, 300 °C was chosen for the experiment at which 90% of the equilibrium hydrogen partial pressure is reached in less than 2 hours. At 300 °C the theoretical storage capacity is 0.272 wt%.

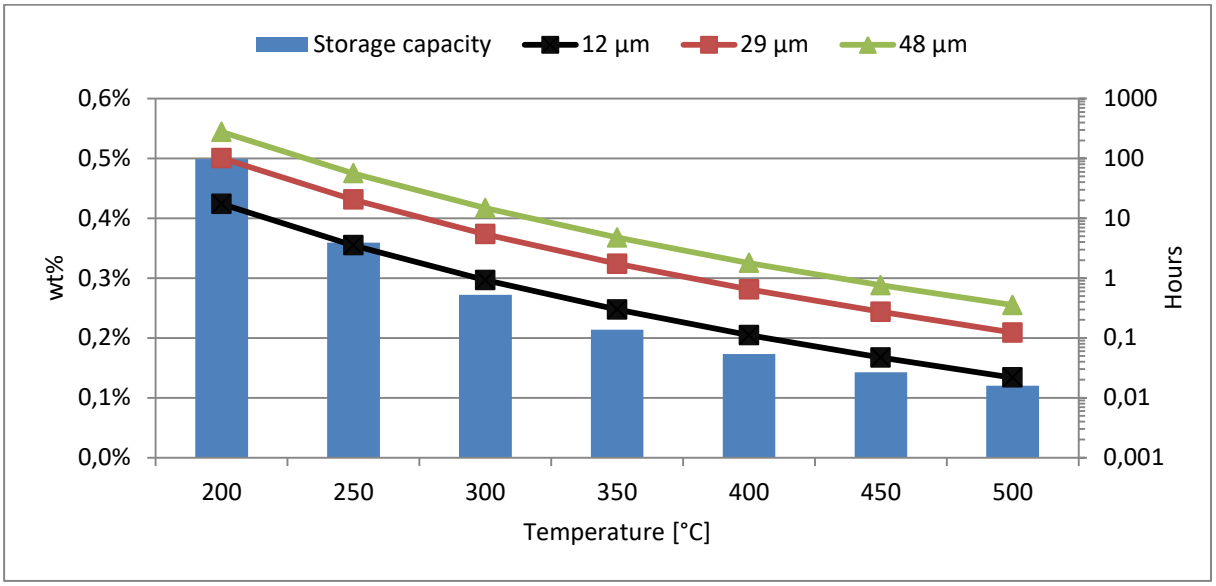

Figure 6 - Theoretical hydrogen storage capacity (bar chart) and fill time (lines) for three monosized microsphere fractions at different temperatures using a 95/5 Ar/H_2 gas mixture at 1000 bar. Note that the fill time is shown with a logarithmic axis.

Once the microspheres are filled they must be able to confine the hydrogen long enough to be transferred into the HIP-capsule before it is evacuated and sealed. Shelby et al. noted a 15 – 24% loss of hydrogen from larger, nickel oxide doped microspheres (D50 between 41.1 – 64.5 µm) filled with 0.93 bar when stored for 35 days at 50 °C. [35] The exact composition is not presented. A small change in the script used to calculate the fill time estimate that about 22% of the hydrogen has escaped after 35 days at 50 °C for a glass composition with M=15%. Therefore, an estimation of the storage capability can be done using the developed Matlab script and the expected fill pressure. Figure 7 shows the loss of hydrogen from microspheres of three diameters stored at 20 °C for 1 year using the same fill conditions as before. Here, it is assumed zero partial pressure H_2 in the surrounding atmosphere. One can according to this calculation expect minor losses of hydrogen during storage and for one year it is estimated that 1 – 16% is lost depending on the microsphere's diameter and thus its wall thickness.

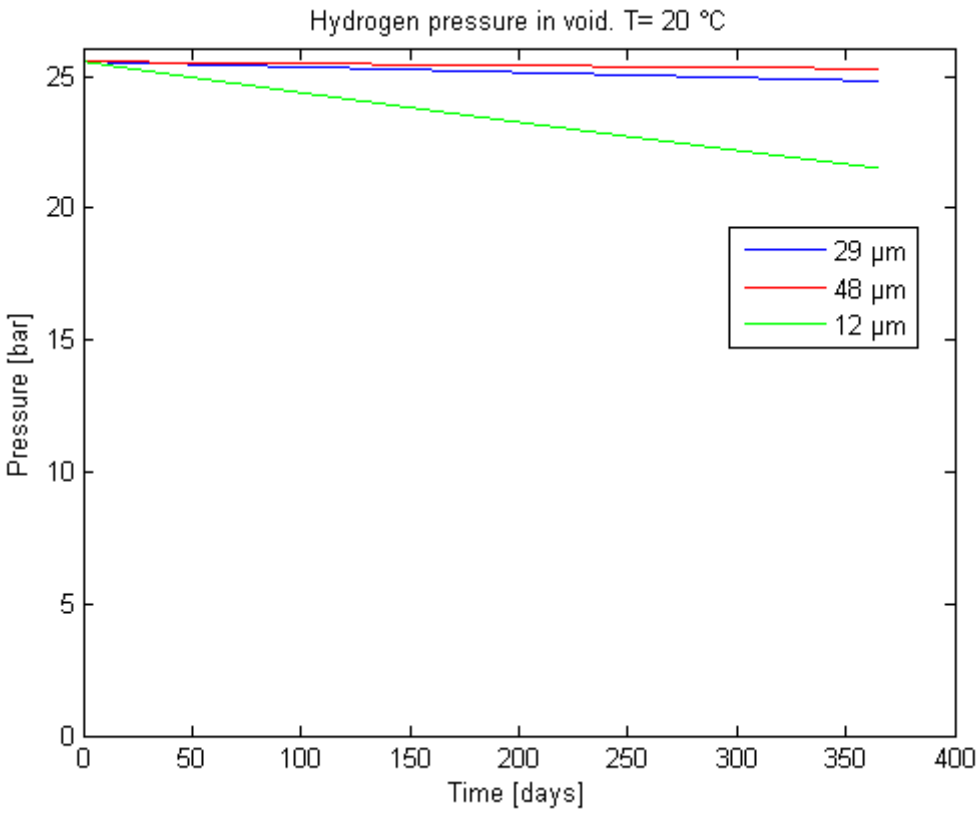

Figure 7 – Storage capability of hydrogen in microspheres. Calculated for the three sizes in its size span, aspect ratio=0.041 and with M=20%.

2.1.3 Amount of microspheres

The volume of microspheres needed to store the required amount of hydrogen can be calculated using the fill conditions determined in the previous chapter (1000 bar, 300 °C, 2 h). The internal pressure will be equal to the partial pressure of hydrogen in the fill gas, i.e. 5% of the total pressure. This together with the volume of the void in the microspheres determines how much hydrogen gas each microsphere can hold. Firstly, the volume of a solid microsphere is calculated using the median particle size $D50 = 29\ \mu m$. [18] Then, the volume of the void can be calculated with as:

$$V_{void} = V_{solid} * \left(1 - \frac{\rho_{tr}}{\rho_{th}}\right) \quad (12)$$

Where $1 - \frac{\rho_{tr}}{\rho_{th}}$ is the true density to theoretical density ratio of the microspheres and material respectively, the void to particle ratio (VtP). Due to the lack of information on the composition of the soda-lime borosilicate S60HS, the density was assumed to be that of the major component, silica $\rho_{th} = 2.65\ g/cm^3$. [44] The wall thickness can also be calculated using the obtained volume to calculate the void's radius , r_{void}, and the microsphere's outer diameter:

$$r_{void} = \left(\frac{3V_{Void}}{4\pi}\right)^{1/3} \rightarrow t = \frac{d}{2} - r_{void} \quad (13)$$

Assuming a constant aspect ratio, i.e. wall thickness to diameter, the resulting wall thickness for the microspheres' size span, D10=12 µm to D90=48 µm [18], is 0.5 µm and 1.97 µm respectively. With the V_{void} known, the theoretical storage capacity of one microsphere of 29 µm can be calculated using the ideal gas law and fill conditions:

$$n_{H_2} = \frac{PV_{void}}{RT} \quad (14)$$

The pressure is in *Pa*, temperature in *K* and *R* is the ideal gas constant. This results in an internal pressure of 25.6 bar at 20 °C. The volume of the gas is then calculated with the ideal gas law and divided by the VtP to obtain the true volume of microspheres needed to store the required amount of H_2. Multiplied with the true density $\rho_{tr} = 0.6\ g/cm^3$ from the manufacturer gives the mass of the required microspheres (m_{MS}).

$$m_{MS} = \rho_{tr} * V_{MS}^{true} = \rho_{tr} * \frac{V_{H2}}{VtP} \quad (15)$$

The mass of the hydrogen is small compared to the microspheres and is therefore neglected. Using the bulk to true density ratio (BtT=0.6) of the microspheres from the manufacturer gives the bulk volume, i.e. the real volume the microspheres will take up. [18]

$$V_{MS}^{bulk} = \frac{m_{MS}}{\rho_{tr} * BtT} \quad (16)$$

Equation 15 results in, m_{MS}, of 41.3 and 16.1 g for the tool steel and the low-alloy steel, respectively. Equation 16 results in a volume of the required microspheres V_{MS}^{bulk} of 114 and 45 cm^3 for the tool steel and the low-alloy steel, respectively.

2.1.4 Amount of ammonia borane

Similar calculations is performed for ammonia borane in order to determine how much to add to the capsules. As previously mentioned ammonia borane releases 2.2 mol H_2 per mol H_3NBH_3. This is used to calculate the required mass ammonia borane.

$$m_{\mathrm{H_3NBH_3}} = \frac{n_{H_2}}{2.2} \quad (17)$$

Then the required volume of the ammonia borane can be calculated with its bulk density of 0.26 g/cm^3. [45]

$$V_{\mathrm{H_3NBH_3}} = m_{\mathrm{H_3NBH_3}} * \rho_{\mathrm{H_3NBH_3}} \quad (18)$$

This yields a mass, $m_{\mathrm{H_3NBH_3}}$, of approximately 0.78 g and 0.31 g as well as a volume $V_{\mathrm{H_3NBH_3}}$ of 3 cm^3 and 1.2 cm^3 for the tool steel and the low-alloy steel, respectively. These amounts represent S60HS filled with pure H_2 at 1000 bar and 300 °C weighing 2.1 and 0.8 g with a bulk volume of 5.7 and 2.2 cm^3 for the tool steel and the low-alloy steel, respectively.

2.1.5 Loss of hydrogen from HIP-capsule

Any loss of hydrogen would require an increased amount of microspheres or ammonia borane to compensate for the loss. Therefore, a numerical calculation was setup in order to estimate the magnitude of the hydrogen loss during the reduction heat treatment. The partial pressure in the free volume of the capsule, i.e. the interparticle void, was calculated using the ideal gas law and by assuming that the entire required amount of hydrogen was released simultaneously as:

$$p_{H_2} = \frac{n_{H_2} RT}{V_f^{porosity} * V_{capsule}} \quad (19)$$

The decrease in hydrogen partial pressure due to reduction reactions forming water vapour is neglected since the water vapour will be taken care of by a confidential method which is unfortunately not possible to describe in detail in this thesis. It also tests the worst scenario with the highest hydrogen partial pressure and thus the fastest hydrogen loss. The result is approximately 15 bar at 500 °C for the two tested cylindrical capsules with the internal dimensions: 162.5 mm in height and 50 mm or 80 mm in diameter, designated as model 1 and 2 respectively. Capsules are constructed of a 2 mm thick sheet of either carbon steel or austenitic stainless steel. It is assumed that the partial pressure is evenly distributed throughout the capsule volume at all times. Thus, the calculations can be performed in one dimension over the capsule wall.

Hydrogen diffuses atomically in metals and the transfer from its gaseous state to dissolved hydrogen occurs in three steps. Firstly, the diatomic hydrogen molecule is adsorbed onto the surface. Secondly, the molecule is dissociated into atomic hydrogen which is also adsorbed to the surface. Lastly, the adsorbed atom is dissolved into the material and start to diffuse. The overall reaction can be written as
$\frac{1}{2}H_2(g) \rightleftarrows \underline{H}$ where the slowest step is the rate limiting step. Since all three reactions occur in succession, the sequential step of diffusion in the solid can also be added.

For instance, below 200 °C, the rate-limiting step is the dissociation of diatomic hydrogen into its atomic state. It is affected by the surface concentration of adsorbed H_2 which in turn is dependent on the partial pressure of the hydrogen gas. [46] An estimation of the hydrogen loss can be determined using hydrogen's permeability through the metal. The permeability, K, was retrieved as an average of six plain carbon ferritic steels, K_{CS}, and several austenitic stainless steels, K_{SS}, from San Marchi and Somerday [47] according to:

$$K_{CS} = 2.592 * 10^{-5} * \exp\left(-\frac{34617}{RT}\right) \quad (20)$$

$$K_{SS} = 1.2 * 10^{-4} * \exp\left(-\frac{59800}{RT}\right) \quad (21)$$

It is assumed once again that all of the hydrogen is released simultaneously inside the capsule and that hydrogen is treated as an ideal gas, i.e. neglecting possible fugacity effects. Noticeable fugacity effects occur above 500 bar according to San Marchi and Somerday. [47] Hydrogen permeates until the partial pressure of hydrogen reaches the hydrogen partial pressure outside the capsule, i.e. 0. This assumption is validated by the fact that the furnace will be filled with pressurised Ar-gas and the escaped hydrogen will therefore be diluted.

With the permeability known, the calculations are possible to set up. The numerical iteration was performed in Matlab implementing equations 20 or 21 into:

$$J = \frac{K}{\Delta x} * \sqrt{\Delta P_{H_2}} \quad \left[\frac{mol\ H_2}{m^2 s}\right] \quad (22)$$

Which describes the flux of H_2 through the capsule wall with a thickness Δx due to a partial pressure difference ΔP_{H_2}. Then, the new hydrogen pressure is calculated as before using equation 19 obtaining the new partial pressure difference. Parameters used in the calculations are shown in Table 4. An appropriate timestep (Δt) was chosen as to fulfil the Von Neumannn stability condition $\frac{2D\Delta t}{\Delta x^2} \leq 1$ for both of the capsule materials. [48]

*Table 4 – Parameters used in numerical iteration.*Calculated as in chapter 2.1.1.*

Capsule material	Capsule model	Wall thickness (Δx) [m]	Inner surface area of capsule (A) [m^2]	Initial amount of H_2* (n) [mol]	Temperature (T) [K]	Timestep (Δt) [s]
Carbon steel	**1**	0.002	0.051	0.056	773	1
	2		0.0295	0.022		
Stainless steel	**1**	0.002	0.051	0.056	773	10
	2		0.0295	0.022		

Figure 8 below shows the calculated hydrogen pressure inside the capsule for the two different materials. Carbon steel is shown to have a much quicker loss of hydrogen compared to capsules made of stainless steel.

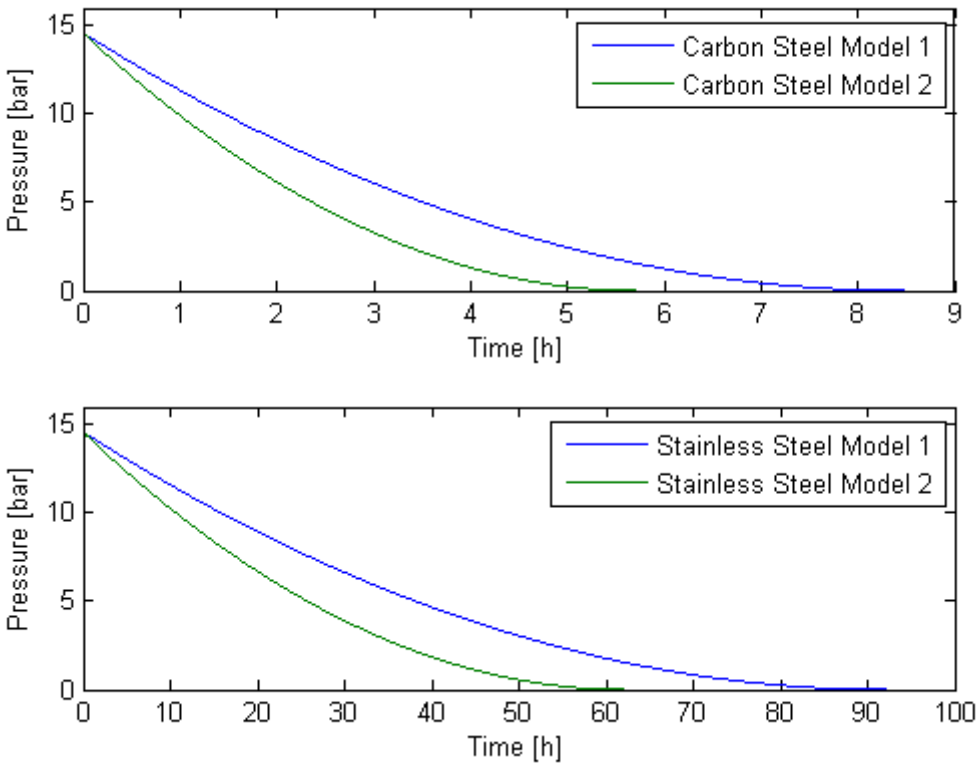

Figure 8 - Hydrogen pressure at inner wall over time for all 4 capsule variations down to p_{H_2} *= 0 bar at T=500 °C.*

3 Experimental

3.1 Metal powders

3.1.1 Chemical analysis of oxygen and nitrogen content

An analysis of the oxygen and nitrogen content of the virgin powders was performed using a "LECO TC 436" nitrogen / oxygen determinator by inert gas fusion. It rapidly heats the powder and detects oxygen in in the form of CO or CO_2 by a Non Dispersive Infrared detector (NDIR) and nitrogen by a Thermal Conductivity detector (TCD). [49] Both virgin metal powders were split into two 1.00 g samples each and the analysis was performed at Swerea KIMAB.

3.1.2 Reduction temperatures

In order to investigate the reduction behaviour of the metal powders an investigation was performed with a Photo Acoustic Spectrometer (PAS) instrument while heating the sample in a hydrogen atmosphere. The instrument continuously measures different gases (CO, CO_2, CH_4 and H_2O) in the process gas. The gas of interest is the measured amount of H_2O in H_2 which indicates the reduction of metallic oxides but also the evaporation of adsorbed water. A 10.00 g sample was heated in a tube furnace up to 1300 °C at a rate of 4 °C/min in H_2 gas flowing at 3 L/min. Afterwards, the samples were retrieved and broken into 2 samples of 0.5-1 g for each material. These were analysed for oxygen and nitrogen in the same procedure as for the virgin powders.

3.1.3 Powder characteristics

An analysis of the microsphere's size distribution and shape was performed by dynamic image analysis using a Camsizer XT from Retsch Technology [50], equipped with air jet dispersion used to break up agglomerates before analysis. From the measurements a number of characteristics were extracted: cumulative distribution (Q3), frequency distribution (q3) in equation 24, sphericity (SPHT3) in equation 25 and particle aspect ratio (b/l3) in equation 26. The "3" in all these characteristics indicate that they are based on volume. All are then plotted against $x_{c\ min}$ which is the shortest chord (width) of a particle which is close to results obtained by sieving. [51]

$$q3 = \frac{dQ_3}{dx} \tag{23}$$

$$SPHT3 = \frac{4\pi A}{P^2} \tag{24}$$

P – measured perimeter of a particle projection.

A – measured area covered by a particle projection.

$$b/l3 = \frac{x_{c\ min}}{x_{Fe\ max}} \tag{25}$$

$x_{c\ min}$ – the shortest chord, see Figure 9.

$x_{Fe\ max}$ – the Feret diameter, see Figure 9.

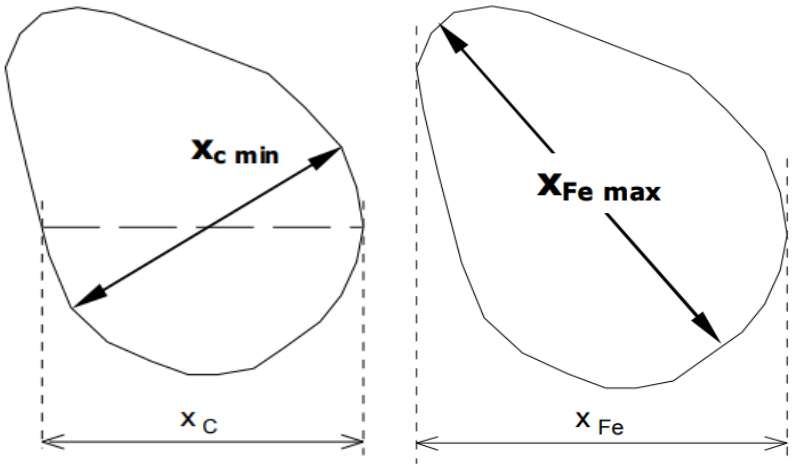

Figure 9 - Difference between x_c and x_{Fe}.

Different measurements of the size distribution exist which yields different values if it deviates from a Gaussian distribution. It is then called right- or left-tailed depending on how the distribution is skewed. Common descriptions of particle size distributions are mode, mean and median. Mode is the peak of the frequency distribution, i.e. how often a size occurs, and represents the most common particle found in the sample. Mean is a similar to the concept of average and is calculated on a volume, number or surface basis and the results are therefore influenced by which basis it is calculated from. Median is defined as the point where half of

the population is larger than this point. It can also be calculated from a volume, number or surface basis but is most often reported on a volume basis. The median is often represented as D50. [52]

3.2 Decomposition analysis of ammonia borane

The analysis of the volatile elements was performed at heating conditions resembling the HIP-cycle. The sample was weighed and placed in an alumina sample holder and slid into the hot-zone of the tube furnace. Thereafter, the sample was heated up to 1160 °C at 5 °C/min under an Ar-gas flow. A dwell time of 30 minutes at 1160 °C was used before the furnace ramped down to room temperature. The off-gas was analysed with a mass spectrometer equipped with a quadrupole mass filter (Pfeiffer Vacuum GSD320). The experimental parameters are shown in Table 5.

Table 5 – Experimental setup for the analysis of ammonia borane's decomposition.

Mass spectrometer		Furnace		Sample	
Maximum mass	120 amu	**Heating rate**	5 °C/min	**Mass**	0.09 g
Scan time	500 ms/amu	**Target temperature**	1160 °C	**Molar mass**	30.87 g/mol
		Dwell time	30 min	**Amount**	0.0029 mol
		Ar-flow	1 L/min		

The resulting mass spectrum was compiled in a spreadsheet and the ion current over time for each measured unit mass (m/z-ratio) was plotted. Mass numbers with a signal-to-noise ratio less than 3 were neglected in agreement with literature. [53, 26] The identified mass numbers were compared with mass spectra of expected species by the use of the NIST database and their agreements were used to link the measured mass number to a certain species. [54] Once a species was identified, its corresponding mass number was plotted against temperature. If a species was released as a result of the decomposition it would here show a peak in ion intensity during heating, while the carrier gas, its contaminants and adsorbed moisture would be relatively constant with temperature. Thus, enabling further distinguishing of where each species originated from and whether all characteristic mass number have been correctly assigned.

3.3 Microspheres

3.3.1 Characteristics analysis

An analysis of the microspheres' size distribution and shape was again performed by dynamic image analysis using a Camsizer XT from Retsch Technology [50], equipped with air jet dispersion used to break up agglomerates before analysis. The same characteristics were collected for the microspheres as for the virgin metal powders.

Morphology and chemical analysis of the microspheres were performed in a Scanning Electron Microscope Microscopy (JEOL JSM 7000F, Japan) equipped with energy dispersive spectroscopy (EDS) X-ray microanalysis (INCA, Oxford Instruments, UK) using an accelerating voltage of 10 kV. A sample was prepared by attaching a conductive carbon

adhesive tape to a small square plate and applying the microspheres onto the tape. The sample was then coated with an approximately 15 µm thin gold film using sputter deposition to achieve a conductive sample suitable for the SEM. Images was taken using the backscattered electron detector in the COMPO mode, showing the difference in atomic mass as contrast with lighter areas showing heavier elements and vice versa. Gold was omitted from the EDS results which give the elements respective contents in weight percent. This was then the base for the quantitative oxide analysis performed in the SEM software INCA. A total of 12 EDS spectra were generated and the average elemental and oxide composition was plotted.

3.3.2 Evolved gas analysis

An analysis of released gaseous elements during heating of the virgin microspheres was performed with the same furnace conditions and mass spectrometer settings as for ammonia borane, see Table 5. The difference was the sample weight of 0.7 g for the microspheres.

3.3.3 Fill procedure

Microspheres were prepared to be filled with hydrogen by loading 54.93 g into an open container with an internal diameter of 50 mm and a height of 163 mm. A fine stainless steel mesh was placed over the open end of the container and held into place by wound steel wires, see Figure 10. The mesh was used to avoid microspheres leaving the container during pressure changes in the furnace, especially during vacuum pumping. The capsule was placed inside an alumina crucible which was in turn placed inside the HIP furnace.

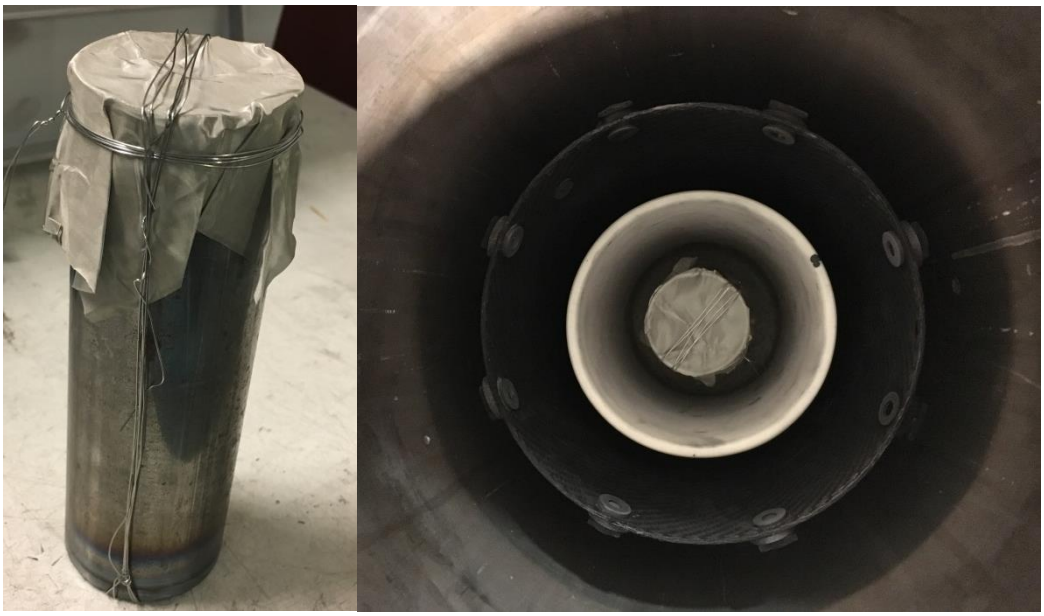

Figure 10 – Mesh covered container used in the fill experiments (left). Container placed in the HIP furnace (right).

The target temperature is limited by the glass softening temperature of 600 °C and was according to the preliminary calculations optimally set to 300 °C. An argon/hydrogen gas mixture consisting of 5% hydrogen gas was used as the pressure gas. After heating to 250 °C in vacuum to remove moisture, the gas mixture was pumped in. Further increase in pressure occur by thermal expansion of the gas during heating up to 300 °C. The target pressure was set to 1000 bar which was held for 1 hour before turning the heating off. When the temperature reached a point where it was safe to release the gas, the furnace was

depressurised as much as possible while still maintaining a temperature above freezing. Figure 11 shows the target pressure and temperature profiles of the fill procedure.

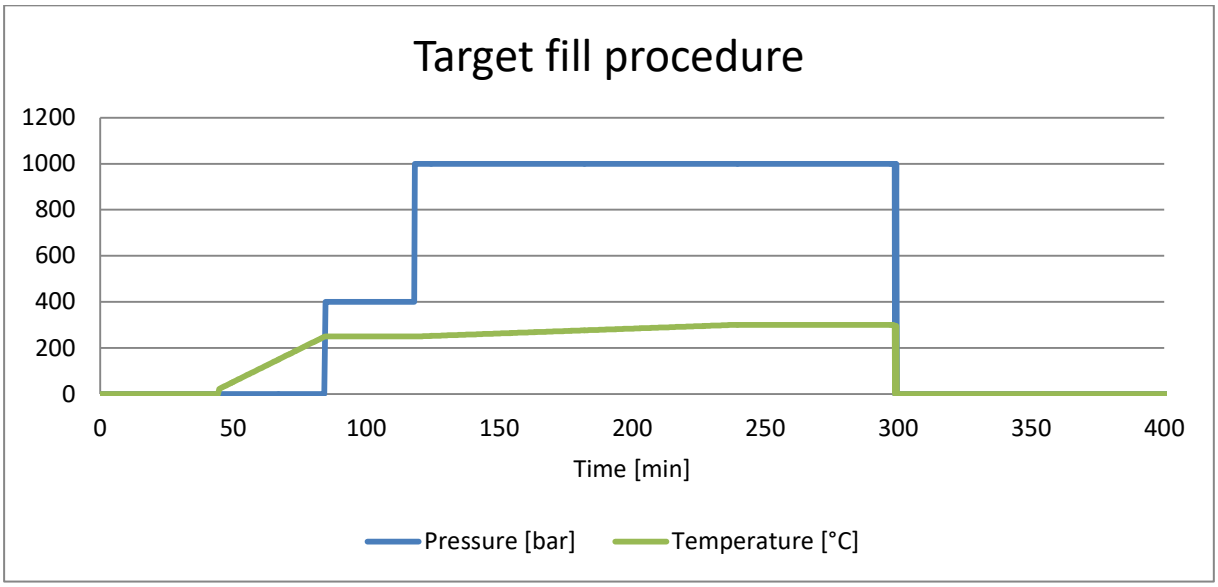

Figure 11 – Target pressure and temperature for hydrogen saturation of the microspheres.

Successfully filled microspheres were separated from damaged ones by the means of flotation in a 99.5% ethanol solution, 0.789 g/cm^3. [55] Microspheres were added into the ethanol filled glass beaker and stirred thoroughly and left for 17 hours. The intact microspheres that are filled with hydrogen have a density between 0.57-0.63 g/cm^3 [18] and damaged ones have the density of the glass, i.e. around 2.65 g/cm^3. Therefore, they separate in the ethanol and the floating microspheres were skimmed off to dry at room temperature until complete evaporation of the ethanol. While the sunken microspheres were together with the beaker heated to 70 °C until complete evaporation of the ethanol. Both fractions were then weighted.

3.3.4 Release of hydrogen

To investigate if the fill procedure was successful and if any argon had entered the internal voids, the microspheres were again analysed with a mass spectrometer at elevated temperatures in a tube furnace. A temperature below the softening point of the microspheres (600 °C) was chosen and the carrier gas was switched to nitrogen to be able to detect possible trapped argon. The setup is shown in Table 6 below. Filled microspheres were tested 4 and 73 days after the fill procedure to investigate the storage capacity and loss of hydrogen while stored in a plastic container at room temperature. Using a slightly altered script of the one used to calculate the hydrogen loss in Figure 7 together with the heating rate in the table below it is possible to estimate whether the time in the furnace is sufficient. This was done by increasing the temperature for each time step (60 s) by 4 °C and recalculating the permeability at the new temperature, thus giving an increased flux. Figure 12 shows that all of the stored hydrogen is expected to be released during heating to the target temperature for the entire size span of the microspheres.

Table 6 – Experimental setup for the release of hydrogen.

Mass spectrometer		Furnace		Sample	
Maximum mass	120 amu	**Heating rate**	4 °C/min	**Mass**	0.98 g
Scan time	500 ms/amu	**Target temperature**	600 °C		
		Dwell time	30 min		
		N_2-flow	1 L/min		

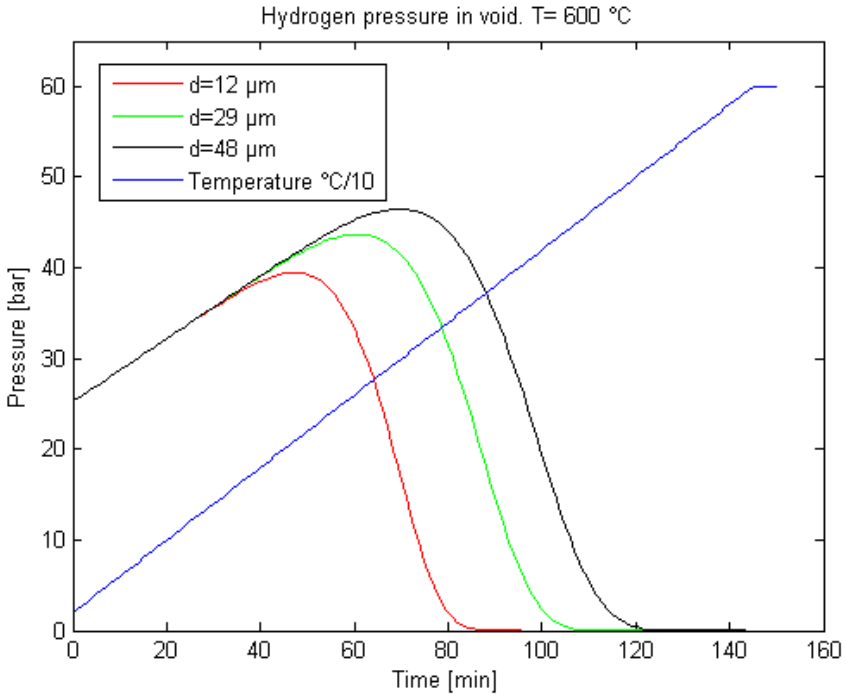

Figure 12 – Internal hydrogen pressure during heating of filled microspheres at 4 °C/min up to 600 °C. With M=20%, T_{fill}=300 °C and P_{fill}=1000 bar.

The storage capacity in the form of wt% H_2 was estimated with the, from literature, known released hydrogen per mol ammonia borane, mass of the microsphere sample (m_{MS}) and the relation between the two respective areas under the measured mass spectrometer curve. Three variants of a Riemann sums were used to calculate the area under the curves (A_{MS} & A_{AB}); left, right and trapezoid. A left Riemann sum approximate the area under the curve by a number of incremental rectangles, with a height corresponding to the measured ion intensity at its lowest x-value for each subinterval (Δx), multiplied with the subinterval. A right Riemann sum instead approximates the curve by the highest x-value for each subinterval (Δx). A trapezoid Riemann sum results in the average between a left and a right Riemann sum. [56] The curves were normalized to the base value of the background noise by subtracting its linear trend line before and after the peak. The amount of mol H_2 ($n_{H_2}^{MS}$) was calculated as:

$$n_{H_2}^{MS} = \frac{A_{MS} n_{H_2}^{AB}}{A_{AB}} \quad (26)$$

The storage capacity of hydrogen in wt% ($w_{H_2}^{MS}$) could then be calculated as.

$$w_{H_2}^{MS} = \frac{n_{H_2}^{MS} M_{H_2}}{m_{MS}} * 100 \quad (27)$$

A theoretical storage capacity could be calculated with equation 28 and the required amount of hydrogen and microspheres from chapter 2. This results in a hydrogen storage capacity of 0.272 wt% when filled at 300 °C with a 5% hydrogen gas mix at 1000 bar.

3.4 Oxide reduction attempt and evaluation

3.4.1 Capsule preparation

This section describes the capsule preparation including capsule construction, testing and loading. Figure 13 show the two capsule models used in this work and the two variations of the fill pipe for ammonia borane and microspheres respectively. The larger capsule model 1, made of stainless steel, was loaded with the tool steel and the smaller capsule model 2, made of carbon steel, was loaded with the low-alloy steel. The confidential method is applied in the capsules containing H_2-carriers. The capsule characteristics are summarized in Table 7.

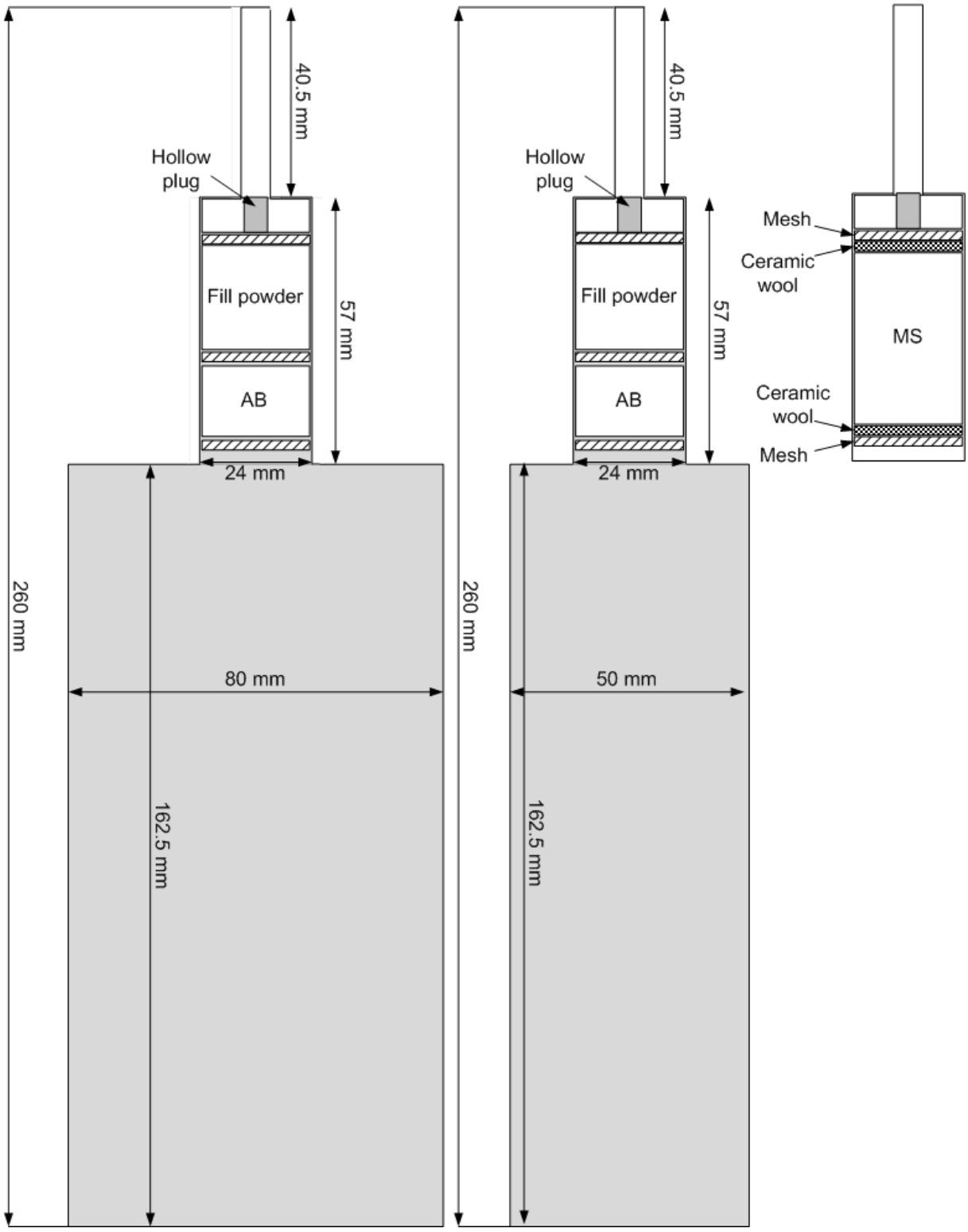

Figure 13 – Sketch of the inner dimensions of capsules model 1 (left) and model 2 (middle) for the ammonia borane capsules with stainless steel meshes separating the metal powder, ammonia borane and fill powder. An alternative approach with the fill pipe without fill powder was used for the microsphere capsules (right).

Table 7 – Dimensions and other properties of the prepared HIP-capsules.

Capsule model	Sheet material	Inner dimensions (h x d) [mm]	Fill pipe inner dimensions (h x d) [mm]	Sheet thickness [mm]	Total dimensions (h x d) [mm]	Metal powder
1	316L	162.5 x 80	57 x 24	2	260 x 80	Tool steel
2	Carbon steel	162.5 x 50	57 x 24	2	260 x 50	Low-alloy steel

The lid with the attached fill pipe and a bottom plate is welded on to the raw tube while argon gas is added inside the capsule, shielding the material. The capsules were then tested for leaks by injecting helium gas inside a covering plastic bag and measuring if any helium had leaked inside with a helium leak detector, see Figure 14 .

Figure 14 - Helium leak test of a HIP-capsule.

Three samples are made for each metal powder; one reference, one with ammonia borane and one with microspheres. The sample nomenclature used in this work is shown in Table 8. The capsules are loaded with the metal powders, ammonia borane or hydrogen filled microspheres according to Table 9. The metal powder is filled just over the connection to the fill pipe to allow for some shrinkage during the HIP process and still obtain a flat top of the cylinder.

Table 8 – Sample nomenclature for the 6 different HIP-capsules. TS=Tool Steel, LAS=Low-Alloy Steel, 1 or 2=capsule model number, R=Reference, AB=Ammonia Borane, MS=MicroSpheres.

Sample nomenclature	Reference	Ammonia borane	Microspheres
Tool steel	TS1R	TS1AB	TS1MS
Low-alloy steel	LAS2R	LAS2AB	LAS2MS

Twice the required mass of ammonia borane was added generating twice the required amount of hydrogen gas. Fine steel meshes are placed above the metal powder, ammonia borane and

fill powder as seen in Figure 13. Because of the small particle size, microspheres will go through the mesh. Thus, a stainless steel foil shaped into a cup was also used in addition to ceramic wool discs, see Figure 15. An additional foil sheet was placed in the bottom of the cups. The cups should hold the microspheres in place and the discs will further protect the metal powder from contamination as well as avoiding extracting the microspheres during capsule evacuation and leak testing. The ceramic discs were placed above and below the microsphere-filled cups with meshes on the outside, securing the discs into place, see Figure 13. Because of the diluted gas mixture used in the microsphere's fill procedure, less hydrogen would be stored. Therefore, no fill powder was used in order to maximize the amount of microspheres added. The reference samples were only loaded with fill powder with meshes placed above and below. The fill powder is a high temperature stainless steel powder (253 MA +250 -1000 µm) which consolidates later then the main powder.

Table 9 – Sample contents.

Sample	Tool steel powder [kg]	Low-alloy steel powder [kg]	Ammonia borane [g]	Hydrogen filled microspheres [g]
TS1R	3.965	-	-	-
TS1AB	3.950	-	1.56	-
TS1MS	4.005	-	-	4.95
LAS2R	-	1.742	-	-
LAS2AB	-	1.757	0.63	-
LAS2MS	-	1.728	-	5.28

Figure 15 – Bottom pair of ceramic wool disc and mesh before pushing them down into place (left). On top of the pair, stainless steel foil cups with an extra bottom sheet were inserted into the fill pipe (right). The cups were then filled with the hydrogen filled microspheres. An inverted pair was then placed above the filled foil cups.

An evacuation pipe is placed onto the uppermost mesh for all samples and a hollow plug is inserted which is secured in placed by a cold pinch of the evacuation pipe just above the plug. After welding the evacuation pipe into place and a subsequent leak test, the capsules are evacuated at a slow rate to vacuum. Once fully evacuated the evacuation pipe is hot pinched and welded shut.

3.4.2 Hot Isostatic Pressing cycle

Appropriate HIP-cycles suitable to reduce surface oxides and consolidate the material was determined after the PAS-measurement. Thus, suitable temperatures where oxides were reduced are taken into consideration when programming the HIP-cycle. The heat transfer into the capsules is another important factor in deciding the cycle times. Optimally, the entire volume of the capsules should be at the reduction temperature long enough. Dwell time was determined from Frisk et al. [57] that modelled the heat transfer into the capsules in addition to the reduction time from the PAS-measurements. After the dwell time has passed the temperature and pressure is raised and the powder is finally consolidated. One factor special for this work is that an increase of internal pressure will occur due to the released hydrogen inside the capsule. In order to avoid excessive bulging of the capsule walls the external pressure has to be raised before any hydrogen is released from the microspheres and ammonia borane.

The resulting HIP-cycle for the tool steel and the low-alloy steel is shown in Figure 16. Firstly, the HIP chamber is evacuated and held at vacuum for 1 hour to remove moisture. Normally, moisture is removed from the HIP chamber at vacuum for shorter times at around 300 °C. However, the temperature was held at room temperature to avoid releasing hydrogen risking bulging and perhaps capsule rupture. After 1 hour in vacuum an argon pressure of 70 bar was established before heating up to 400 °C for the tool steel and 600 °C for the low-alloy steel which was held for 2 hours to reduce the oxides. This together with 40 minutes of heating is sufficient for the center of both capsule models to reach the target reduction temperature according to a confidential study. Heat transfer will be further assisted by the high external and internal pressure. The pressure was then increased to 1000 bar during an increase in temperature to 1160 °C over 2 hours. This was then held for 3 hours before the heating was turned off and pressure released. Further reductions of oxides are expected to occur during heating up to the final temperature.

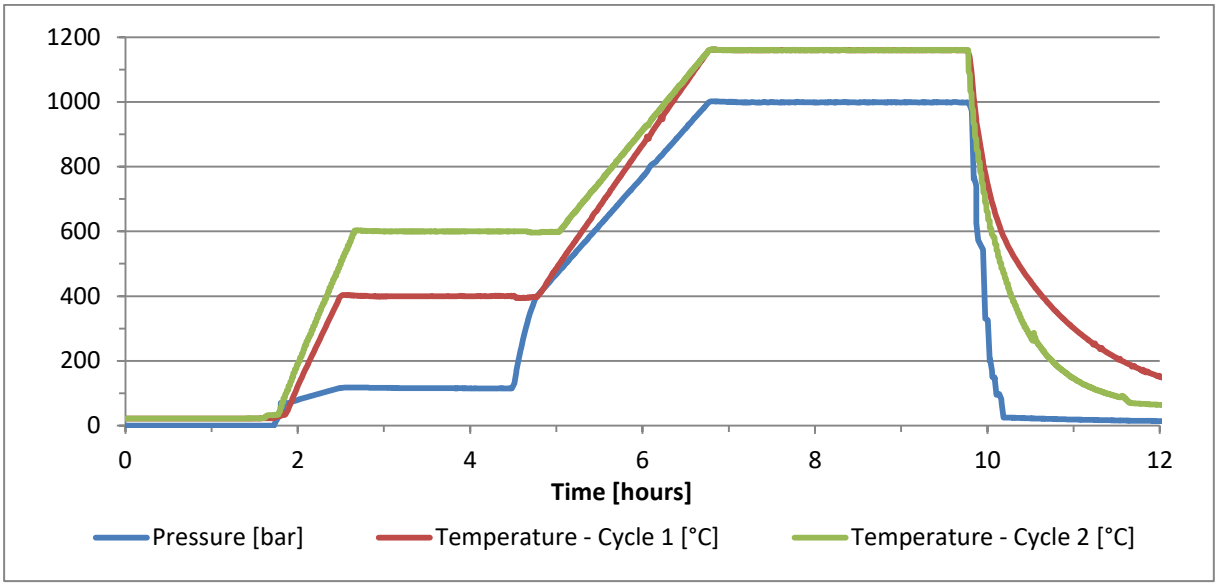

Figure 16 – HIP-cycle designed to both reduce metallic oxides by hydrogen and consolidate the metal powder. Cycle 1 was used for the tool steel and cycle 2 was used for the low-alloy steel.

3.4.3 Oxygen and microstructural analysis

Once a capsule was retrieved from the HIP furnace it was cut in certain positions to assess the amount of oxygen reduction both radially and vertically. The low-alloy steel capsules were first heat treated, using the procedure explained in the next chapter, before being cut into oxygen samples and impact testing bars at Swerea KIMAB, see Figure 17. The top and bottom slices of the tool steel capsules, shown in Figure 18, were cut before heat treatment. This was done since the oxygen samples and impact testing bars were tested at different locations. Oxygen samples were cut 5 millimetres from the capsule wall to avoid any surface effects. Chemical analysis was performed in the same way as for the virgin and sintered powders using inert gas fusion. Whether any reduction has occurred is determined by comparing the oxygen content between the reference capsule and the other two capsules.

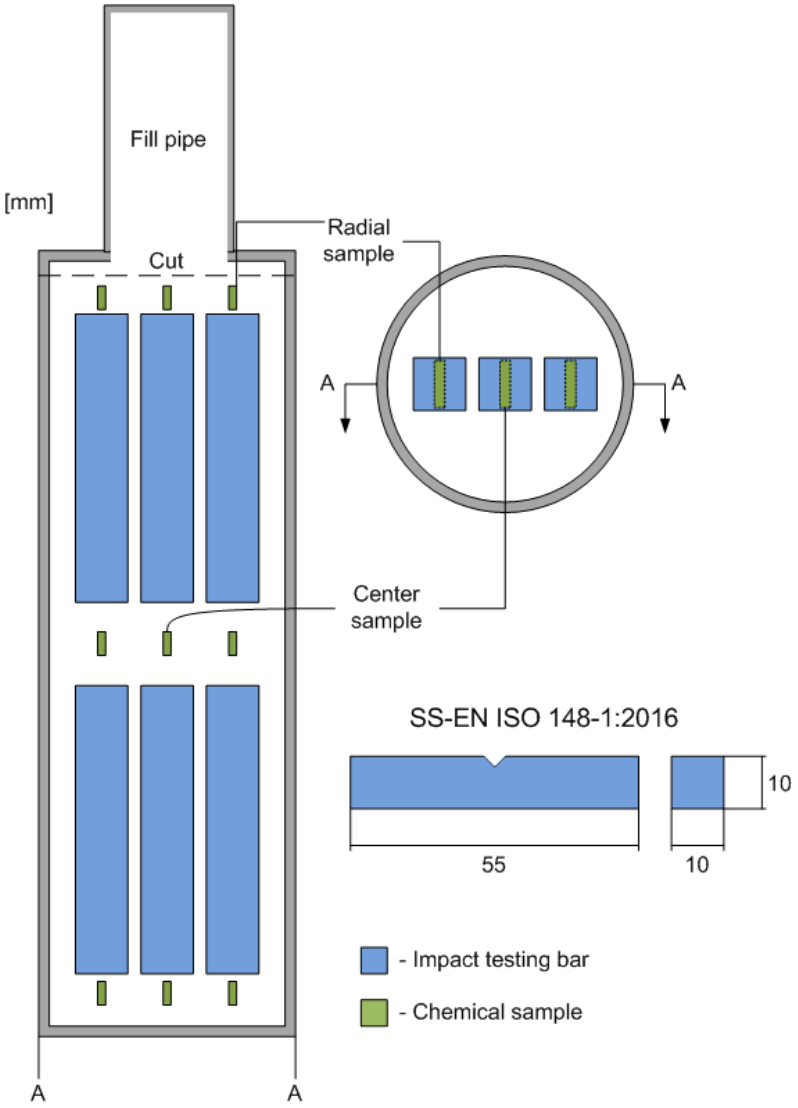

Figure 17 – Position of the impact test bars (blue) and oxygen samples (green) for capsule model 2 (low-alloy steel). Microspheres and Ammonia Borane were placed in a fill pipe above the capsule.

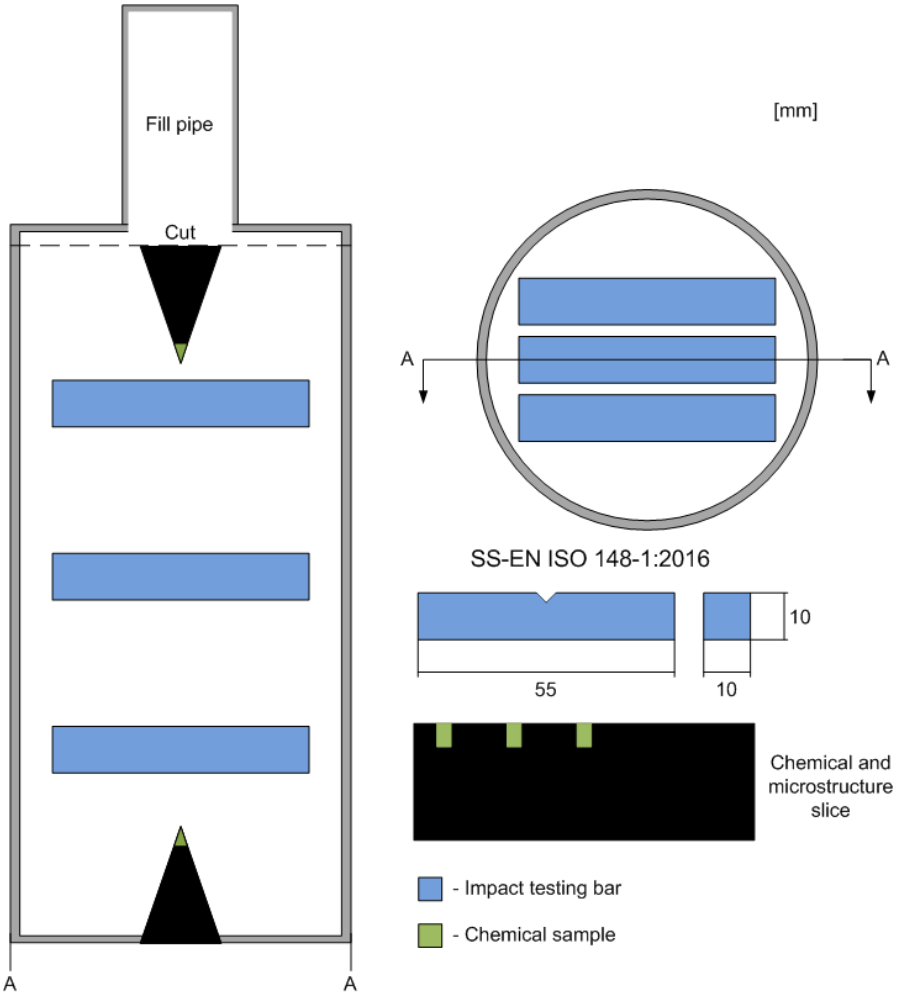

Figure 18 – Position of the impact test bars (blue) and oxygen samples (green) for capsule model 1 (tool steel). Microspheres and Ammonia Borane were placed in the fill pipe above the capsule.

Microstructural samples were retrieved from the top of each capsule as a part of the slice (tool steel) and an area adjacent to the chemical samples (low-alloy steel), both surfaces facing down. They were then analysed with Scanning Electron Microscopy (JEOL JSM 7000F, Japan) equipped with energy dispersive spectroscopy (EDS) X-ray microanalysis (INCA, Oxford Instruments, UK). Inclusion size, measured as the maximum Feret diameter, was then determined from the SEM images using a public domain image processing program (ImageJ 1.52a, National Institute of Health). The cumulative percentage of the inclusion sizes obtained from a number of images is plotted for each capsule. This plot show whether the inclusions have increased or decreased in size due to the incorporation of hydrogen into the capsules.

3.4.4 Impact toughness

Before cutting impact testing bars, the low-alloy steel is heat treated as follows:

- 1120°C for 1 h for every 25 mm of material thickness, thus 2 h for a 50 mm capsule material. Quenching in water.
- 900°C for 2 h, quenching in water.
- 675°C for 20 h, cooling in air.

Charpy-V samples were then cut-out from different locations in order to test the impact toughness radially and vertically, see Figure 17 for the low-alloy steel and Figure 18 for the tool steel. Unfortunately, results from the impact testing of the tool steel were not included due to time constraints. The fill pipe containing the hydrogen carriers was cut off to obtain a flat top before further sectioning. Impact test bars were manufactured and tested according to SS-EN ISO 148-1:2016 at room temperature and with a striker radius of 2 mm. [58]

4 Results

The following chapters contain the result of the initial investigation on the metal powders, ammonia borane, microspheres and the final experiment on the hydrogen carriers' ability to reduce surface oxides in the metal powders.

4.1 Metal powders

4.1.1 Chemical analysis and reduction temperatures

The results from the oxygen and nitrogen analysis of the virgin powders are shown in Table 10.

Table 10 - Oxygen and nitrogen analysis of the virgin metal powders.

Material	O [ppm]	Std. dev.	N [ppm]	Std. dev.
Tool steel	103.2	1.1	497.2	5.0
Low-alloy steel	120.5	6.2	319.5	3.5

A mass loss was observed for both powders, 0.07 g and 0.05 g for the low-alloy steel and the tool steel respectively. Figure 19 shows the change in measured gases as an effect of the reduction. The amount of water vapour show that the oxides in the low-alloy steel are reduced between 250 – 320 °C with the peak at 274 °C in approximately 20 minutes and between 710 – 815 °C. Oxides present in the tool steel are reduced between 268 – 377 °C with a peak at 309 °C for approximately 30 minutes.

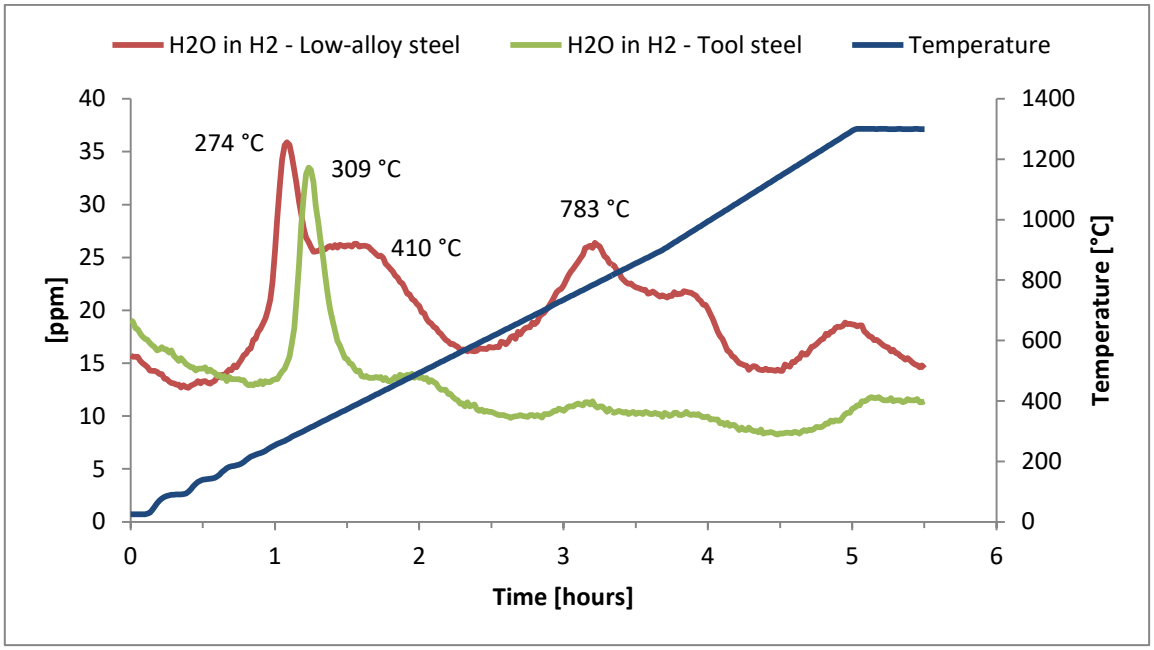

Figure 19 – PAS measurement of the low-alloy steel and the tool steel virgin powders in hydrogen gas.

The chemical analysis of the materials after the PAS measurements shown in Table 11 indicate that not all oxygen was removed. Nitrogen contents were reduced to below 5 ppm.

*Table 11 – Chemical analysis of the powders after treatment at 1300 °C in a H_2 atmosphere. *Nitrogen contents were too low for accurate measurement with the applied settings calibrated for higher nitrogen contents.*

Material	O [ppm]	Std. dev.	N [ppm]	Std. dev.
Tool steel	37.0	2.0	< 5*	-
Low-alloy steel	58.7	2.1	< 5*	-

4.1.2 Characteristics

The result of the size distribution obtained by dynamic image analysis in Figure 20 and Figure 21 shows a right-tailed appearance with the most common particles, the mode, found at around 35 µm and 65 µm for the low-alloy steel and the tool steel, respectively. The median, D50, is shown in Table 12 along with the size span D10 to D90 acquired from the cumulative size distribution (Q3).

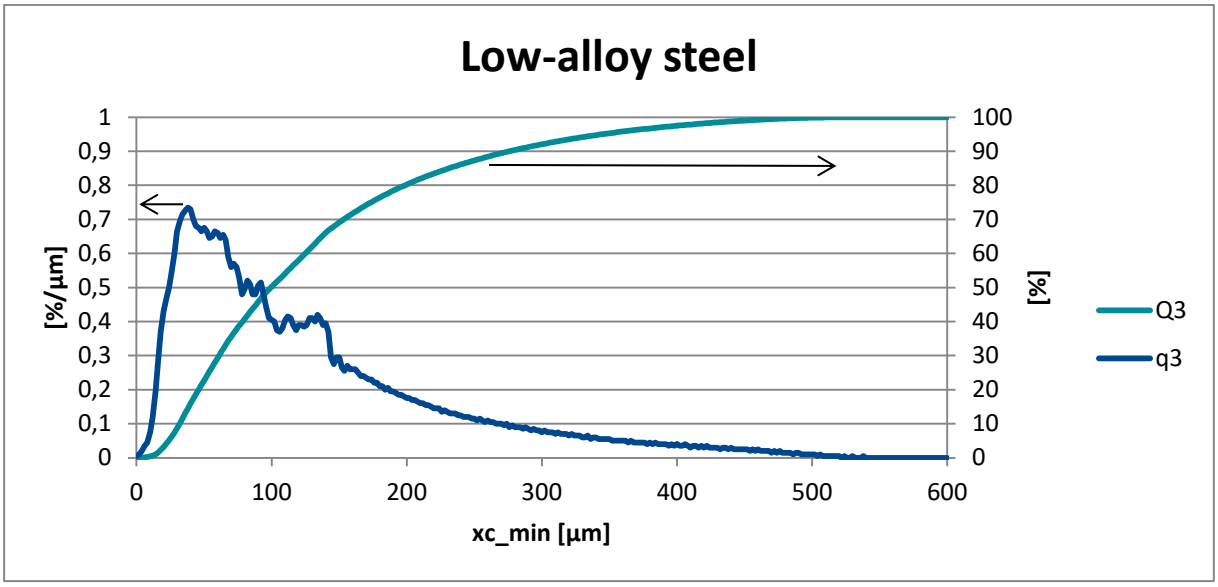

Figure 20 – Cumulative size distribution (Q3) and frequency distribution (q3) by volume of the low-alloy steel powder.

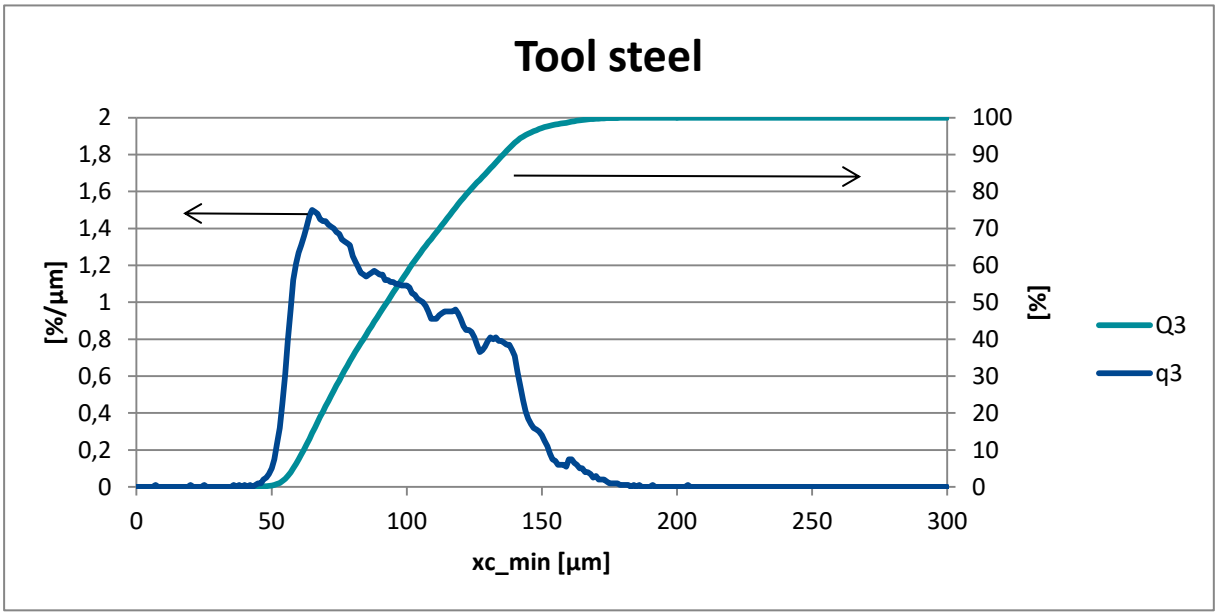

Figure 21 – Cumulative size distribution (Q3) and frequency distribution (q3) by volume of the tool steel powder.

Table 12 – Size span of the low-alloy steel and the tool steel.

Material	Distribution [µm]		
	D10	D50	D90
Low-alloy steel	32	99	276
Tool steel	63	94	137

Sphericity and particle aspect ratio for the low-alloy steel is shown in Figure 22 as a relative steady, decreasing trend except for the largest particle sizes and the dip in sphericity up to 30 µm. For the tool steel, the shape factors are not as steady, see for example the dip between 10 – 25 µm and 175 - 190 µm in Figure 23.

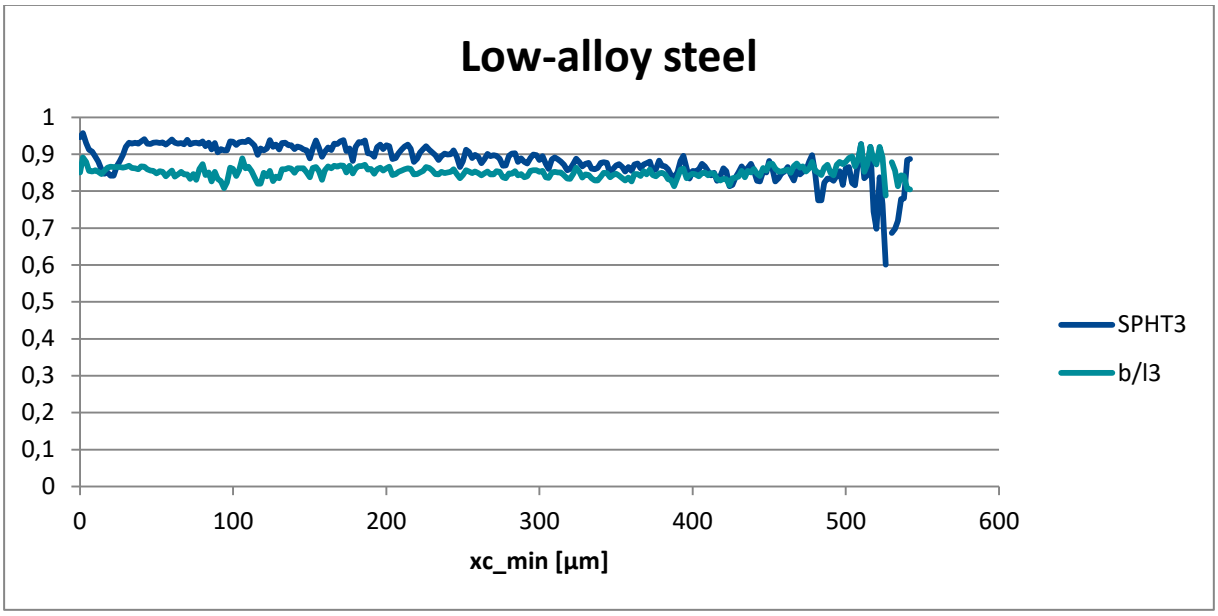

Figure 22 – Sphericity (SPHT3) and particle aspect ratio (b/l3) of the low-alloy steel powder.

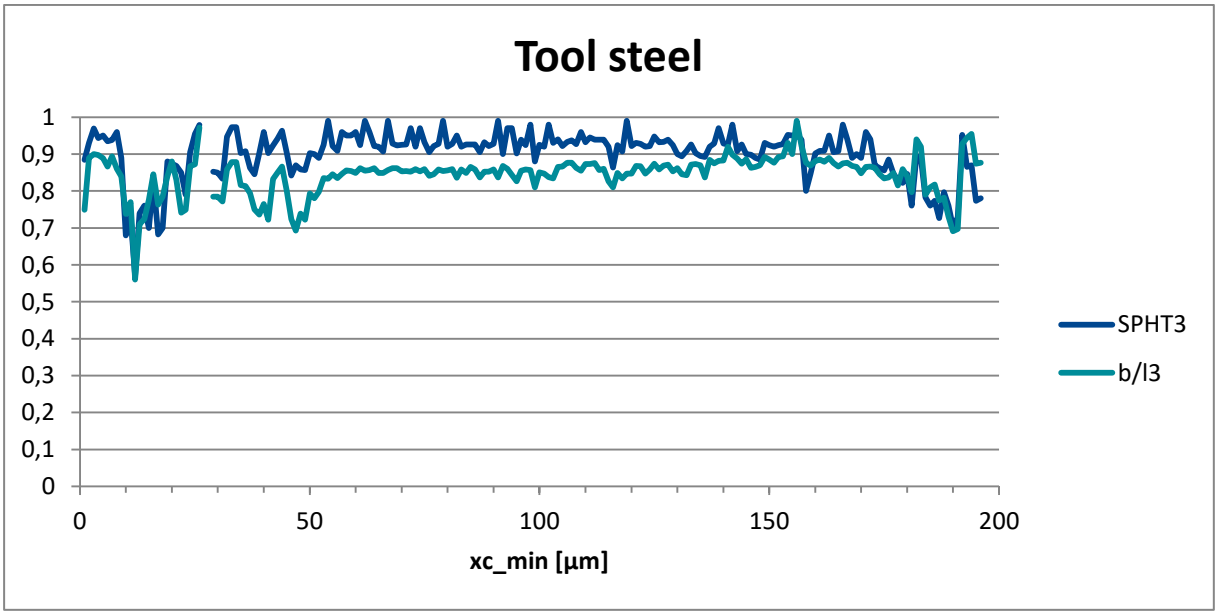

Figure 23 – Sphericity (SPHT3) and particle aspect ratio (b/l3) of the tool steel powder. Gaps in the curve represent sizes where no measurements exist.

4.2 Ammonia borane

4.2.1 Decomposition analysis

The expected species, established in the literature study, were Ar, H_2O, H_2, NH_3, aminoborane (BH_2NH_2), borazine $(BHNH)_3$ and diborane (B_2H_6). Some originate from the ammonia borane while others from the carrier gas or from adsorbed atmospheric gases.

Decomposition species of ammonia borane was identified with their characteristic mass number and the correlation between the measured and reference data is shown in Figure 24. Mass numbers that had a signal-to-noise ratio less than 3 were neglected. Some species share certain mass numbers which makes the assignment of peaks more difficult, for instance water and ammonia share mass number m16 and m17 for some molecular fragments. Argon, hydrogen, water and diborane (B_2H_6) show good correlation with reference data while other species cannot conclusively be confirmed from the peak assignment alone. Borane (BH_3) is the one exception which has low correlation with reference data which in addition to overlapping mass number with other species add up to the dismissal of borane as a detected species. The significant mass numbers, i.e. signal-to-noise ratio above 3, which were unassigned were m30, m32, m41.

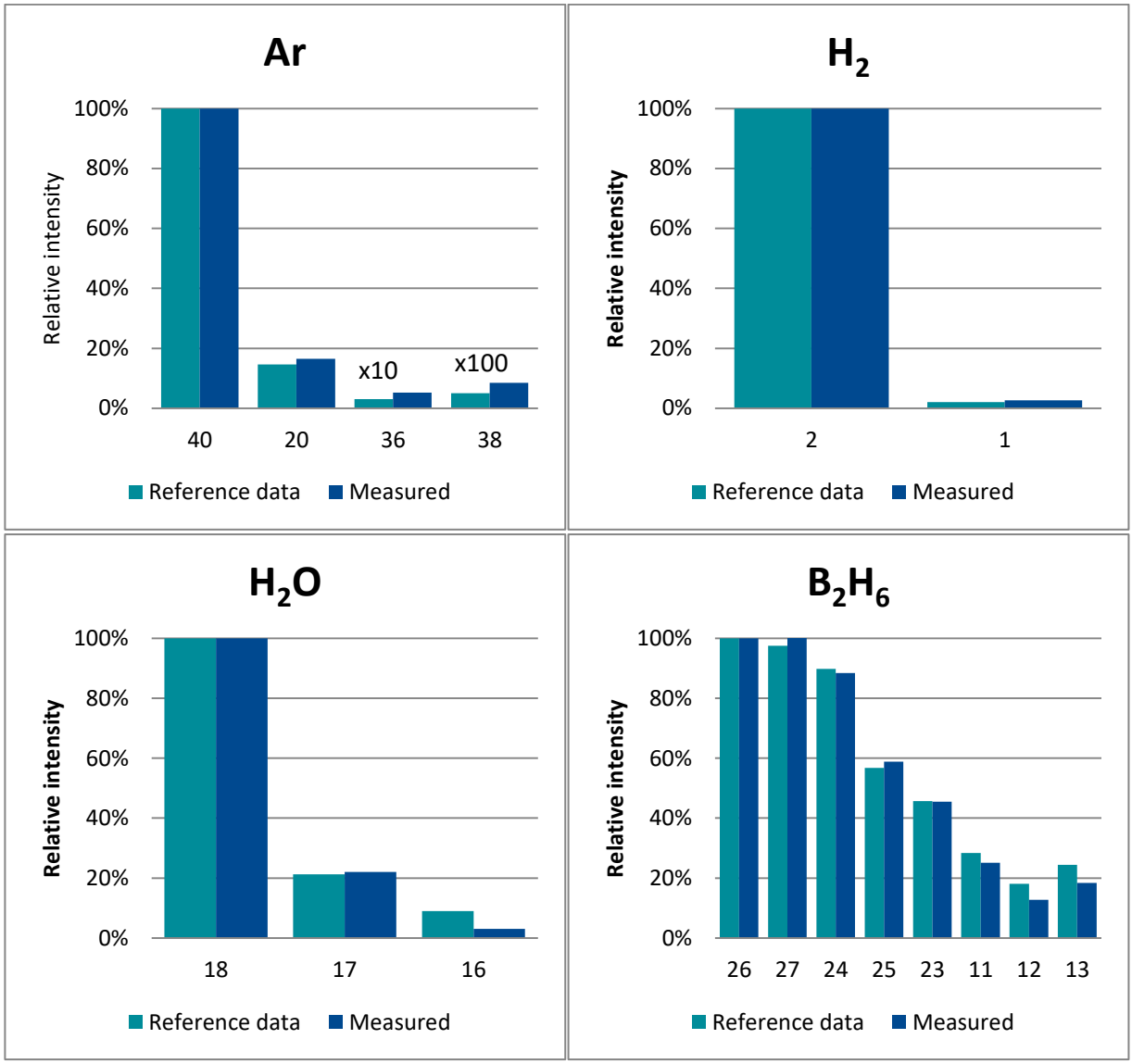

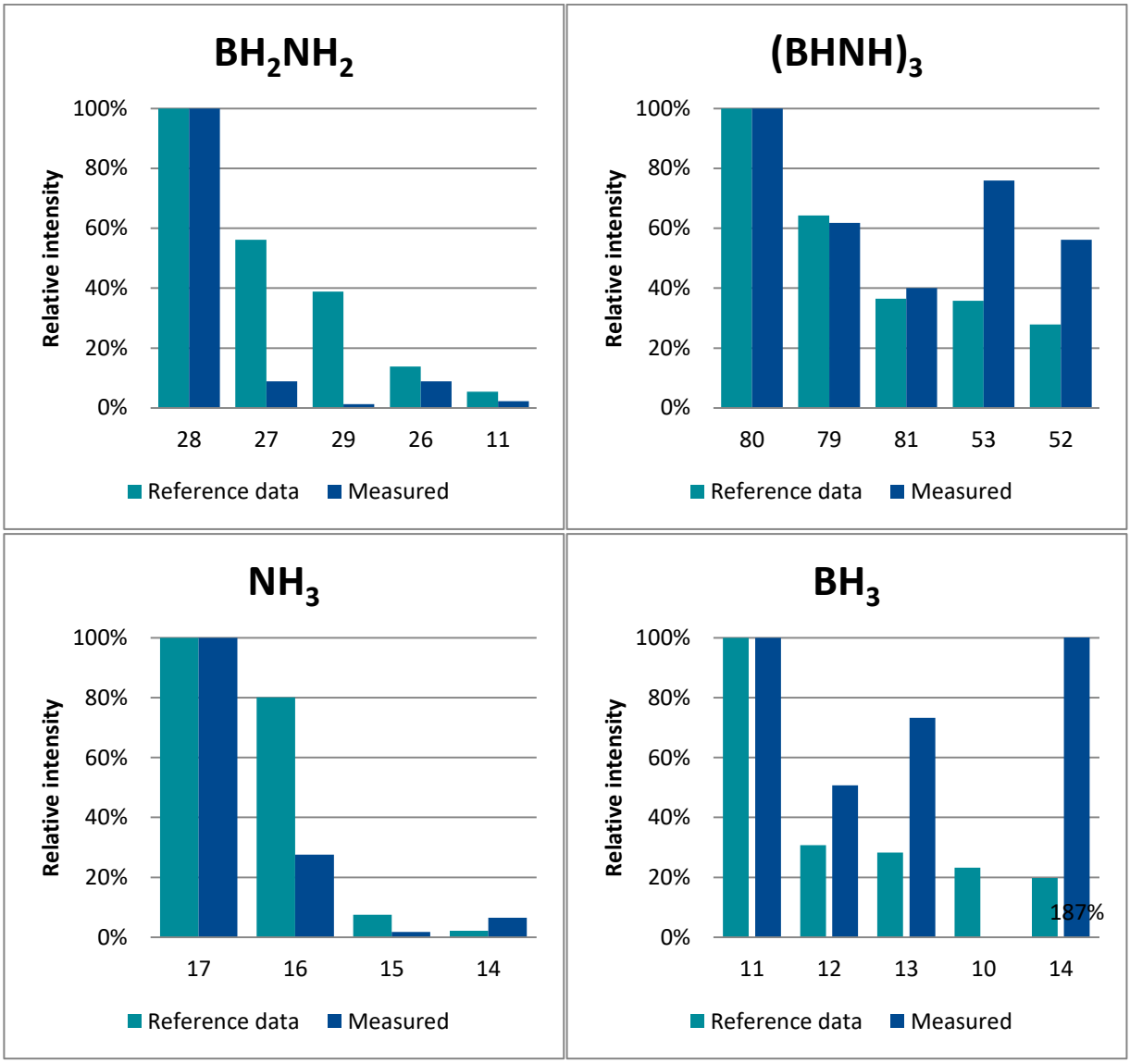

Figure 24 – Correlation between expected species' mass number and measured mass numbers' relative ion intensity. Small values are multiplied by a factor of 10 or 100.

Figures 25 – 30 show the identified assigned mass number for different species as a function of temperature during heating up to 1160 °C. There was a slight shift in the peak intensity from integer mass numbers due to possible calibration error of the mass spectrometer. Therefore, the mass numbers were adjusted to the closest integer for clarity. Also, temperature fluctuations in the furnace can explain why some curves have an irregular shape. It is clear that diborane and borazine is released during heating because of their multiple well-defined and correlating peaks, see Figure 25 and Figure 26. Furthermore, borazine is supposedly released in two steps at around 140 °C and 170 °C. Hydrogen shows a clear peak in ion intensity for m2 but not for m1. The carrier gas argon show a stable intensity with temperature as expected. Water and ammonia show an increase in intensity at temperatures where other species are released. An observation is that, ammonia's increase is in the peaks that it shares with water, i.e. m16 and m17.

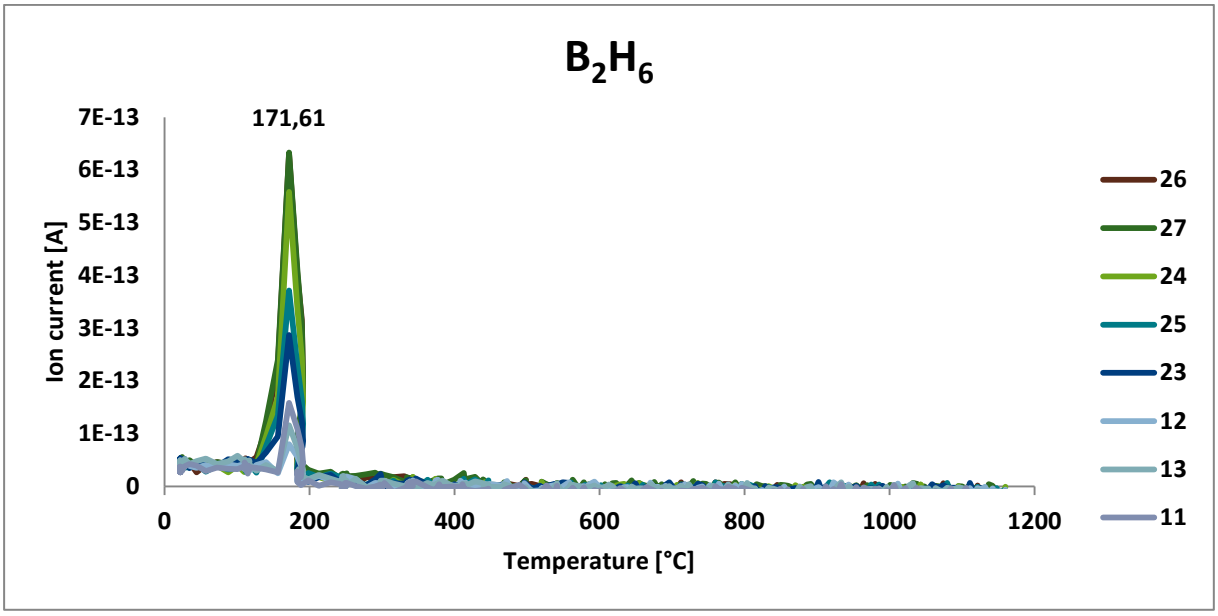

Figure 25 – Change in intensity with temperature for diborane's characteristic peaks. The data point shows the temperature at the peak.

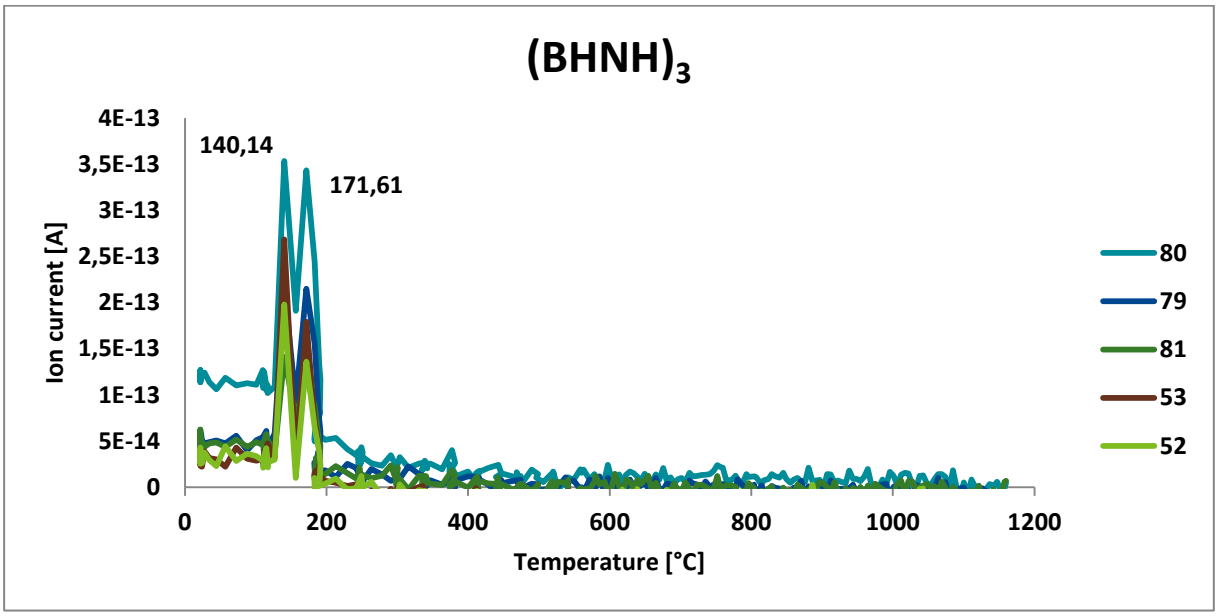

Figure 26 – Change in intensity with temperature for borazine's characteristic peaks. The data points show the temperature at two distinct peaks.

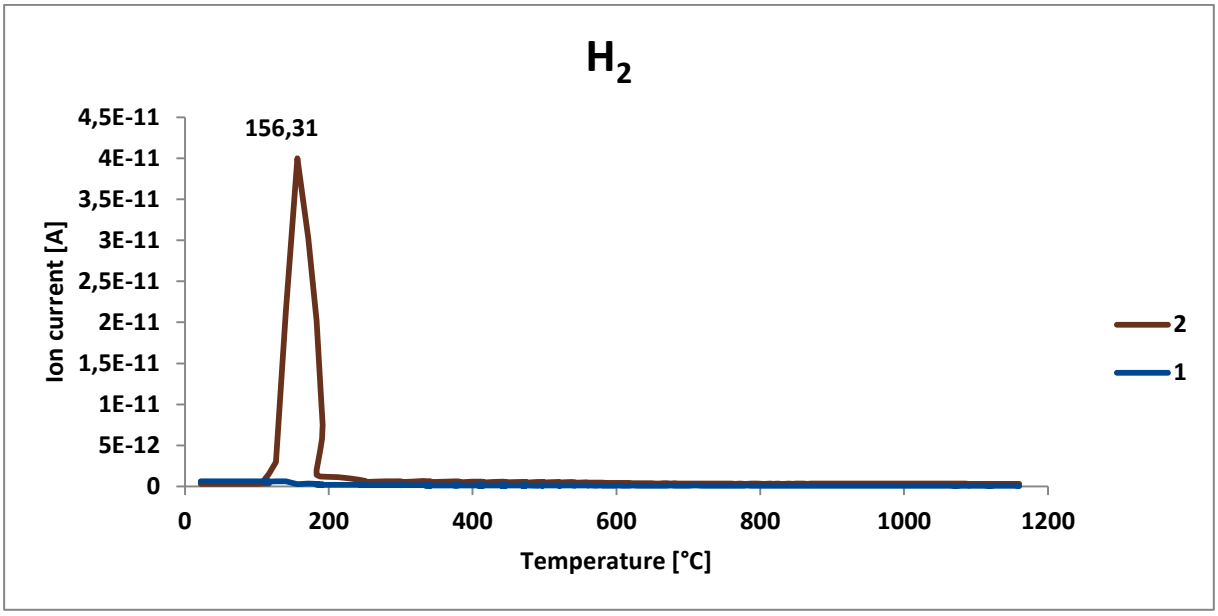

Figure 27 – Change in intensity with temperature for hydrogen's characteristic peaks.

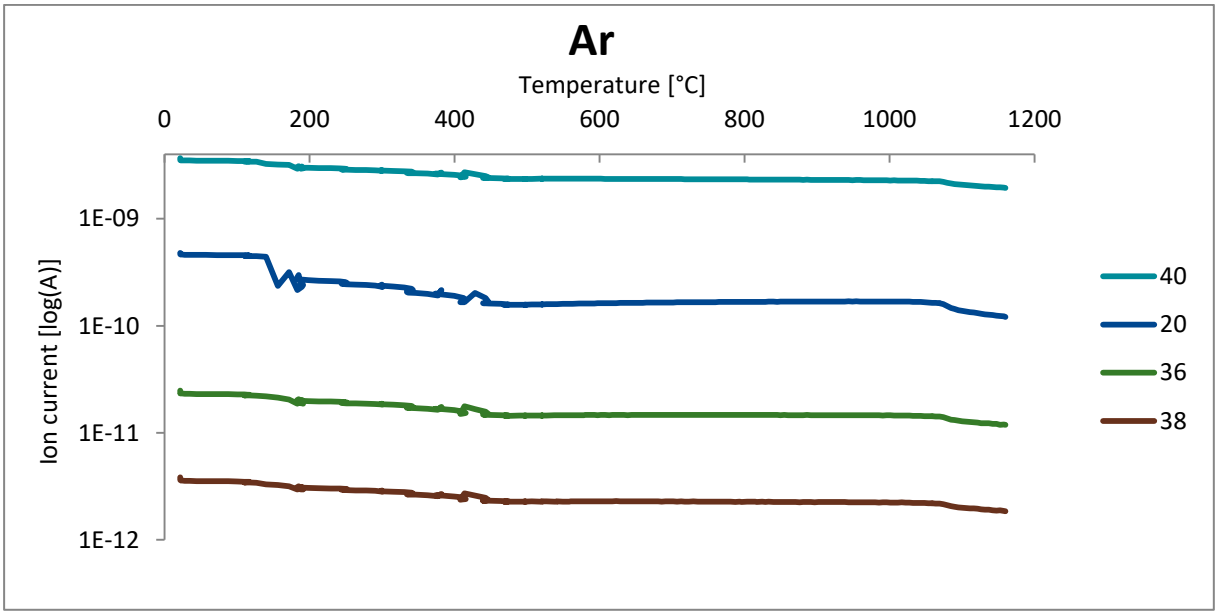

Figure 28 – Change in intensity with temperature for argon's characteristic peaks.

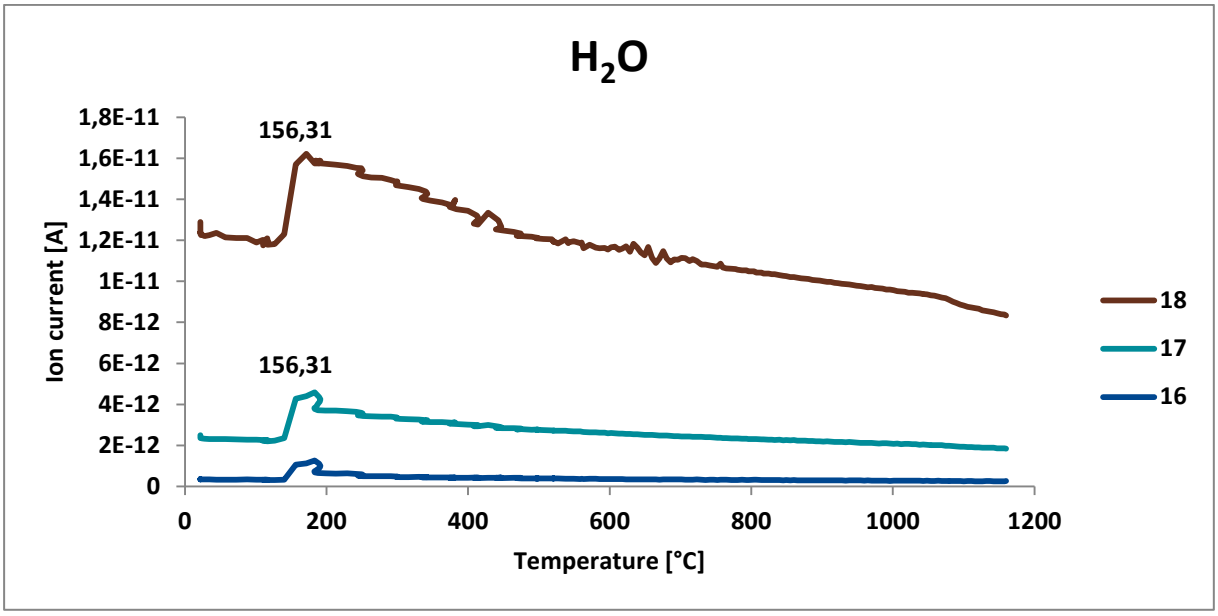

Figure 29 – Change in intensity with temperature for water's characteristic peaks. The data points show the temperature at end of the rapid increase in intensity.

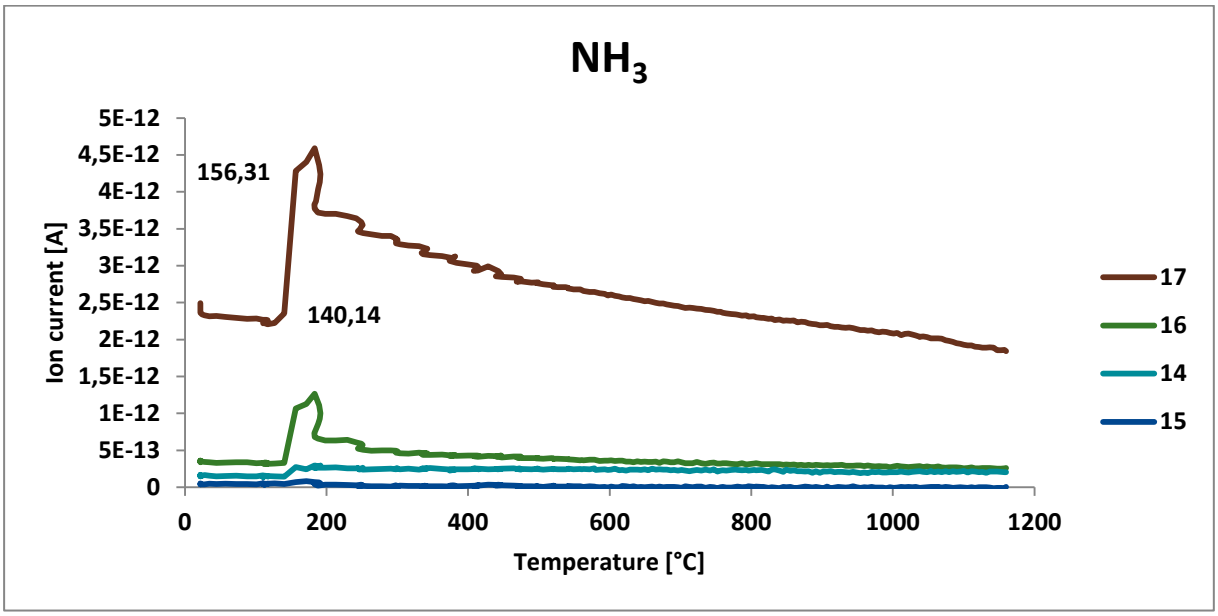

Figure 30 – Change in intensity with temperature for ammonia's characteristic peaks. The data points show the temperature at the onset and end of the rapid increase around 145 °C.

4.3 Microspheres

4.3.1 Characteristics

An example of an area used in the SEM EDS analysis is shown in Figure 31**.** In this specific area the darker spots in the microspheres were investigated. There was no significant difference in composition in these spots.

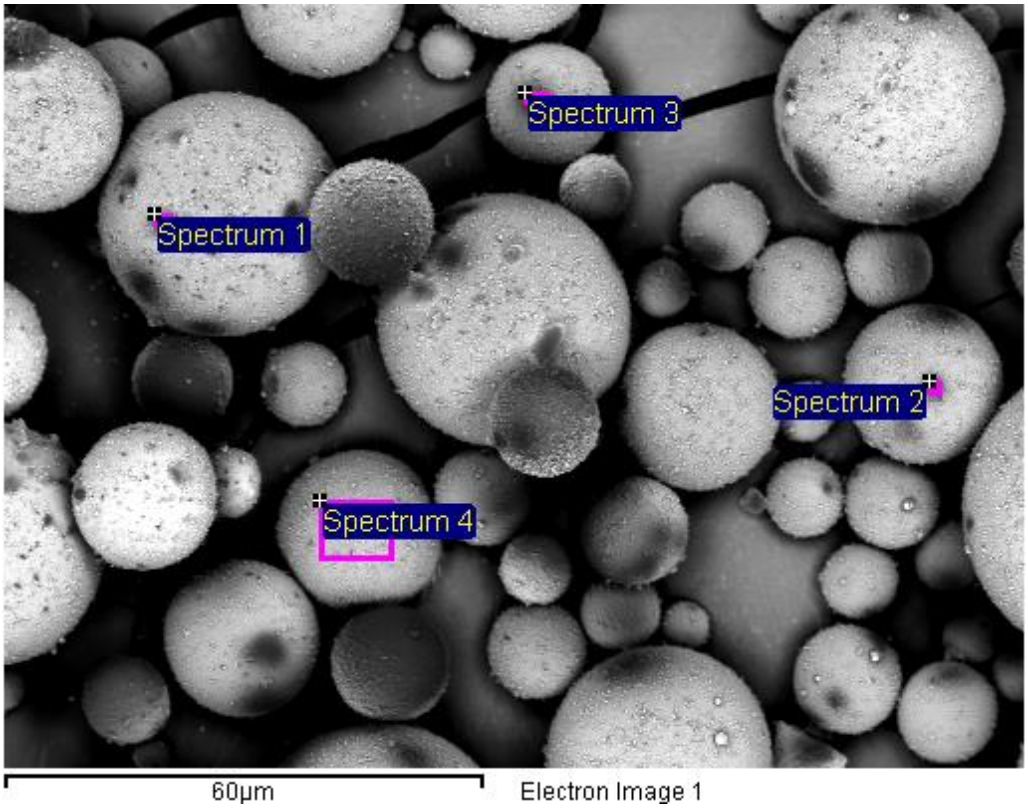

Figure 31 - Example area used in EDS analysis. Note that the fuzzy appearances of the microspheres' surfaces are gold deposits as a result of the sample preparation.

Figure 32 below shows the resulting elemental and oxide compositions acquired from the SEM EDS analysis. Note that magnesium was only present in 2 out of 12 spectra while the other elements were present in all spectra. The resulting percentage of non-network formers in the glass (Na_2O and CaO) is 16.91%.

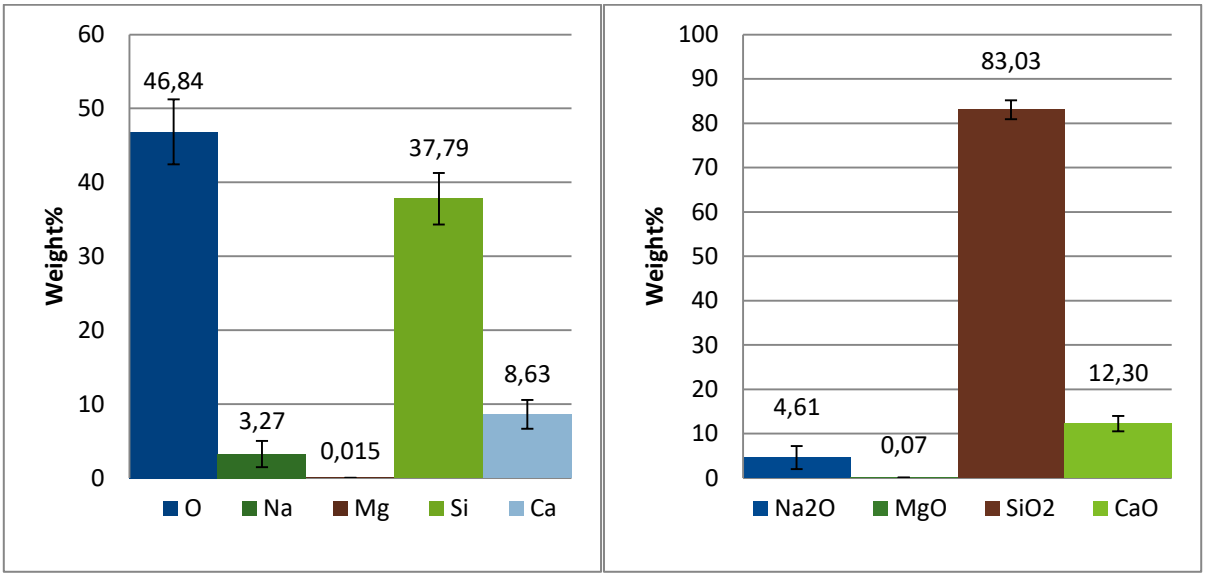

Figure 32 – Elemental composition (left) and oxide composition (right).

Figure 33 shows two SEM images of a broken microsphere with wall porosity. It is shown that the wall thickness of the broken microsphere is in the same magnitude as expected by the preliminary calculations, around 1 µm.

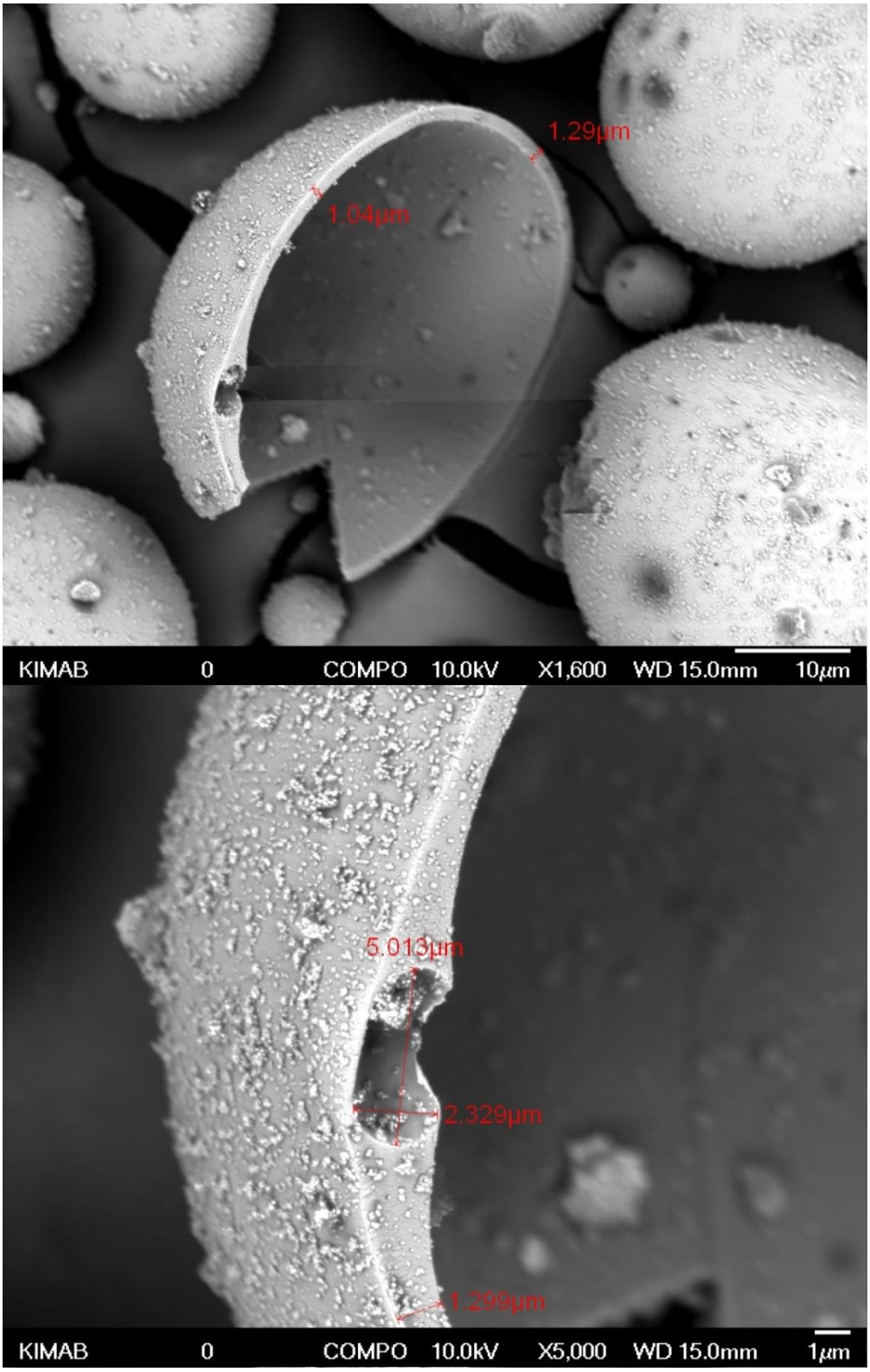

Figure 33 – Measurement of wall thickness (top) and wall porosity (bottom). Note that the granulate appearance of the microspheres' surfaces are gold deposits as a result of the sample preparation.

Figures 34 and 35 show the result of the dynamic image analysis of the microspheres. Figure 35 show lower values than expected for the supposedly spherical microsphere powder. Table 13 show the size span obtained from the cumulative size distribution (Q3). It is slightly lower than the size span given by the manufacturer.

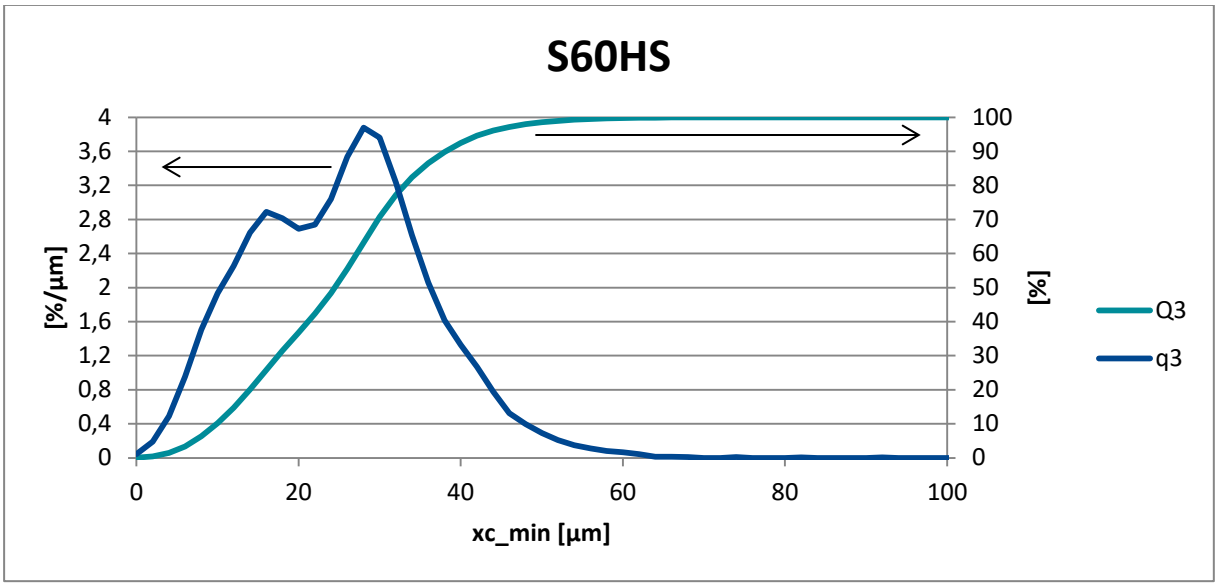

Figure 34 – Cumulative size distribution (Q3) and frequency distribution (q3) by volume of the microspheres.

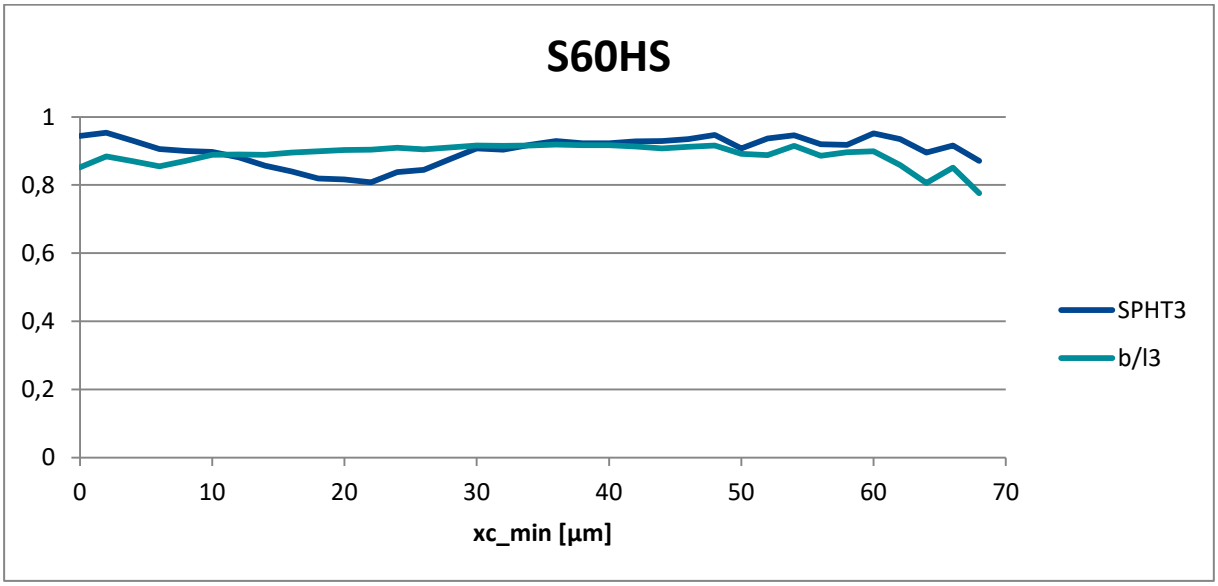

Figure 35 – Sphericity (SPHT3) and particle aspect ratio (b/l3) of the low-alloy steel powder.

Table 13 – Size span of S60HS comparing measurement in this work and from the manufacturer.

	Distribution [µm]		
	D10	D50	D90
Measured	10	24	38
From 3M [18]	12	29	48

4.3.2 Gas analysis of virgin microspheres

Expected species decided from the literature study were Ar, H_2O, N_2, O_2, CO_2 and SO_2. In figure 36 – 41 below the results from mass spectrometer measurement during heating virgin microspheres up to 1160 °C is shown. Figure 36 show the significant, characteristic mass numbers and the correlation between the measured and reference data from NIST. [54] Fragment mass numbers of the expected species are shown relative to the precursor/molecular mass number. No significant peaks could be assigned to SO_2 and CO_2 and there is therefore no diagram investigating the correlation with reference data. Argon, water, nitrogen and oxygen show good correlation with the reference data. One peak, m30, was significant, i.e. signal-to-noise ratio above 3 but could not be assigned to a specific species. Moreover, it showed no peak in intensity as a function of temperature.

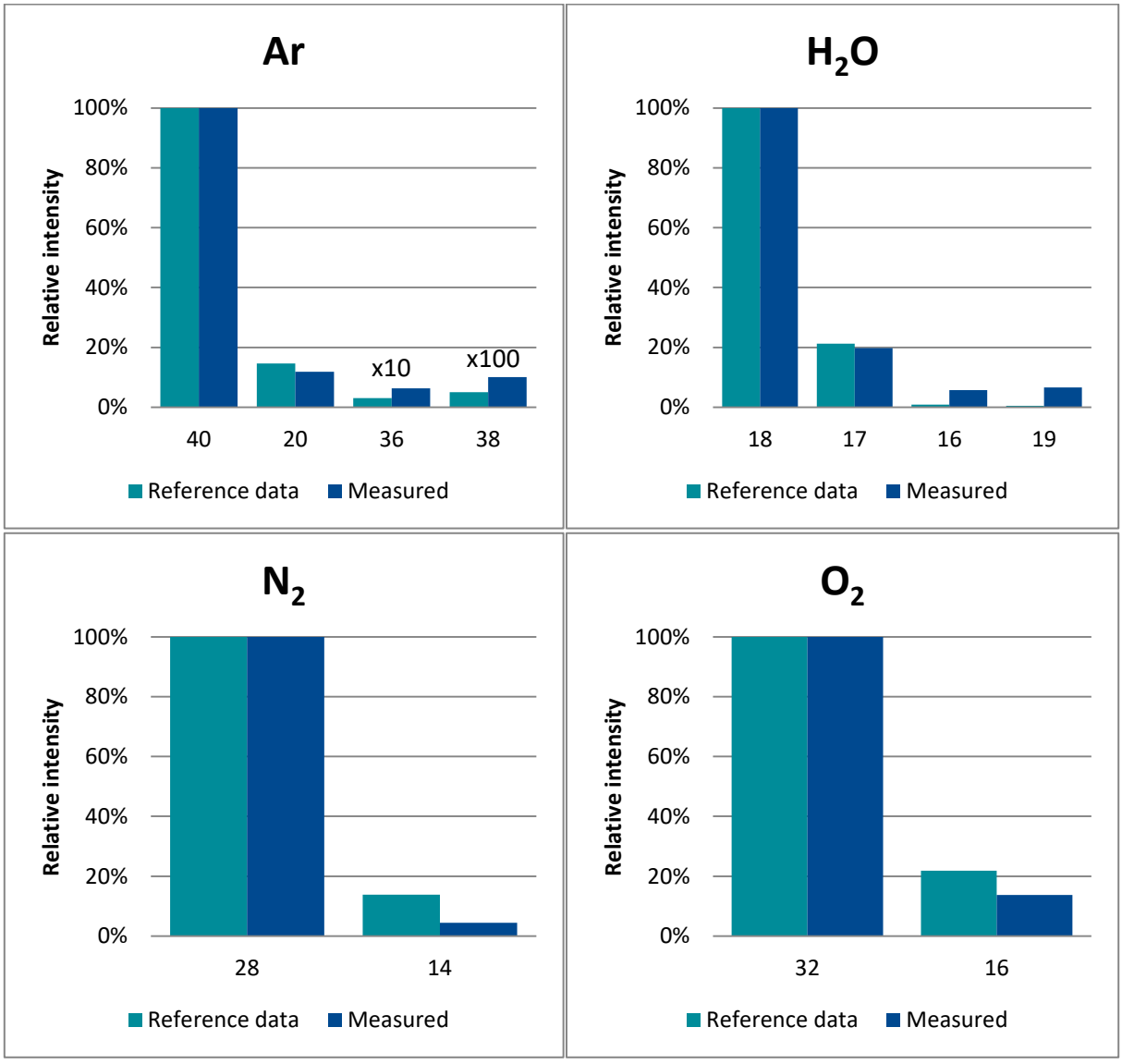

Figure 36 – Correlation between expected species' peaks and measured peaks' relative ion intensity. Small values are multiplied by a factor of 10 or 100.

Figures 37 – 41 show the significant and assigned mass numbers for different species as a function of temperature during heating up to 1160 °C. There was a slight shift of the peak intensity from integer mass numbers due to possible calibration error of the mass spectrometer. Therefore, the mass numbers were adjusted to the closest integer for clarity.

Also, temperature fluctuations in the furnace explain the inconsistent shape of some curves. All species show a stable or decreasing ion intensity with increasing temperature indicating that no gaseous elements where released from the virgin microspheres. However, a small peak in intensity is visible for water at 177 °C.

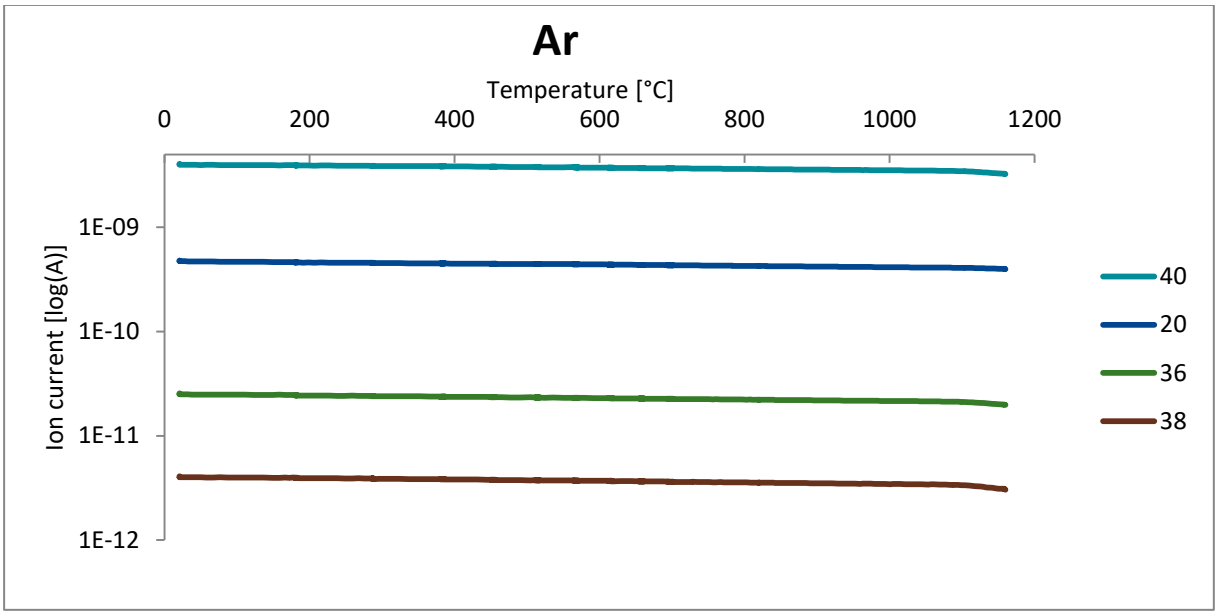

Figure 37 – Change in intensity with temperature for argon's characteristic peaks.

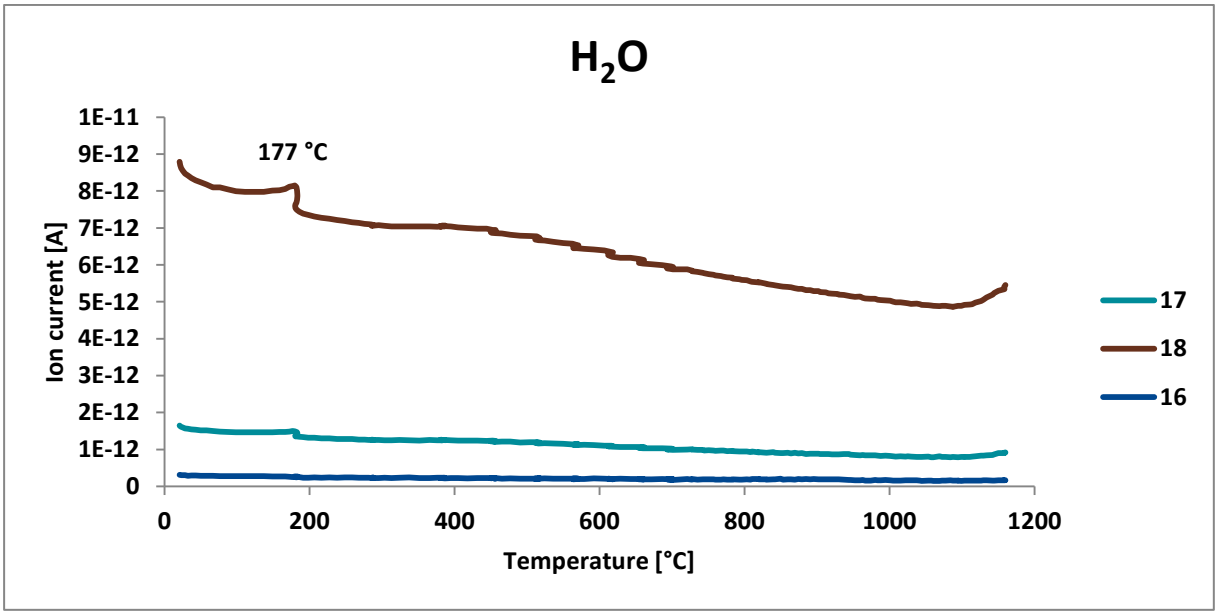

Figure 38 – Change in intensity with temperature for water's characteristic peaks. The data point shows the temperature at the peak.

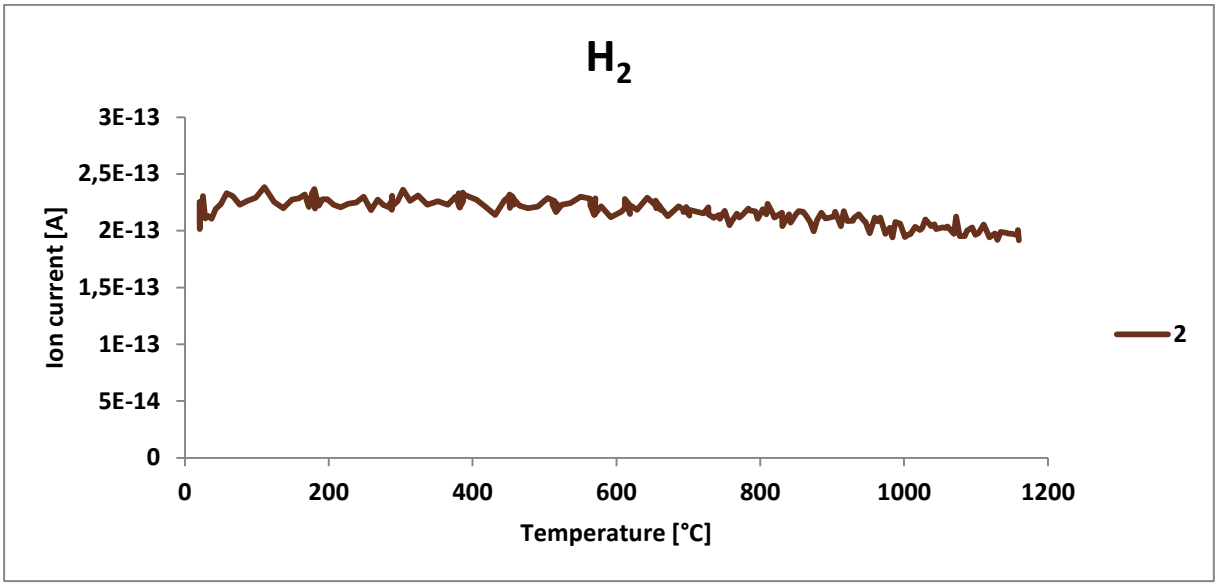

Figure 39 – Change in intensity with temperature for hydrogen's characteristic peaks.

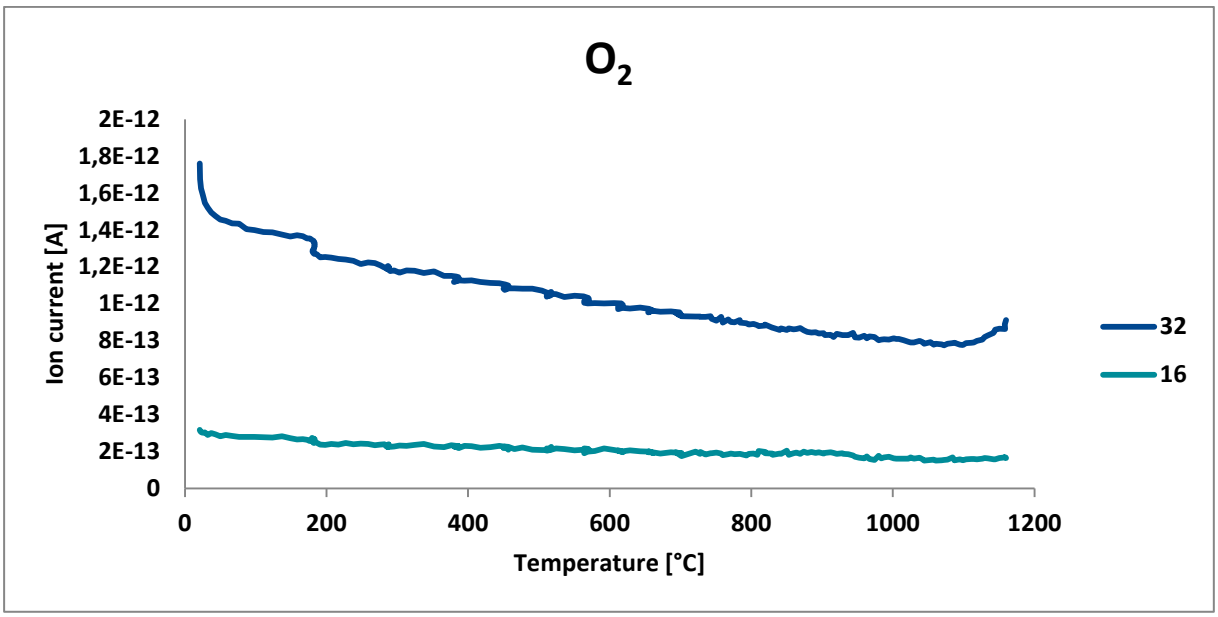

Figure 40 – Change in intensity with temperature for oxygen's characteristic peaks.

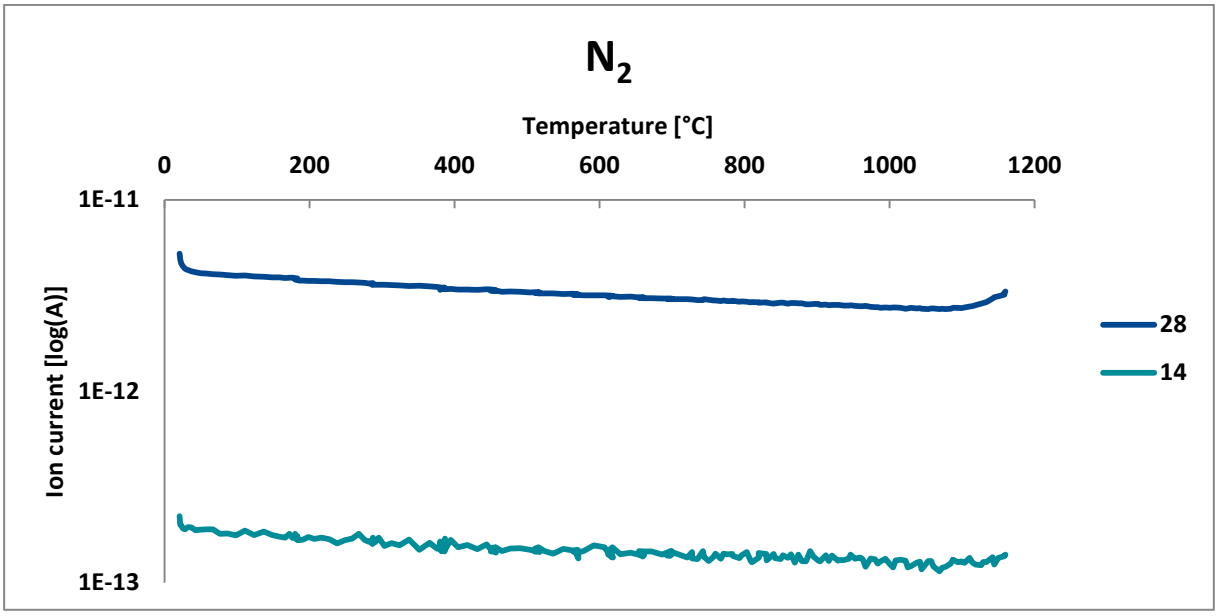

Figure 41 – Change in intensity with temperature for nitrogen's characteristic peaks.

4.3.3 Hydrogen storage capability

An investigation of the hydrogen storage capability was performed with the gained knowledge from the preliminary calculations. The recorded fill cycle is shown in Figure 42. The target pressure of 1000 bar was not reached because of an insufficient amount of gas in the connected gas bottle resulting in a maximum pressure of 675 bar. It was furthermore not possible to evacuate the gas at 300 °C and there was no additional gas to maintain the maximum pressure during the decent in temperature. Therefore, a decrease in pressure occurred until it was safe to quickly evacuate the gas at 100 °C.

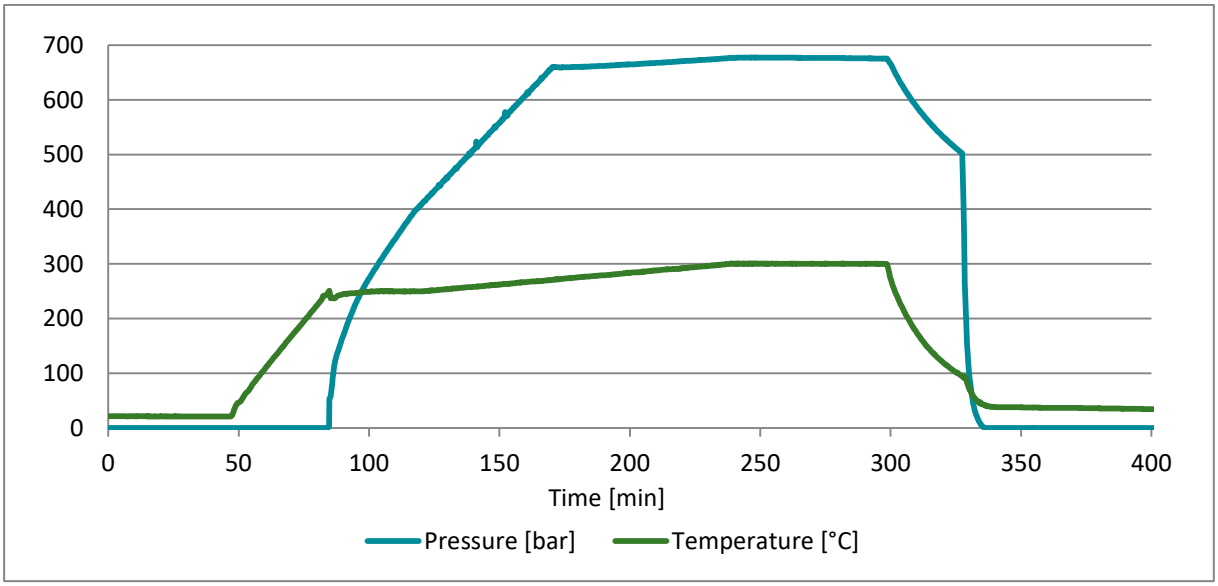

Figure 42 – Recorded fill cycle from the attempt to fill microspheres with hydrogen gas.

Microspheres that were intact and therefore filled with hydrogen were separated from broken ones by floatation in ethanol. Figure 43 show the state of the separation process at certain point after the initial stirring. No significant change was noticed between 3 and 17 hours and

it was decided that the floated microspheres would be skimmed off, dried and weighted. The weights were 37.50 g for the skimmed off microspheres and 17.43 g for the sedimented and suspended microspheres.

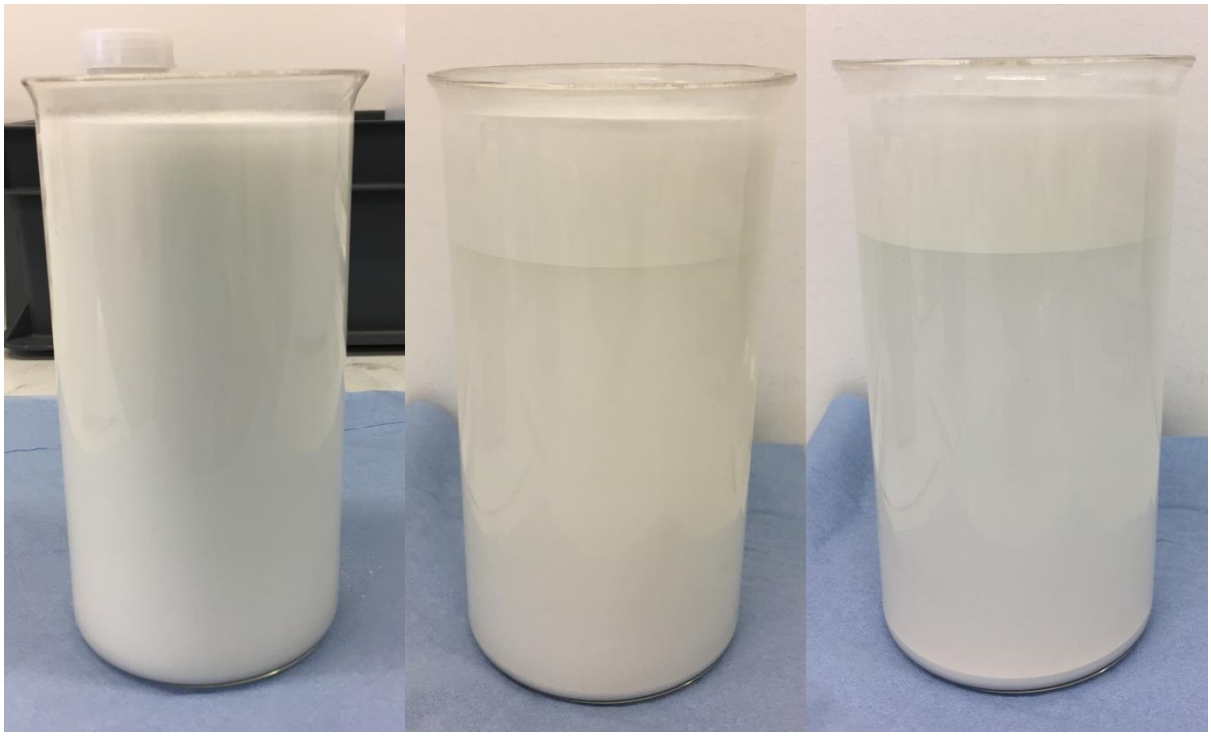

Figure 43 – Separation of filled and broken microspheres in ethanol after 0 h (left), 3 h (middle) and 17 h (right).

Once the skimmed off microspheres had been dried they were heated while measuring released gaseous species with a mass spectrometer. Figure 44 shows the detected species and their characteristic peaks' correlation with reference data. The carrier gas, nitrogen, and water agrees well while argon was detected in such small amounts that only the precursor m40 and second, m20, fragment could be distinguished from the background noise. Oxygen and water share m16 and both thus contribute to the same mass number, explaining why m16 is too high for both water and oxygen. Some concerns existed whether the ethanol used to separate broken microspheres was not fully evaporated which could contaminate the samples. However, no peaks of ethanol or any of its characteristic molecular fragments were detected.

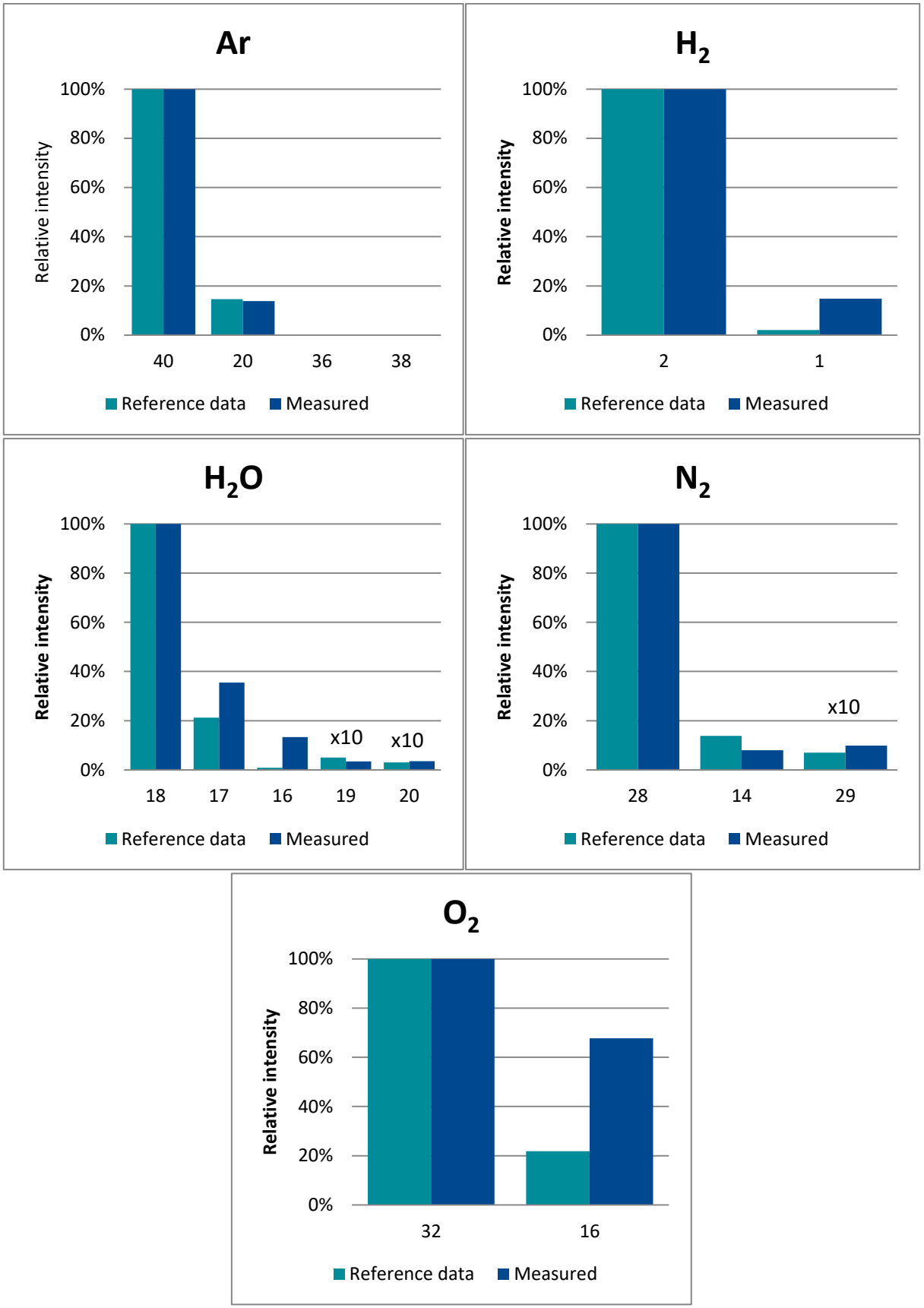

Figure 44 – Correlation between expected species' peaks and measured peaks' relative ion intensity. Small values are multiplied by a factor of 10.

Hydrogen only occurs in two peaks and the correlation is not conclusive. However, Figure 46 clearly shows that hydrogen is released between approximately 200 – 500 °C and that m1 cannot be assigned to hydrogen gas since its ion intensity does not follow m2. The significant but unassigned mass numbers were m15, m30, m42 and m44. They all showed no peak in ion intensity with increasing temperature. The change in ion intensity for each detected species with temperature is shown in Figure 45 – 48. Over all, all intensities show a decreasing trend except the characteristic precursor peak for H_2, m2, after both 4 and 73 days, see Figure 46. After 73 days, hydrogen's peak remained while the other species showed similar behaviour as in the first measurement. They were thus not included. There was no measurable mass loss of the sample before and after heating.

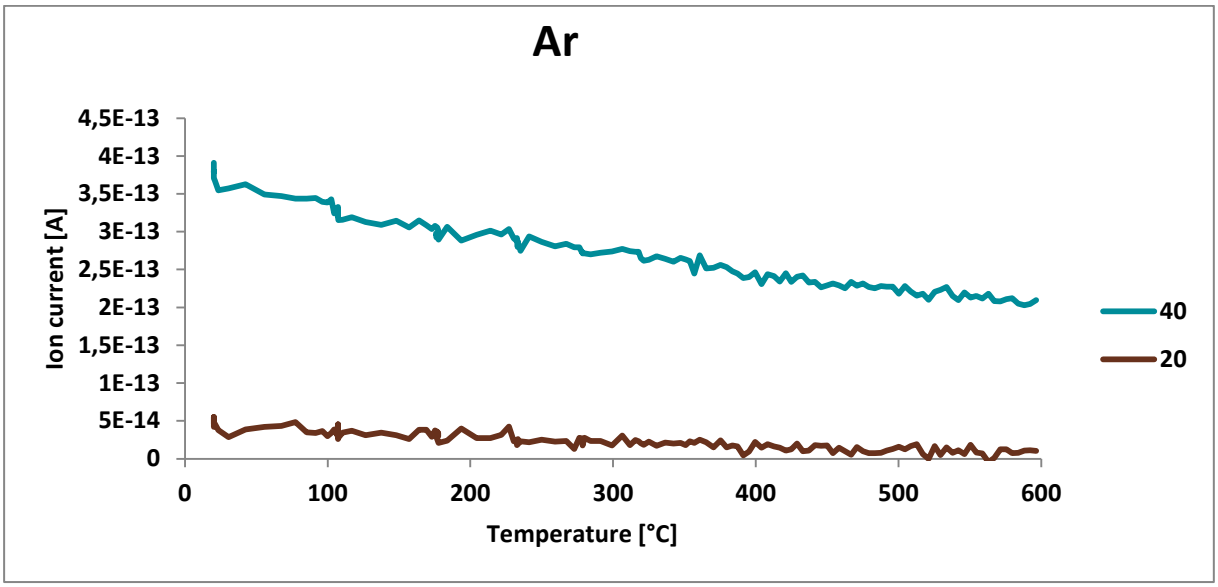

Figure 45 – Change in intensity with temperature for argon's characteristic peaks.

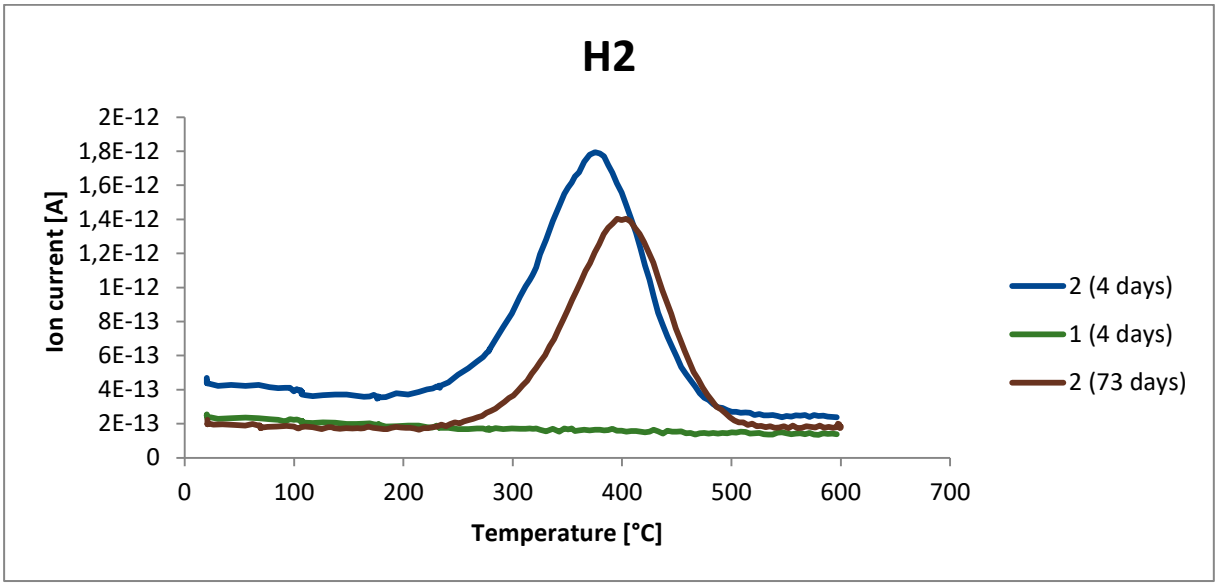

Figure 46 – Change in intensity with temperature for hydrogen's characteristic peaks at the first (4 days) and second (73 days) measurement.

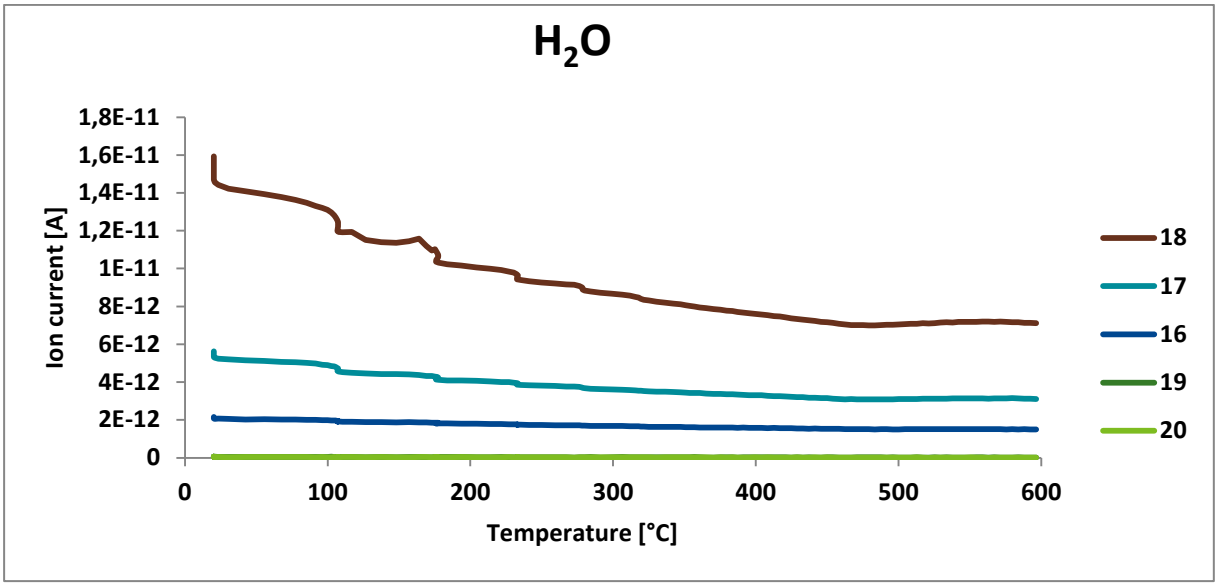

Figure 47 – Change in intensity with temperature for water's characteristic peaks.

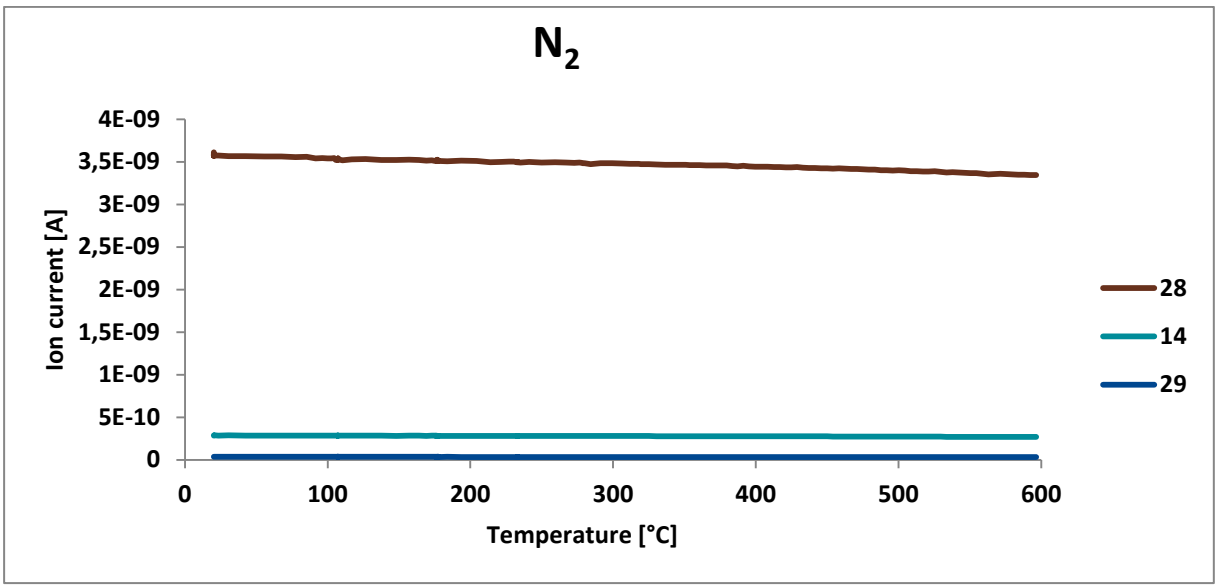

Figure 48 – Change in intensity with temperature for nitrogen's characteristic peaks.

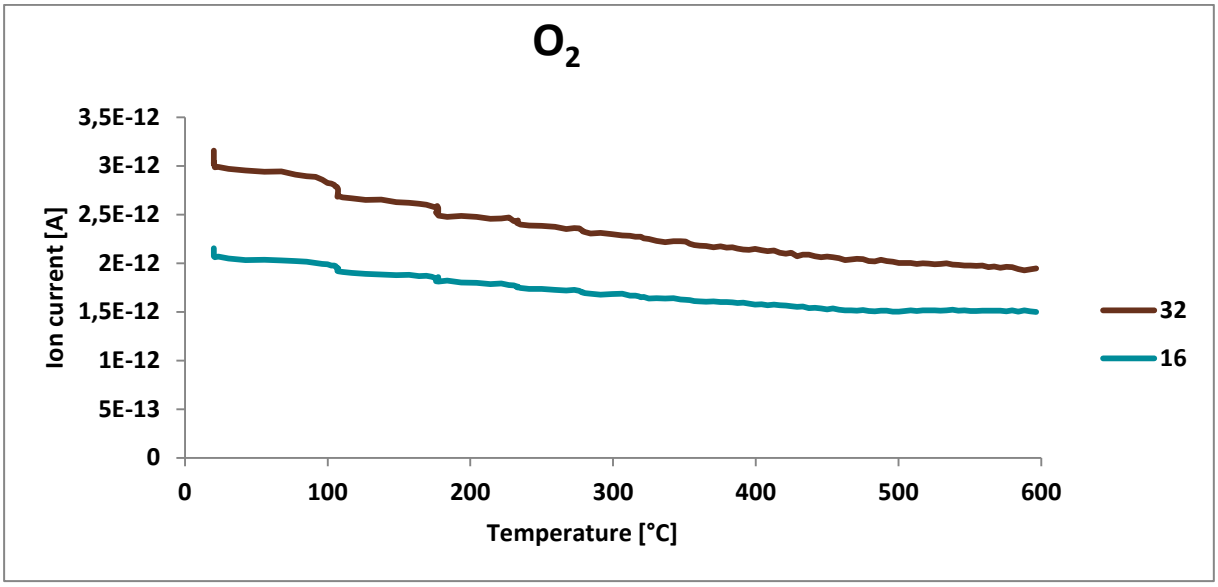

Figure 49 – Change in intensity with temperature for oxygen's characteristic peaks.

From the data in Figures 46 and 27 the area under the H_2 curve could be calculated using three variants of a Riemann sum, see Table 14. The relation between the areas and amount of mol H_2 released per mol ammonia borane gives the amount of hydrogen stored in the microspheres:

$$w_{H_2}^{MS} = \frac{n_{H_2}^{MS} * M_{H_2}}{m_{MS}} * 100 = n_{H_2}^{AB} \frac{A_{MS}}{A_{AB}} \frac{M_{H_2}}{m_{MS}} * 100 \ \ [wt\%] \qquad (28)$$

With $m_{MS} = 0.98\ g$ and $M_{H_2} = 2.016\ g/mol$. The added amount of ammonia borane is known from Table 5 and the literature value of 2.2 mol H_2 per mol ammonia borane gives $n_{H_2}^{AB} = 0.0064\ mol$.

Table 14 – Calculated area under the hydrogen curve with three different methods of calculating a Riemann sum.

Riemann sum method	Ammonia borane	Microsphere, 4 days	Microsphere, 73 days
Left	1.43E-09	1.80E-10	1.37E-10
Right	1.67E-09	1.82E-10	1.37E-10
Trapezoid	1.55E-09	1.81E-10	1.37E-10

Depending on the method of Riemann sum used different storage capacities are obtained. Therefore, the average of all 9 different combinations of the areas results in a storage capacity of 0.1548 wt% after 4 days and 0.1148 wt% after 73 days.

4.4 Microstructural analysis

Common inclusion morphology and composition from the top of each capsule, closest to the hydrogen carriers, is shown in the following paragraphs. The low-alloy steel was heat treated before SEM analysis while the tool steel was not.

4.4.1 Low-alloy steel – Reference

Figure 50 show the microstructure of the reference capsule containing the low-alloy steel. No clear PPBs could be seen and common inclusions were around 1 µm in size consisting of both oxides and sulphides.

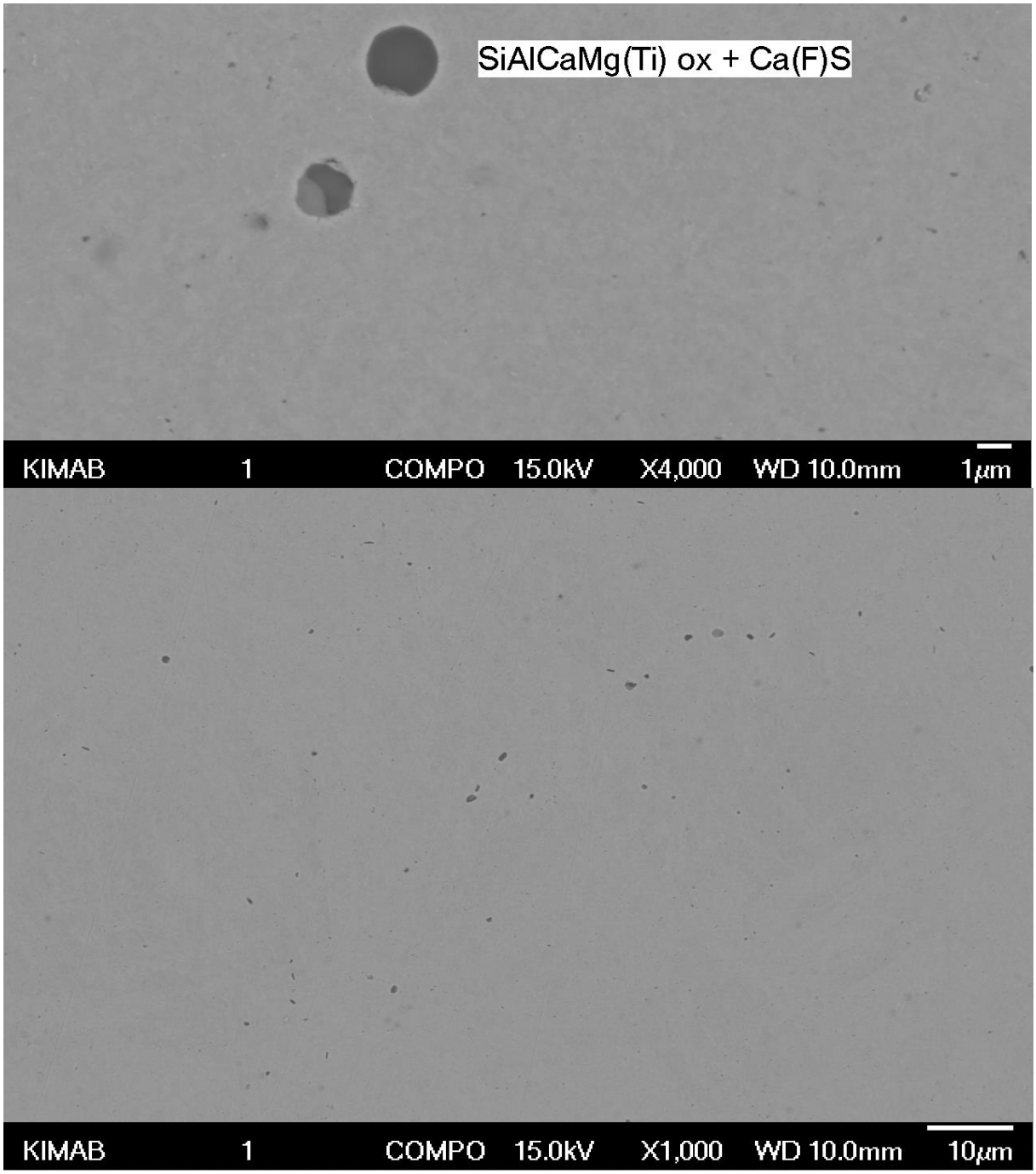

Figure 50 – Common oxide and sulphide (top) and overview of the microstructure (bottom)

4.4.2 Low-alloy steel – Ammonia Borane

Large unknown porosities could be found scattered throughout the material around 10 µm in size. These areas had a high iron and oxygen content but also higher carbon content compared to the bulk composition and other inclusions. No boron or nitrogen could be detected in these areas. Otherwise, similar oxides and sulphides as in the reference can also be found.

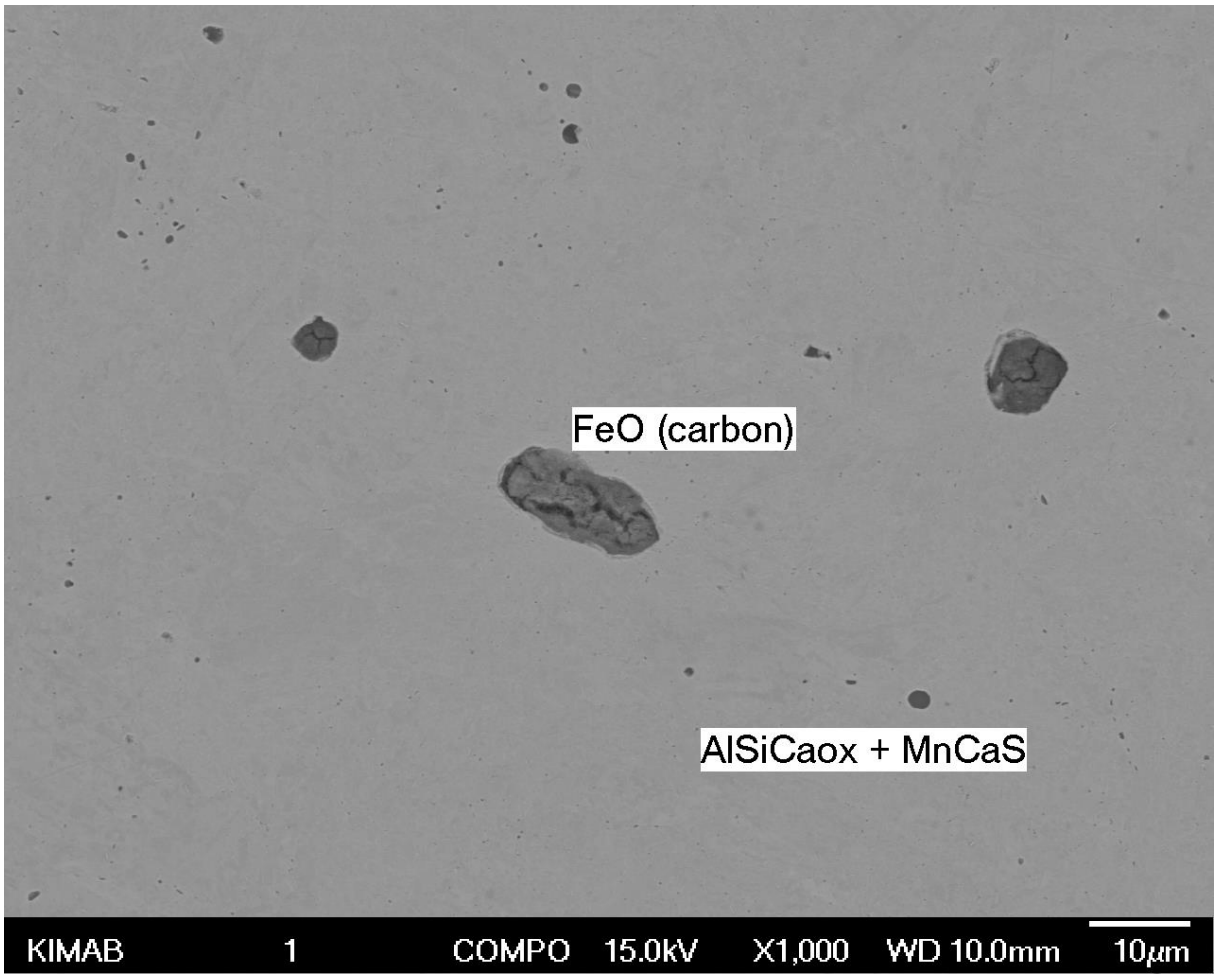

Figure 51 – Example area displaying 3 larger cavities and multiple smaller oxides and sulphides.

4.4.3 Low-alloy steel – Microspheres

Larger inclusions containing boron and nitrogen were determined to be microspheres, see Figure 52. A few inclusions, larger than any individual microsphere, were also found containing boron and nitrogen, see Figure 53. The size indicates that it is a cluster of several microspheres. Smaller inclusions were similar to the other two low-alloy steel capsules regarding size and composition.

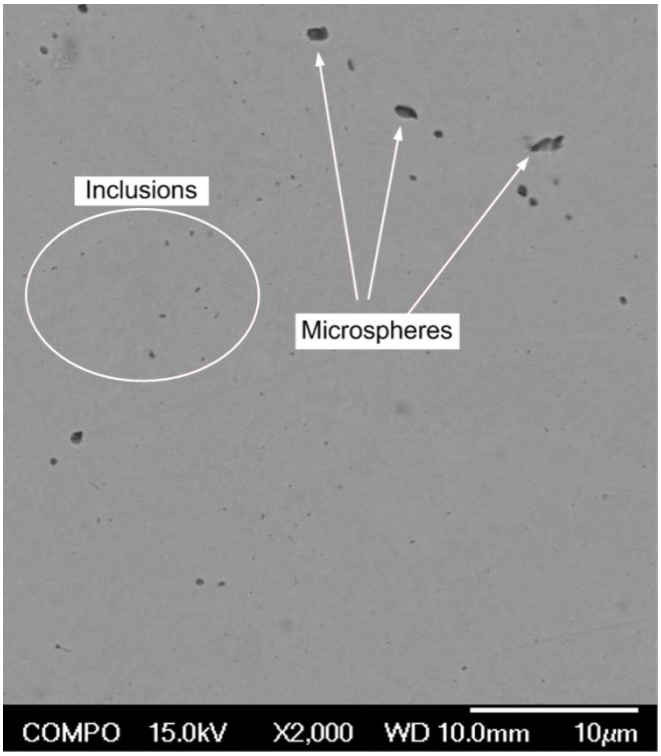

Figure 52 – Areas containing boron and nitrogen (microspheres) and smaller inclusions such as MnS and SiAlNi-oxide.

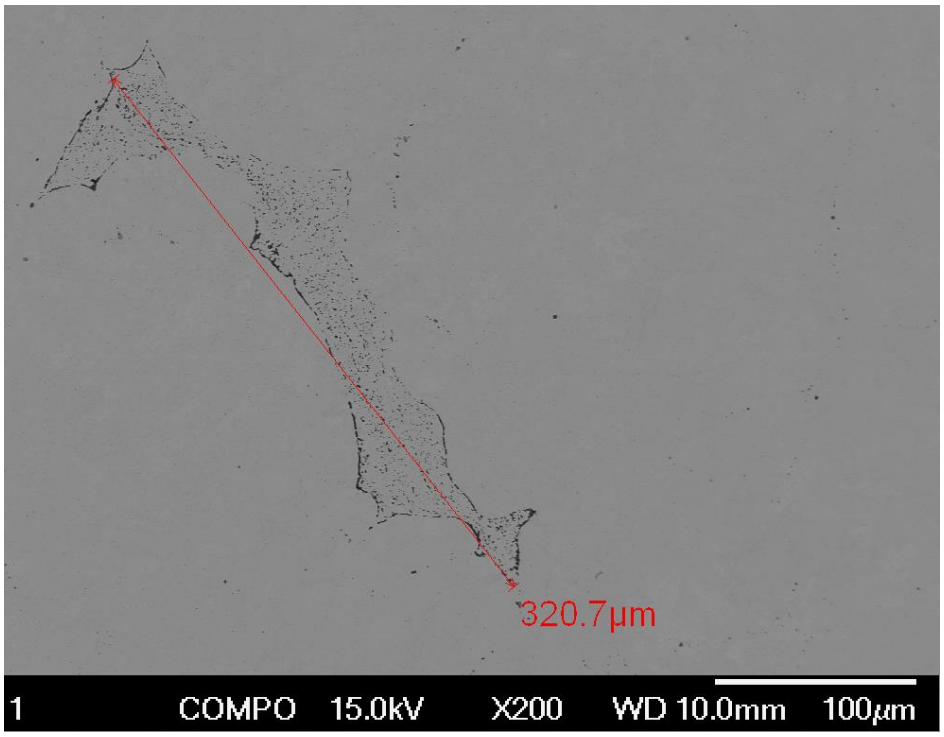

Figure 53 – Area containing B, N, O and Ca determined to be a cluster of microspheres.

4.4.4 Tool steel – Reference

Figure 54 show the microstructure of the reference capsule containing the tool steel. PPBs could be seen consisting of oxides of Mo, Cr and Mn less than 1 µm in size. Larger inclusions

were randomly distributed throughout the material and were around 1 µm in size consisting of both oxides and sulphides as seen in figure 55. Much smaller carbides containing Cr, V and Mo were also randomly distributed.

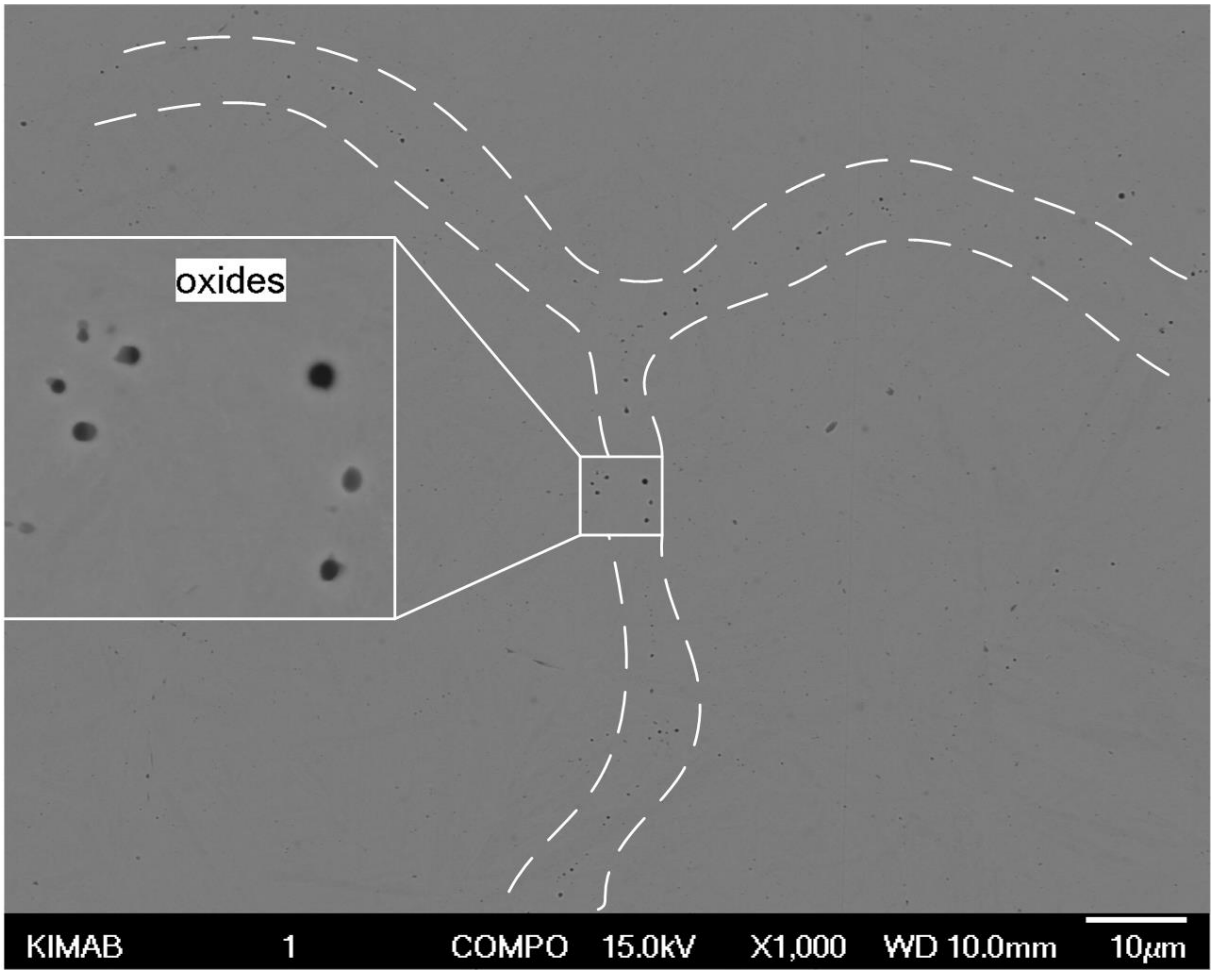

Figure 54 – Oxides (Mo, Cr and Mn) mainly distributed in sequence between the dashed lines.

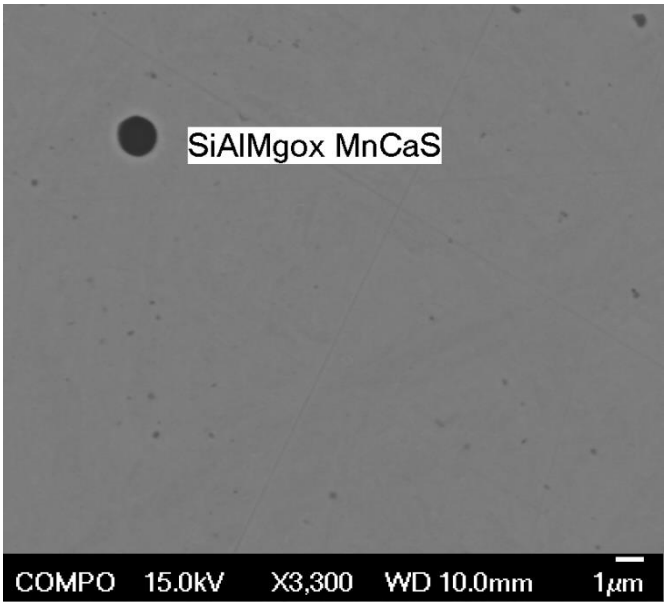

Figure 55 – Larger inclusion surrounded by smaller carbides containing Cr, V and Mo.

4.4.5 Tool steel – Ammonia Borane

Areas rich in boron and nitrogen were found in the center of the capsule. In Figure 56, these areas are surrounding the metal powder particles while closer to the capsule wall, see Figure 57, there is instead some pores. These pores contain no boron and significantly less nitrogen but also carbon which is absent in the darker areas in the center of the capsule. They resemble the pores found in the low-alloy steel regarding composition and appearance.

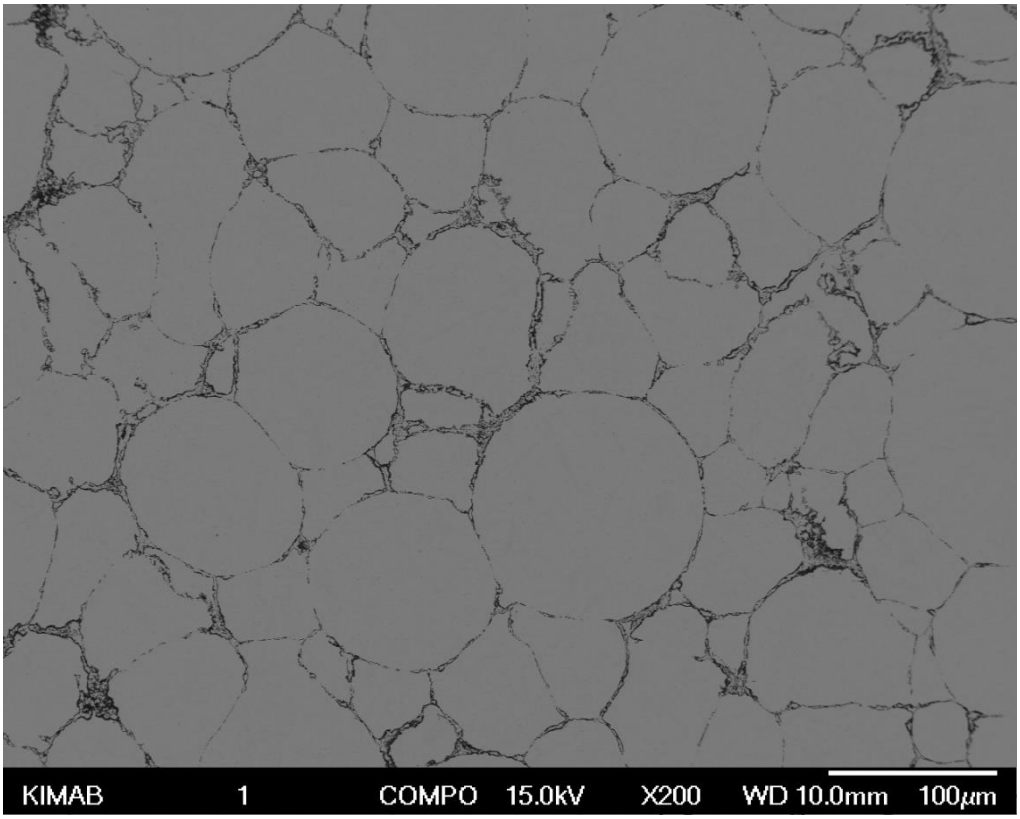

Figure 56 – Microstructure in the center of the capsule, directly below the fill pipe.

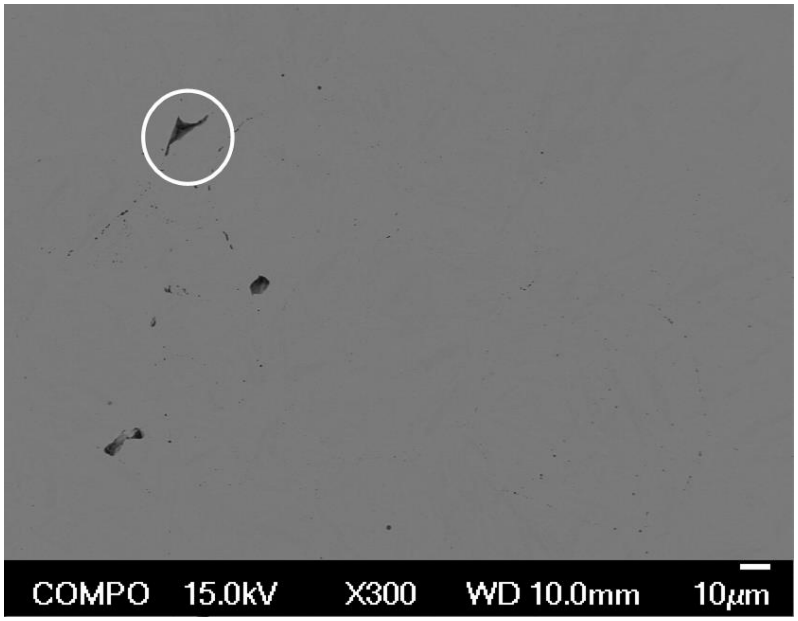

Figure 57 – Microstructure close to the capsule wall. One of the pores containing elevated carbon contents is encircled.

4.4.6 Tool steel – Microspheres

Inclusions lined in sequence were found in the center of the capsule, see Figure 58. Closer to the capsule wall, disperse inclusions were found such as the one displayed in Figure 59.

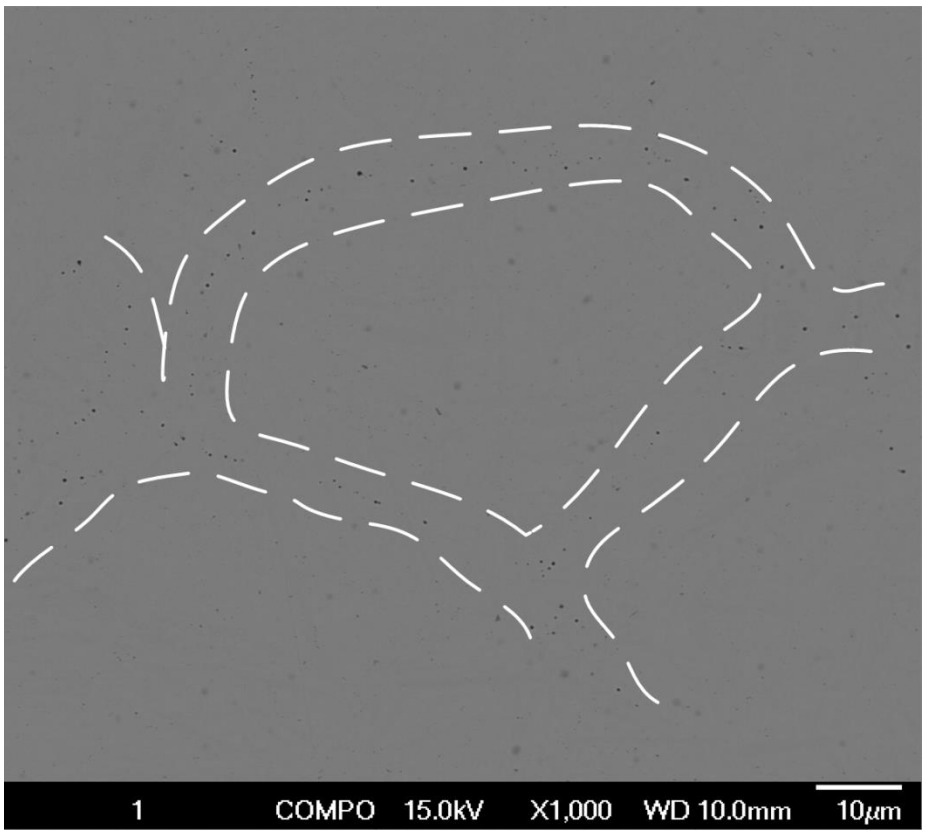

Figure 58 – Oxides distributed in sequence between the dashed lines.

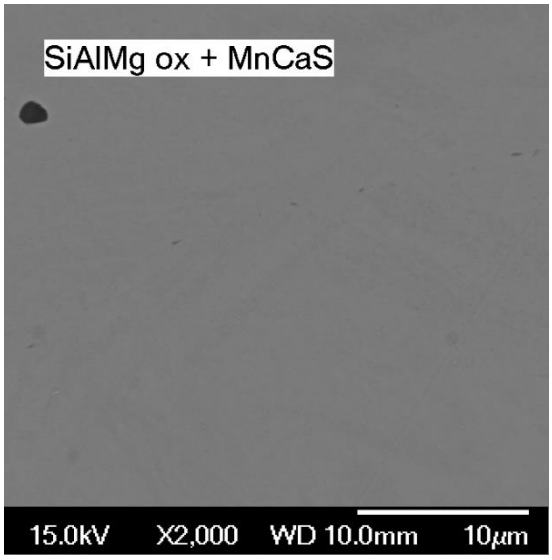

Figure 59 – Inclusion close to the capsule wall.

4.4.7 Inclusion size distribution

The following plots show the maximum Feret diameter of measured inclusions in 0.05 µm intervals. Obvious large inclusions caused by the additives, for instance large clusters of microspheres (Figure 53) or pores (Figure 57), were excluded in the measurement since the additives effect on surface and bulk oxides were of interest. Figure 60 shows that both tool steel capsules containing hydrogen carriers exhibit slightly larger inclusion compared to the reference (which reaches 100 % sooner). Figure 61 shows a similar trend for the low-alloy steel.

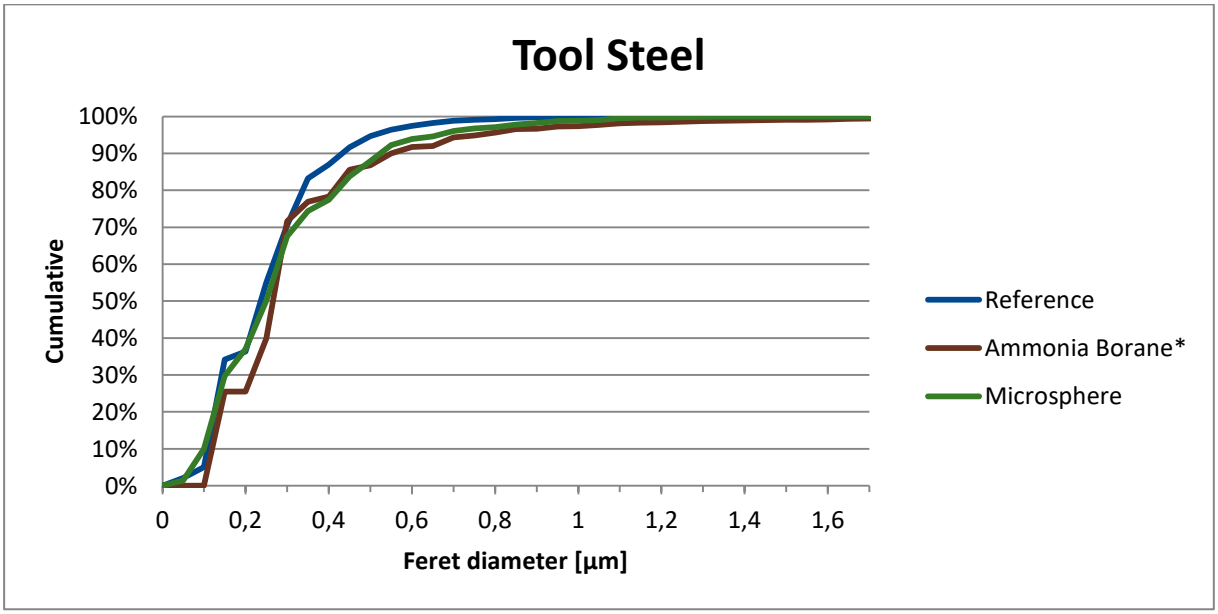

*Figure 60 – Cumulative percentages of inclusion sizes for all 3 of the tool steel capsules. *Large pores as well as the contaminated area in the center were excluded from the measurement.*

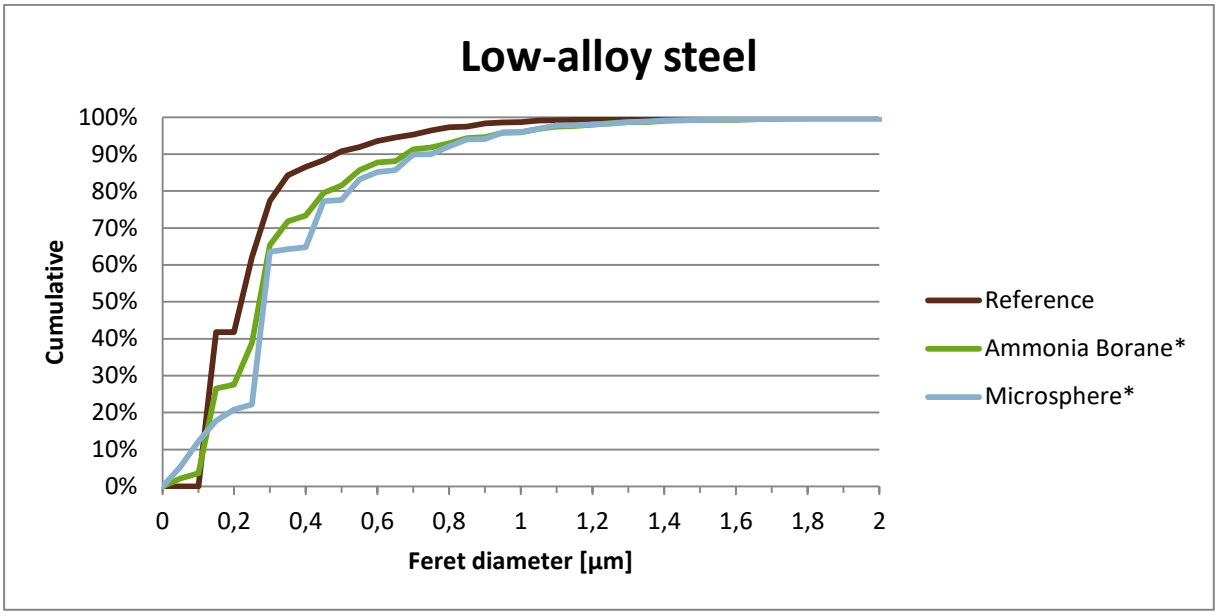

*Figure 61 – Cumulative percentages of inclusion sizes for all 3 of the low-alloy steel capsules. *Large clusters of microspheres and pores are excluded from the measurements.*

4.5 Oxide reduction and impact toughness

4.5.1 Low-alloy steel

Figure 62 shows the results of the chemical analysis and impact toughness for the low-alloy steel. Note that the radial chemical samples at each vertical position not necessarily correspond to the impact testing bar above or below. They were however cut at the same distance from the capsule wall, i.e. 5 mm.

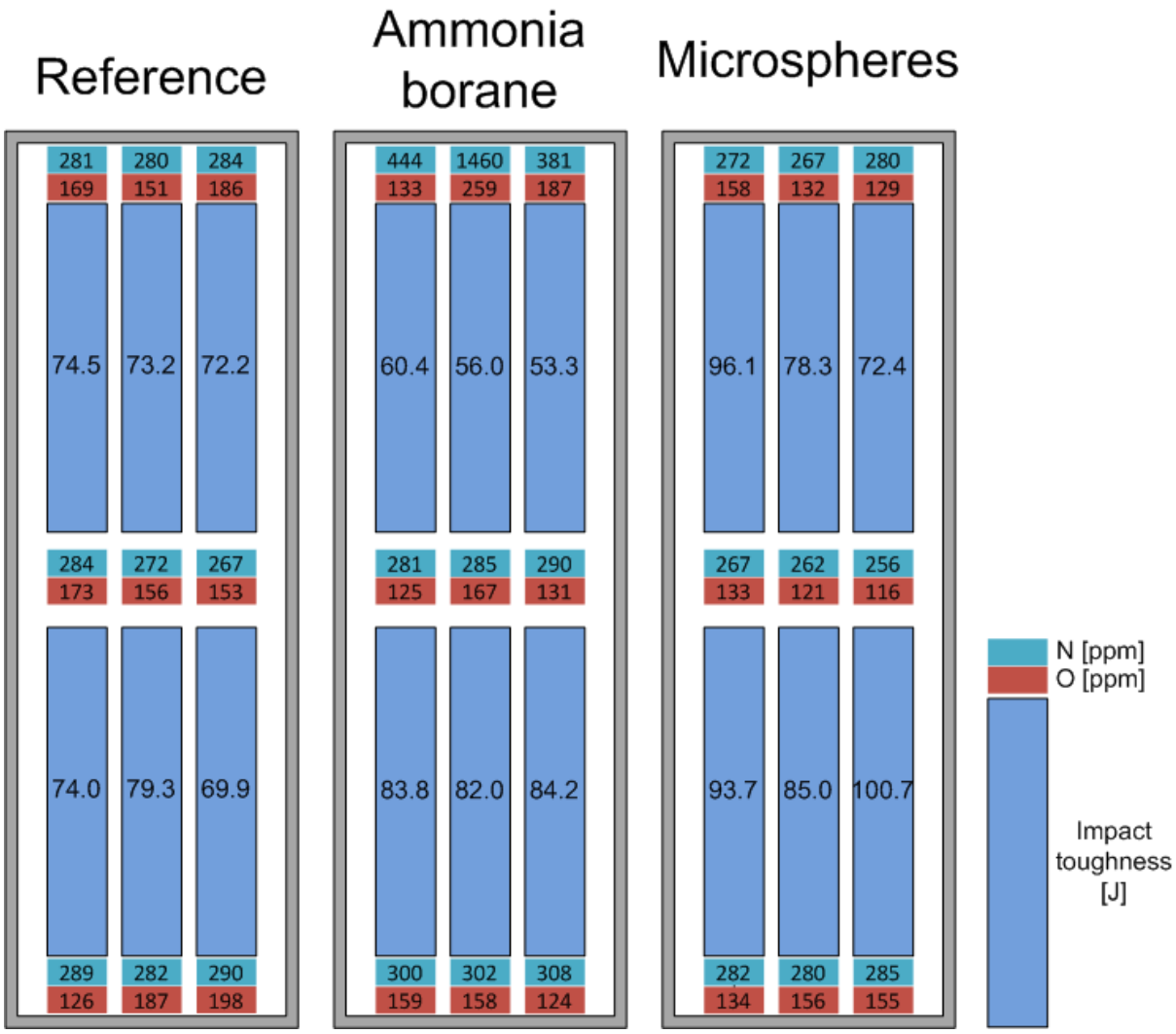

Figure 62 – Impact toughness and chemical analysis of the three capsules containing low-alloy steel. From the left: LAS2R, LAS2AB, LAS2MS.

Impact toughness is rather stable for all positions in the reference capsule, with a standard deviation of 2.85, see Table 15. The two capsules containing hydrogen have a larger standard deviation of 13.56 and 10.04 for LAS2AB and LAS2MS respectively. A significant decrease in impact toughness can be seen in the three top impact bars in LAS2AB compared to LAS2R. Furthermore, impact toughness was slightly increased in the bottom positions. Impact toughness was in general increased for LAS2MS, especially in the bottom positions. However, the standard deviation in each vertical position is greater for LAS2MS than the other two capsules, 10.1 and 6.4 in the top and bottom position respectively. The other two capsules have standard deviations below 4 at each vertical position.

Table 15 – Average impact toughness of the low-alloy steel for all, top and bottom positions.

	LAS2R	LAS2AB	LAS2MS
Average [J]	73.9	70.0	87.7
Std. dev.	2.855	13.559	10.044
Average - top	73.3	56.6	82.3
Std. dev.	0.9	2.9	10.1
Average - bottom	74.4	83.3	93.1
Std. dev.	3.8	1.0	6.4

No significant decrease in oxygen content was noticed in LAS2AB, instead an increase occurred at the top along with a drastic increase in nitrogen content. Nitrogen content was otherwise comparable with the other capsules in the middle and bottom positions. Oxygen content in LAS2MS was similar to the other two capsules in the bottom position. However, it was decreased by at least one standard deviation in the middle and top positions. Nitrogen content was reduced below the contents in the virgin powder while oxygen was not. There was no sign of a radial gradient in either nitrogen or oxygen content and the major differences were thus vertical.

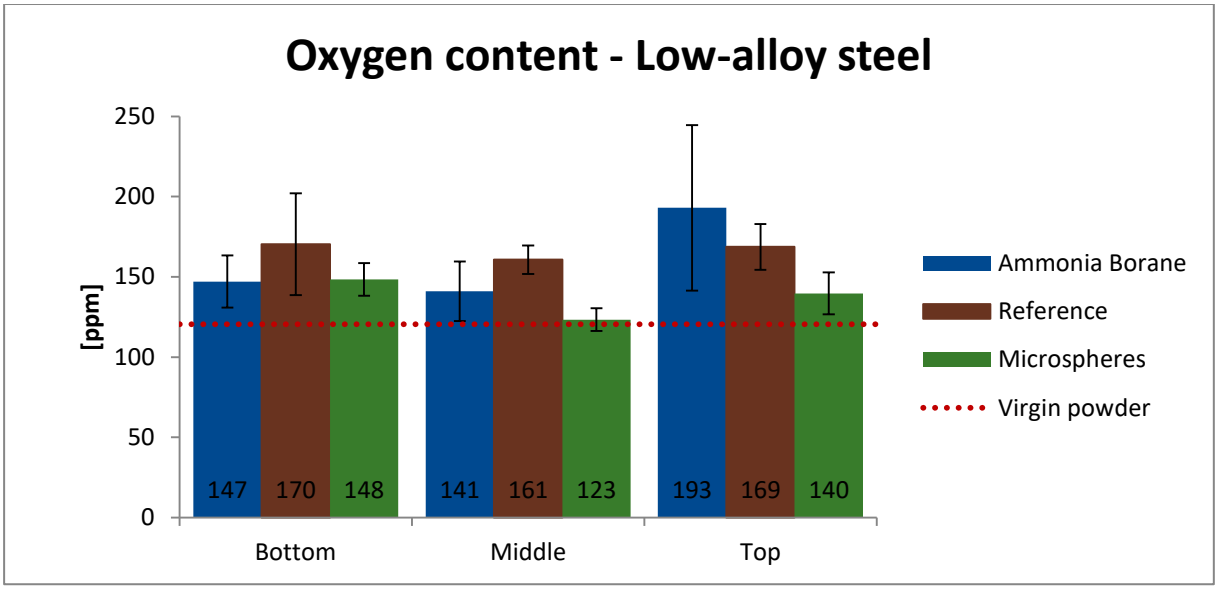

Figure 63 – Oxygen content in the low-alloy steel for the three vertical positions.

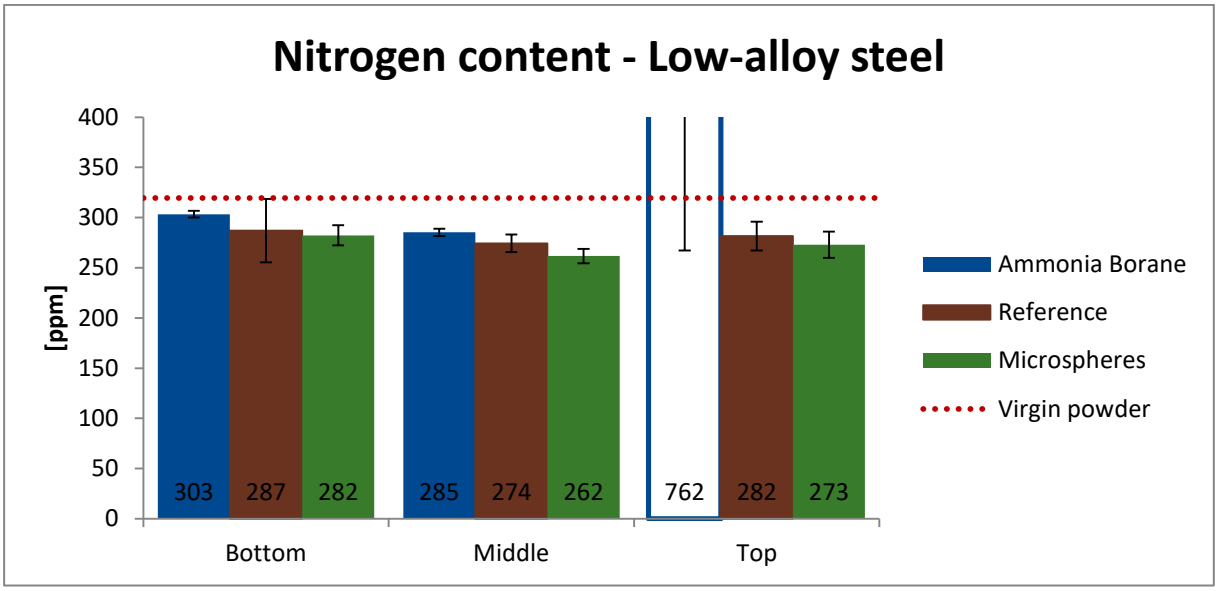

Figure 64 – Nitrogen content in the low-alloy steel for the three vertical positions. The large value for LAS2AB in the top is cut for better comparison of the other values.

4.5.2 Tool steel

Due to time constraints, impact toughness for the tool steel is not included. Nitrogen content was lowered compared to the virgin powder for TS1R and TS1MS but not TS1AB which had a large standard deviation in the top. Oxygen content also varied greatly in the top of TS1AB but was more than one standard deviation lower in the bottom position compared to the reference. The same was true for the bottom of TS1MS while the top instead was more than one standard deviation above the reference. No sign of a radial gradient in nitrogen or oxygen content was found.

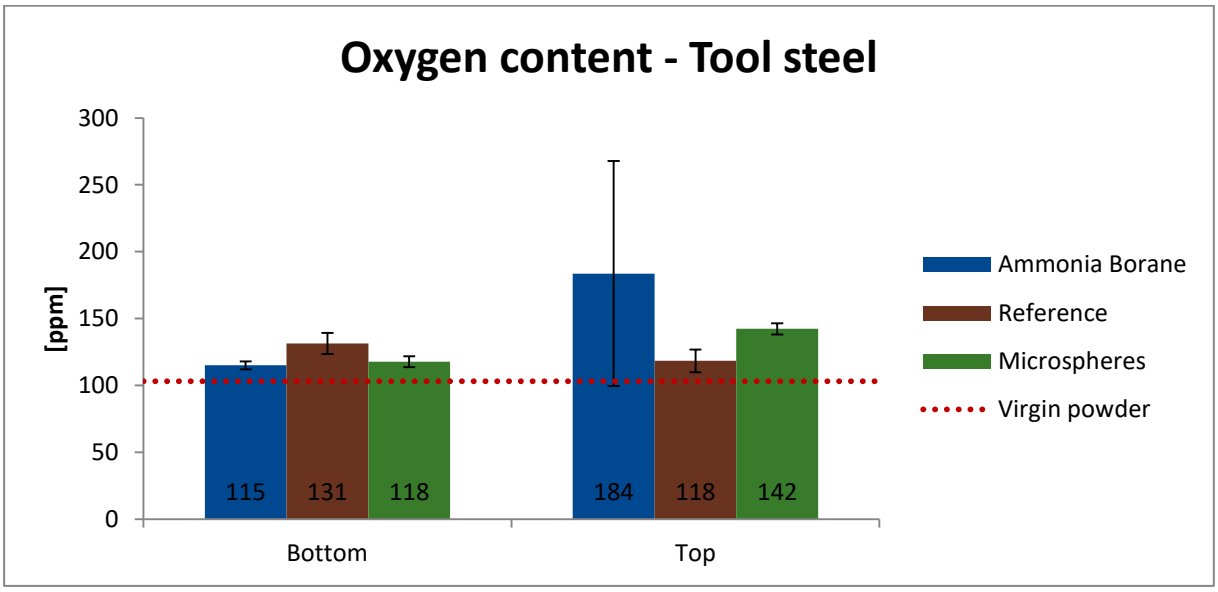

Figure 65 – Oxygen content in the tool steel for the two vertical positions.

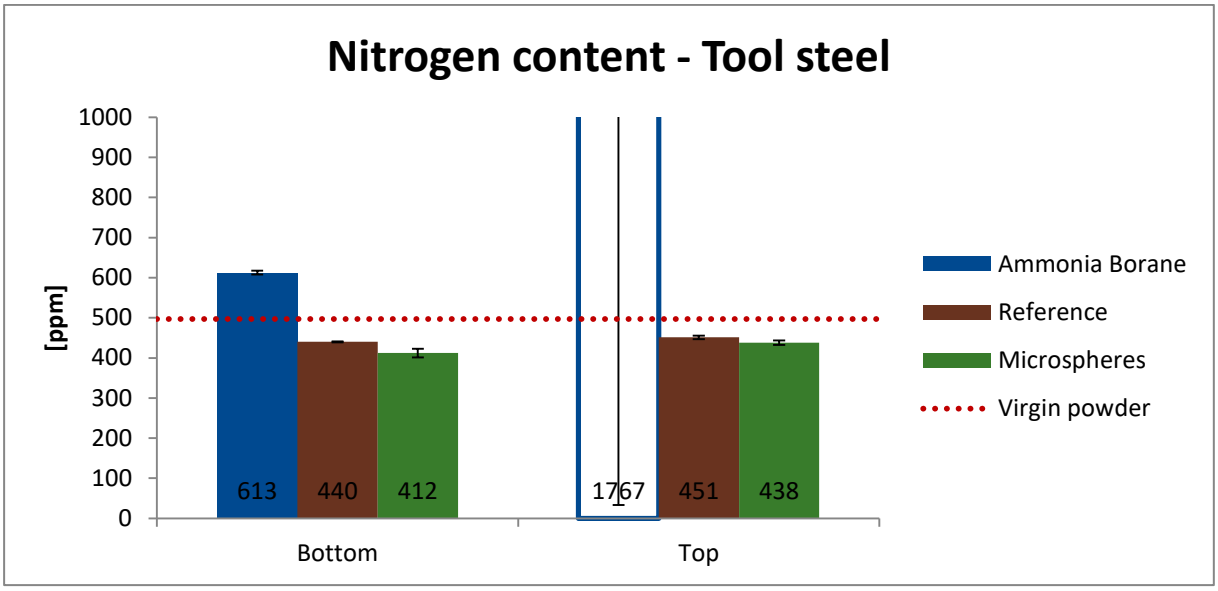

Figure 66 – Nitrogen content in the tool steel for the two vertical positions. The large value for TS1AB in the top is cut for better comparison of the other values.

5 Discussion

5.1 Decomposition analysis of ammonia borane

The water and ammonia peaks exhibited similar behaviour with an increase in intensity around 150 °C in the peaks they share, see Figure 29 and Figure 30. One possibility is that the increase in water intensity is from evaporation of adsorbed water present in the sample and furnace. Similar peaks at these temperatures could also be seen for both measurements of the microspheres, see especially Figure 38 but also a slight peak in Figure 47. Another oddity is that the increase in intensities occurs along with the detection of ammonia borane's decomposition products. The water peak occurs in three different measurements of both ammonia borane and microspheres, at almost the same temperature. It is therefore most likely due to evaporation of adsorbed water from the equipment which just happens to co-occur with the decomposition of ammonia borane. Furthermore, because of the shared mass numbers, a raise in intensity due to evaporation of adsorbed water is probably not correlated with a release of ammonia. Thus, no significant amount of ammonia is released.

Borane (BH_3) was not detected as expected from the study by Babenko et al. as it quickly forms diborane which was indeed detected. [26] The mass spectrometer filament is placed far away from the hot-zone which gives species time to react or condense before being analysed. According to Baitalow et al., aminoborane (BH_2NH_2) converts into non-volatile oligomers at room temperature. [24] A slight white condensate could be seen on the inside of the transparent silica tube downstream from the sample, outside the box furnace. Whether this is aminoborane that had condensed on the colder silica tube outside the furnace is not known. This could be the reason for not detecting aminoborane, contradictory to what has been reported in literature. Baitalow et al. [24] had the detector closer to the sample and could thus detect unstable products such as aminoborane within subseconds of formation. Hydrogen was expected to be released in two steps which were not distinguishable at a 5 °C/min heating rate, in agreement with Baitalow et al. [24] In contrast to that study where borazine was only detected at the second step, two peaks were detected at around 140 °C and 170 °C. It is not

certain if this is accurate or caused by the experimental setup. For instance, the peak only consists of three data points which influence the peak's shape as measurements were performed 60 seconds apart. A better distinction would have been possible if a shorter scan time than 500 ms/amu was used. However, accurate detection of each atomic mass unit decreases with a decreased scan time. This is because the relative statistical error is inversely proportional to the square root of the number of detected ions per second. [59] Instead, the maximum mass to be scanned for could have been set to a lower value than 120 amu since the heaviest detected species was about 80 amu. Then, a shorter scan time would yield the same accuracy but measurements would be taken more frequently resulting in a more accurate distinguishing of the reaction mechanism.

The unassigned m30 and m32 are most likely lower intensity contaminants of the carrier gas due to similar profiles, see Figure 67. However, m41 show a rapid increase in intensity at 140 °C linking it to the decomposition of ammonia borane. Exactly which specie it is cannot be conclusively determined. Babenko et al. [26] could by using a H_2/NH_3 atmosphere detect triborane (B_3H_x) and aminodiborane (NB_2H_x) which both have their characteristic peak fragments around m40. By using an argon atmosphere in this work resulted in a strong and wide argon peak at m40, it could have obscured the detection of these species. The resolution of the scan was therefore not sufficient to fully distinguish these species. A better distinguishing would be possible if a measurement was performed under identical conditions but without the sample, creating a standard curve of the background gases. It could then be compared to the sample further distinguishing the origin of the gaseous species. Overall, the detected species and the confirmed release of hydrogen agree well with literature when considering the difference in experimental setup.

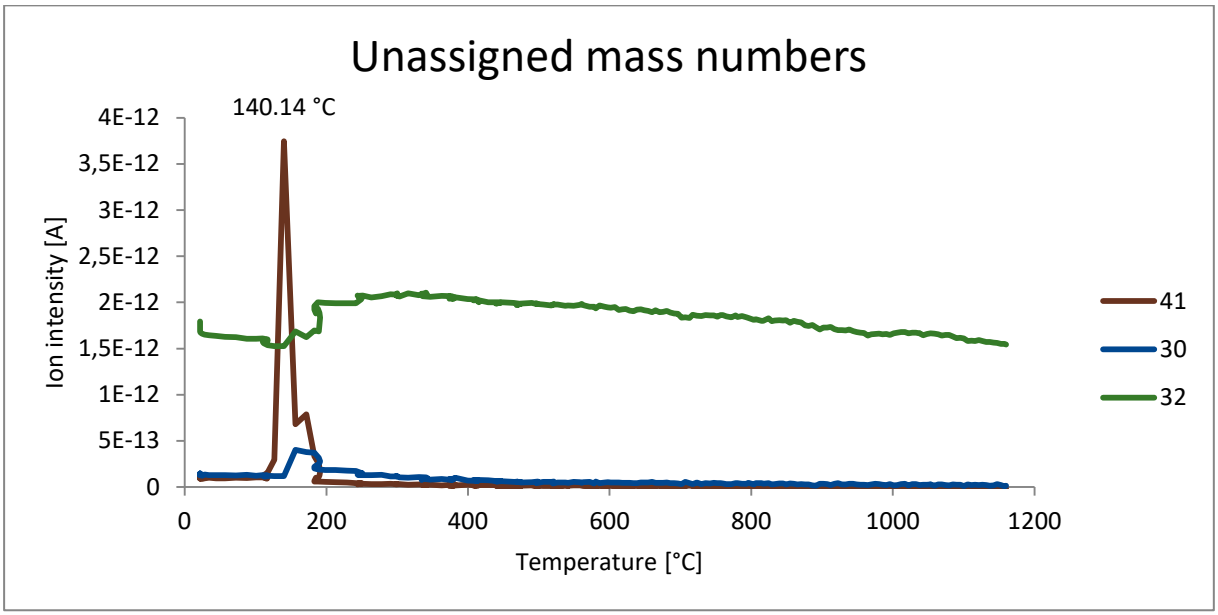

Figure 67 – The unassigned mass numbers' change in ion intensity with temperature.

5.2 Microspheres – fill experiment and calculations

5.2.1 Gas release from virgin and filled microspheres

A promising result was obtained from the gas analysis of the virgin microspheres as there was no detectable release of gaseous species. Especially important, no SO_2 was detected which together with the moisture from oxides reduced by hydrogen could cause corrosion of the

metal powders. [60] However, it may seem rather peculiar that no sulphur dioxide was detected even between the softening point of the glass (600 °C) and the peak temperature up to 1160 °C. During the SEM analysis, some pores were seen in the sintered samples, see Figure 68. Due to their round shape, they are most likely gas pores either originating from trapped atmospheric gases in the void between particles or the gas present in the internal void of the microspheres. It is difficult to determine which but nevertheless, no sulphur dioxide was detected so it was either trapped in these pores or there was such a miniscule amount inside the microsphere voids that it could not be detected. The detection limit of SO_2 in Ar is 2 ppm for the mass spectrometer, so the amount of SO_2 could be less than 2 ppm. However, the important point is that microspheres do not seem to release any potential harmful gaseous species that can contaminate the metal powder or obstruct reduction reactions.

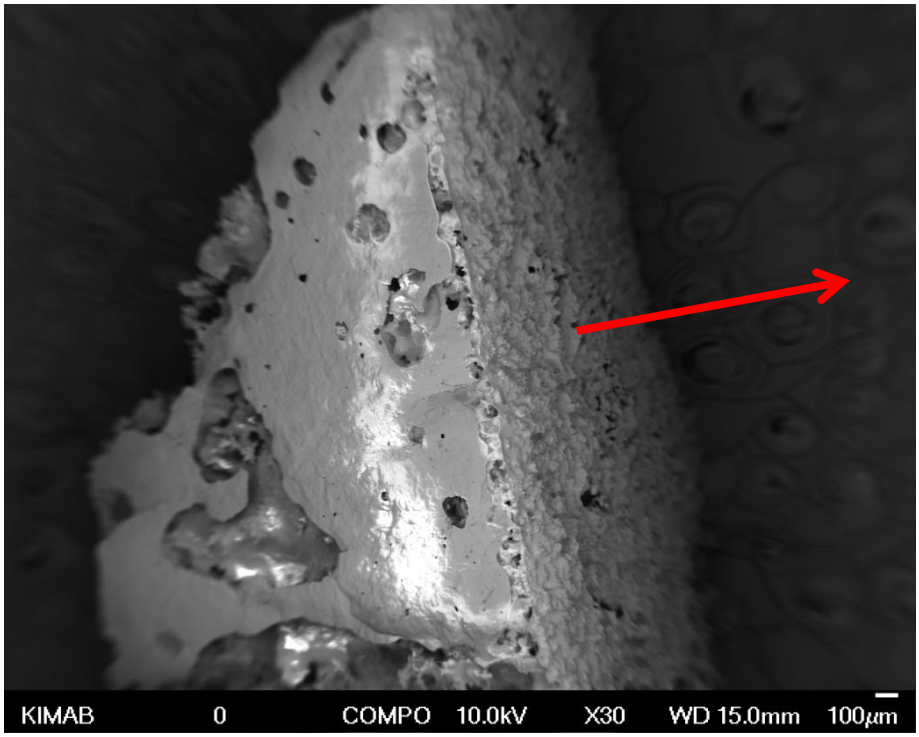

Figure 68 – Microspheres after heating to 1160 °C. Arrow is orthogonal to the upper surface of the sample in the furnace.

Additional evidence that no gaseous species was released emerged during the gas analysis of the filled microspheres. The fast permeating hydrogen emerged from the microspheres in sufficient amounts above 200 °C as shown in Figure 46. It is highly unlikely that a slower permeating, larger molecule such as argon, water or sulphur dioxide is released faster than hydrogen. As mentioned previously, water show an increase in intensity linked to evaporation of adsorbed water in the furnace, but it occurs below 200 °C. Furthermore, there was no detectable argon released from the microspheres which demonstrate their filtering ability. If argon was released from the microspheres, an increase in intensity would be visible when argon's diffusivity in the glass matrix increases. Instead, argon and all other species except hydrogen decreased or were stable with increased temperature demonstrating that only hydrogen was stored in the microspheres. Additionally, the detection of these gases could be explained by an adsorption of atmospheric gases or species in the carrier gas during flushing of the system. The intensities of these gases drop faster at lower temperatures likely linked to adsorbed gases merely electrostatically bonded to the surface as described by Shelby. [39] The adsorbed gases can originate from the microspheres but more likely from the larger surface of the equipment. Ideally, a background measurement should have been performed

enabling the subtraction gases originating from contaminated equipment. Unassigned peaks are likely these adsorbed gases where only the main characteristic peak could be significantly distinguished from the background noise. For example, m30 could possibly be nitric oxide (NO) which has a large main peak but much smaller fragment peak intensities. With similar reasoning, m44 is probably carbon dioxide (CO_2), both these species are trace elements in the atmosphere. [54, 61] Ultimately, it can be concluded that only hydrogen was stored in the microspheres.

One can compare the measured hydrogen release interval with the preliminary calculations and assumptions of the amount of non-network formers. Figure 69 show the difference between the measured and calculated release interval for two M-values and two diameters, D10 and D90 from 3M. [18] It shows the relative flux during identical heating conditions which was normalized to each maximum value, thus the release intervals can be compared. The agreement is better for the larger D90 diameter compared to the smaller D10 for both M-values. This could be a result of the flotation separation which yielded more of the larger microspheres resulting in a shift in size distribution to larger sizes and therefore also larger average wall thicknesses. A larger wall thickness delays the release of hydrogen as the average diffusion distance increases. Note that this figure was calculated for a monosized microsphere fraction. The measured relative flux shows the release from a broader size distribution. Smaller sizes store less hydrogen per microsphere and release hydrogen faster due to the thinner shells while the opposite is true for the larger sizes. In conclusion, the developed model shows a good agreement with the measured hydrogen release concerning at which temperatures hydrogen is released.

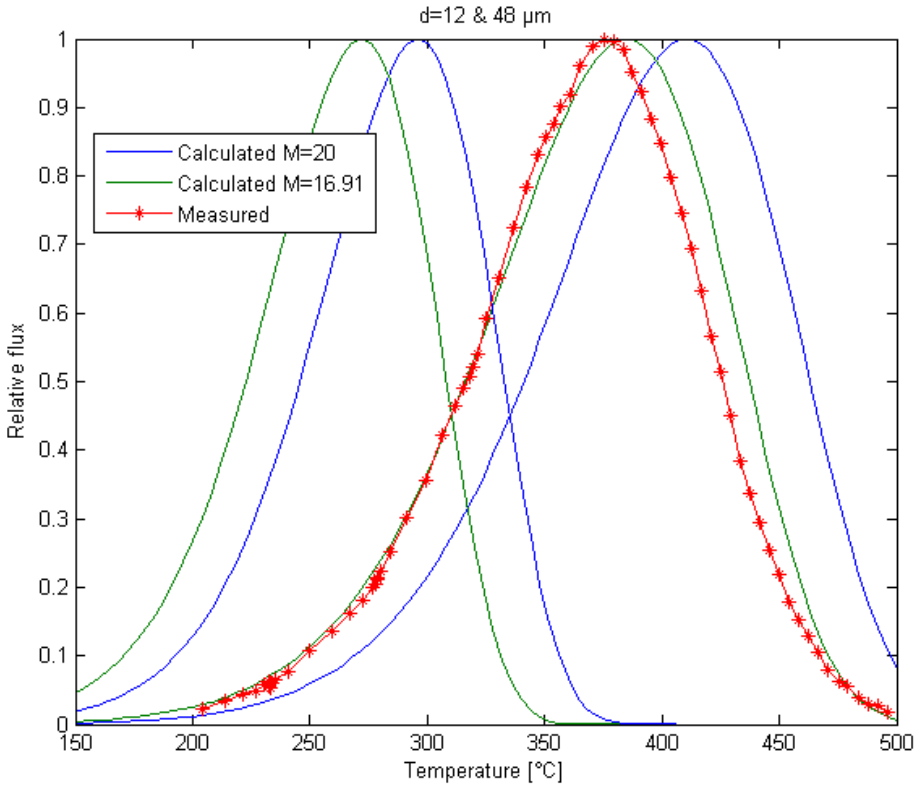

Figure 69 – Comparison of the hydrogen release interval of calculated and measured by mass spectrometry. The calculated curves consist of two diameters with two different amounts of non-network formers. The two curves to the left are for D10=12 µm and the right two curves are for D90=48 µm.

5.2.2 Storage capacity and evaluation of the fill attempt

At an early stage it was determined that an optimal fill of the microspheres could not be achieved. Firstly, the available HIP furnace could not pump pure hydrogen gas, only gas mixtures containing a lower amount of hydrogen. This meant that the theoretical optimal hydrogen pressure of 1241 bar, which comes from the critical buckling pressure, could not be reached. The target fill pressure was set to 1000 bar but the 95/5 Ar/H_2 gas mixture meant that the internal pressure would only be maximum 50 bar. Secondly, the target fill pressure was not reached because of the low temperature used. The gas mixture was pumped in at 250 °C to 400 bar and the temperature was then raised to 300 °C with further pressure increase by thermal expansion. However, there was not enough gas in the gas bottle to raise the pressure up to the target pressure of 1000 bar and instead fell short with a maximum pressure of 675 bar. Therefore, the full hydrogen storage potential could not be determined and much less hydrogen was subsequently added into the HIP-capsules for the oxygen reduction experiments. However, the concept of using microspheres as a way of introducing hydrogen inside HIP-capsules was still proven by the successful release of hydrogen from the filled microspheres.

Previous studies have proven that microspheres can be filled with high pressures of hydrogen. For example, Tajmar and Reissner filled the grade S38 with 700 bar pure hydrogen gas in a high pressure autoclave at 250 °C. [36] However, many microspheres were broken because of its lower isostatic crush strength of 275 bar. S60HS used in this work is stronger and have an isostatic crush strength of 1241 bar. Theoretically, by using a high pressure autoclave, S60HS would have a storage capacity of 5.17 wt% with the same setup as used in this work (1000 bar, 300 °C). Then, only 2.2 g and 0.86 g would be required to reduce all 200 ppm oxygen in the tool steel and the low-alloy steel respectively, instead of 41.3 g and 16.1 g. Consequently, twice this amount would easily fit inside the fill pipe together with the meshes, ceramic wool and a sufficient amount of fill powder.

The resulting storage capacity in this work of 0.1548 wt% is 84% of the theoretical fill capacity at 300 °C and 675 bar. It corresponds to an internal pressure of approximately 28 bar at 300 °C instead of the maximum hydrogen partial pressure at 675 bar of 33.75 bar. There are two possible explanations to this. Firstly, the fill time was too short. Since the flux in the microsphere shell is only dependent on temperature, wall thickness and pressure differential the fill time is independent of the external pressure. A lower external pressure yields a reduced pressure difference and thus a lower flux compensating for the lower internal equilibrium pressure. In the end, the total fill time equals out assuming the solubility of the glass is not reached and that the isostatic crush strength is not surpassed. Therefore, the fill time at 1000 bar is the same as at 675 bar with only the resulting internal pressure differing. Furthermore, the internal pressure reaches 84% of the external hydrogen partial pressure in 46 minutes (300 °C, M=16.91%). The pressure was above 84% of the maximum pressure, i.e. 600 bar, for over 2 hours as shown by Figure 42. In addition, the temperature was at 300 °C for 1 hour. Thus, except the 70 minutes it took to reach 600 bar, an additional 2 hours was spent above this and the internal pressure should therefore have equalized during the slow increase in pressure up to the maximum pressure.

The second possible explanation for not obtaining the maximum internal pressure could be that the microspheres were not cooled quickly enough at the end of the cycle and some hydrogen escaped. In 30 minutes, the temperature decreased from 300 °C to 100 °C and the

pressure from 675 bar to 508 bar. Further knowledge is obtained by comparing the equilibrium internal pressure, which is independent of the microsphere's diameter, as calculated in chapter 2.1.2. Table 16 shows the equilibrium internal pressure, i.e. the hydrogen partial pressure in the gas mixture, at the two temperatures and pressures during cooling as well as the resulting pressure at room temperature. From the calculated storage capacity, equivalent to 28.35 bar at 300 °C, it is clear that the equilibrium internal pressure was not maintained or increased during cooling. If the internal pressure was maintained from equilibrium conditions at 675 bar and 300 °C, the pressure at room temperature would be approximately 17 bar. The internal pressure was neither increased along with the temperature decrease which enables a higher storage capacity due to the gas contracting. Equilibrium at 508 bar and 100 °C would result in 19.95 bar at room temperature, higher than the actual internal pressure of 14.5 bar. In conclusion, hydrogen gas was most likely lost during cooling and not because of a too low fill time.

Table 16 – Equilibrium hydrogen partial pressure inside the void of a microsphere at different measured temperatures and external pressures. Before cooling (675 bar), after cooling to 100 °C (508 bar) and from measured storage capacity calculated internal pressure (567 bar)

Temperature	External pressure		
	675 bar	508 bar	567 bar
300 °C	33.75 bar	-	28.35 bar
100 °C	-	25.40 bar	-
20 °C	17.25 bar	19.95 bar	14.50 bar

After 73 days, the calculated storage capacity had decreased by 24.3% to 0.1158 wt%. The curve is also shifted to higher temperatures as seen in Figure 46. This is most likely caused by segregation of the microspheres during storage. The sample for the test after 73 days was taken from the bottle without proper homogenization. Thus, larger microspheres that had gathered on the top were tested, missing smaller particles that had segregated to the bottom of the bottle. Larger particles generally have thicker shells and therefore a longer diffusion path for the hydrogen molecules. [35] This yields a delayed release of hydrogen compared to the broader size distribution of the better mixed sample that was tested after 4 days. However, the storage capacity is still the same if the aspect ratio (wall thickness to diameter ratio) is assumed to be constant for all sizes. This is not always the case as presented by Shelby et al. where larger microspheres were found to have a lower aspect ratio, i.e. thinner shells. [35] The storage capacity would then be higher than calculated because of an increased void volume and reduced weight of the microspheres. However, this would only change the storage capacity slightly and there are other variables affecting the accuracy of the result.

Uncertainties in the measurements could explain why the storage capacity did not agree with the theoretical, for example calculation of the amount of hydrogen released based on the mass spectrometry data. Because of the rapid release of hydrogen from the decomposition of ammonia borane the peak is narrower than for the microspheres. Therefore, fewer data points were recorded which decrease the accuracy of the Riemann sum and the choice of method affects the result more. Furthermore, the oscillation of the temperature in the furnace at lower temperatures creates a "folding" curve affecting the area under the curve. Basing the storage

capacity of hydrogen on the hydrogen release from ammonia borane is therefore influenced by the accuracy of the measured areas. A more accurate measurement could be obtained using thermogravimetric analysis (TGA) determining the mass loss during heating as Baitalow et al. used to measure the hydrogen storage capacity of ammonia borane. [24]

In order to maximize the amount of hydrogen added to the HIP-capsules, broken microspheres were separated away from the filled microspheres in ethanol. Between 3 and 17 hours the solution showed no further separation and it was determined that the floated microspheres would be skimmed off. The solution was still opaque as there were still microspheres suspended in the ethanol. These were smaller microspheres with a higher density, i.e. closer to the density of ethanol, which could not be separated from the sedimented microspheres. Some intact microspheres were therefore lost but they were considered a necessary loss to maximize the amount of hydrogen added by ensuring that only filled microspheres were added into the capsules. This could have been avoided by choosing a liquid further apart from the densities of the broken and intact microspheres. For example, in the manufacturing of microspheres they are often separated by floatation in water which would increase the yield of the filled microspheres. [17] However, ethanol was chosen due to its low evaporation temperature. Thus, no additional heating was required to evaporate the ethanol, minimizing the risk of losing hydrogen. For future applications where microspheres are filled with pure hydrogen at high pressure the limited space in the fill pipe is a smaller issue. Therefore, the flotation step could be neglected in order to minimize the amount of steps in the fabrication of hydrogen filled microspheres.

5.2.3 Validation of the preliminary calculations

Due to the lack of composition data of the microspheres a number of approximations had to be done for the calculations of the internal void and diffusion of hydrogen through the wall. The approximation which affected the result the most was found to be the amount of non-network formers, M. A value of 20 % was chosen from a study investigating a grade (S60) similar to the one used in this work (S60HS) from the same manufacturer. From the small SEM EDS analysis of the composition this value was determined to be 16.91% which deviates from the approximated value. A lower amount of non-network formers yield a higher permeability and thus a quicker fill time of few hours, see Figure 70. This is of course beneficial as less time is needed to produce hydrogen filled microspheres.

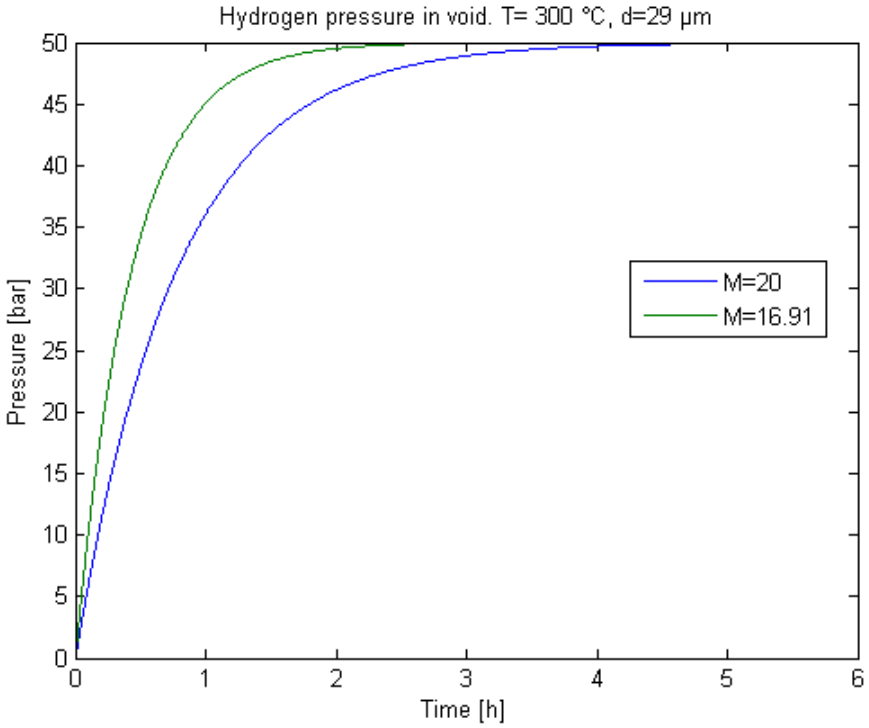

Figure 70 – Filling a 29 µm sized microsphere with hydrogen gas and the effect of different amounts of non-network formers. P_{fill}=1000 bar.

Instead, a major consequence could be a faster loss of hydrogen during storage as seen in Figure 71 which shows the long term storage capability with different amounts of non-network formers (M). However, as this plot shows there is not a significant difference between the measured M-value (16.91%) and the M-value used in the preliminary calculations (20%). While both these values lose 3-13% of the hydrogen pressure over 1 year, compared to a lower amount (M=10%) of non-network formers that loses 97%. After 73 days, the storage capacity decreased with 24.3 %. If the pressure is assumed to decrease proportionally, as depicted by the ideal gas law, it would after 73 days be 19.4 bar assuming that 1000 bar was reached during the fill procedure. This is closer to an M-value of 10% than the other two M-values, as seen in Figure 71. This could be due to the actual microsphere composition deviating from what was measured or that the storage capacity calculated by using ammonia borane as reference has a large error.

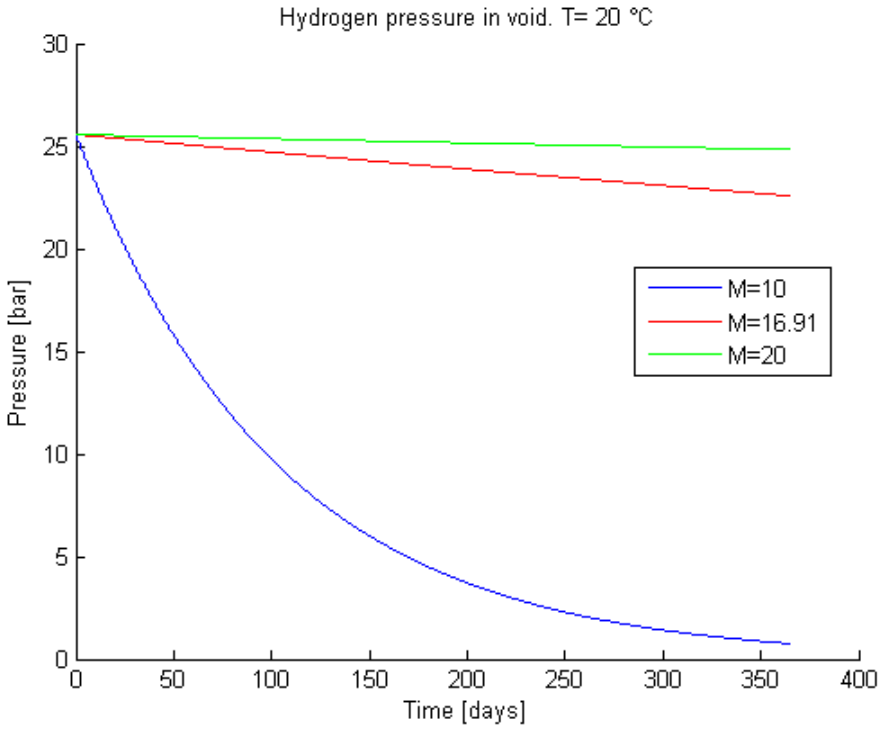

Figure 71 – Hydrogen loss from a 29 µm sized microsphere over 1 year with different amounts of non-network formers. P_{fill}=1000 bar and T_{fill}=300 °C.

The glass is a soda-lime borosilicate glass which should contain between 1-25 wt% boric oxide (B_2O_3). The limited information of the exact composition of S60HS makes it difficult to estimate how much B_2O_3 was neglected in the EDS analysis. An older study by Campbell et al. reported a typical soda-lime-silicate glass composition for microspheres from 3M of 80.7 wt% SiO_2, 10.3 wt% CaO, 6.9 wt% Na_2O, 2.1 wt% B_2O_3 and 1.9 wt% other. [62] This yields an M-value of 17.2%, between the assumed and measured values.

However, the glass S60HS used in this work is a soda-lime borosilicate glass therefore containing a higher boric oxide content. Alkaline earth containing borosilicate glasses, i.e. calcium (lime) containing borosilicate glasses, contain between 8-12 wt% boric oxide according to the classification. [63] Most likely, all boric oxide was undetected resulting in a lower M-value as it is counted as a network former. [42] A lower M-value increases the hydrogen permeability resulting in quicker fill and release times as explained previously. Furthermore, the lower density of boric oxide, 2.46 g/cm^3 [64], would also decrease the glass's density. By exactly how much is not possible to know without the exact composition of the glass.

Another consequence of the lack of composition data is the calculation of the internal volume which affects the storage capability. From the preliminary calculations the density of the glass was assumed to be that of silica, i.e. 2.65 g/cm^3. Again, the result from the SEM EDS analysis can be used to estimate the density of the actual composition of the microspheres. This can be calculated using each components weight fraction and their respective density using:

$$\rho_{MS} = \frac{m}{V} = \frac{m}{\rho_{SiO_2} w_{SiO_2} + \rho_{Na_2O} w_{Na_2O} + \rho_{CaO} w_{CaO}} = 2.699\ g/cm^3 \quad (29)$$

Assuming m=1 g, $\rho_{SiO_2} = 2.65\ g/cm^3$, $\rho_{Na_2O} = 2.27\ g/cm^3$ and $\rho_{CaO} = 3.34\ g/cm^3$. [44] The calculated density from the glass composition is close to the assumed value and the resulting void fraction is only 0.53% larger, justifying the assumption of using 2.65 g/cm^3 for the calculations. Boric oxide have a lower density compared to silica and will therefore lower the glass's density resulting in smaller voids and thicker shells. It is not included in the equation below since its present could not be proven in the SEM EDS analysis.

Another assumption was that the aspect ratio was the same for all diameters. It is however not certain that wall thickness scales with increases in diameter. For instance, Shelby et al. found that for microspheres above about 50 µm in diameter, wall thickness increase but not with the same ratio as below 50 µm. Larger microspheres thus have a lower aspect ratio, i.e. ratio of wall thickness to diameter, resulting in a lower strength. [35] As a consequence, larger microspheres likely have a quicker fill and release time as well as larger voids than what was calculated.

For the calculation of the hydrogen loss through the HIP-capsule wall a reliable value of the permeability was difficult to estimate since the composition of the carbon steel used was not known. Permeability for the different grades used to calculate an average differed with a factor of 3. Another aspect influencing the permeability for both steels is whether they have been deformed. San Marchi and Somerday reported a decrease in permeability by almost a factor of 10 for cold-worked steels compared to their annealed counterparts because of hydrogen being trapped at microstructural features. Both sheets used to form the capsules are likely cold-worked and therefore have a slower loss of hydrogen than calculated. This is beneficial for the experiments since it will contain the hydrogen longer during the reduction step than first anticipated. At the consolidation temperature, 1160 °C, hydrogen is no longer trapped due to the available thermal energy. [65] The higher permeability should empty both capsules in less than an hour assuming the permeability returning to that of an annealed material.

5.3 Powder characteristics

5.3.1 Metal powders

Fortunately for this work where only a limited amount of hydrogen could be loaded into the capsules, the chemical analysis showed lower oxygen contents than first assumed. It measured 120.5 ppm and 103.2 ppm for the low-alloy steel and the tool steel respectively compared to the assumed 200 ppm used in the preliminary calculations. The required amount of hydrogen is therefore decreased by 48% for the tool steel and 40% for the low-alloy steel. Consequently, the H_2/H_2O ratio is increased improving the oxide reduction conditions for both hydrogen deliverers.

Both metal powders exhibited some differences in reduction behaviour during the PAS measurement. The tool steel showed a single peak in water vapour while the low-alloy steel had multiple peaks indicating a difference in oxide composition between the two materials. Reduction of iron oxides can be assigned to the clear low temperature peaks in the tool steel and the low-alloy steel in agreement with literature. [29] For the tool steel, no other oxides

were supposedly reduced. It is possible that these were monolithic or spinel oxides of Cr, which likely exist because of the powder's base composition (5 wt% Cr), but they were not reduced. Other stable oxides of, for instance, Si could also remain unreduced. As a matter of fact, SiAl-oxides were found in the consolidated microstructure, see the following chapter. The surface oxides of the low-alloy steel were reduced in multiple steps after the first reduction of ferrous oxides. It contains less chromium but more manganese, with higher oxygen affinity than iron, compared to the tool steel powder. It is therefore likely that the surface composition of the low-alloy steel contains a larger fraction of MnO. The low-alloy steel also contains nickel which oxide is reduced at similar heating rates around 300 °C according to Jankovic et al. [32] The knee at 410 °C after the initial peak in Figure 19, which does not exist for the tool steel, could therefore be the reduction of NiO. Peaks at higher temperatures are likely some form of spinels. However, without a deeper microstructural investigation of the surface oxides in the virgin powders it is impossible to assign its composition with the PAS measurements alone.

An interesting result was the chemical analysis of the reduced powders. Nitrogen was almost completely removed from both powders. Oxygen was surprisingly not removed as much even under these ideal conditions. Oxygen can still be present in solution or as oxides. Reduction of oxides performed in ideal condition, such as the PAS measurements, gives the minimal, reachable oxygen content by hydrogen reduction. For this reason, one cannot expect a lower oxygen content to be achieved within the HIP-capsules where the condition is not ideal. However, it is possible that the measurement is not entirely accurate since oxygen uptake into the sintered powder likely occurred during the 3 weeks between the reduction and oxygen measurements.

Concerning the size distribution of the two metal powders shown in figures 20 and 21, there is no surprise that the tool steel have a narrower size span since it is sieved to a specific span compared to the low-alloy steel which was received as a full fraction, -500 µm. Therefore, the low-alloy steel contains a larger amount of fine particles which affect the measured oxygen content in the virgin powders as smaller particles exhibit a larger specific surface and consequently higher oxygen contents. [66, 67] This is one explanation, other than the chemical composition, why the virgin powder of the low-alloy steel displayed a higher oxygen content compared to the tool steel.

5.3.2 Microspheres

Size span of the microspheres were generally slightly smaller than the value provided by the supplier which could be due to different measuring techniques or how the diameter is determined. However, the difference is rather small and the agreement is deemed sufficient. The measured shape factors, sphericity and particle aspect ratio, were not as high as the manufacturer states, i.e. 1. Likely explanations are incomplete particle dispersion where overlapping particles are counted as non-spherical, measurement of particles out of focus or that the small transparent microspheres are not as easily characterised as opaque metal particles. An example from the dynamic image analysis of how the software has analysed two particles is shown below. It clearly shows that some particles that were out of focus are measured, affecting the results.

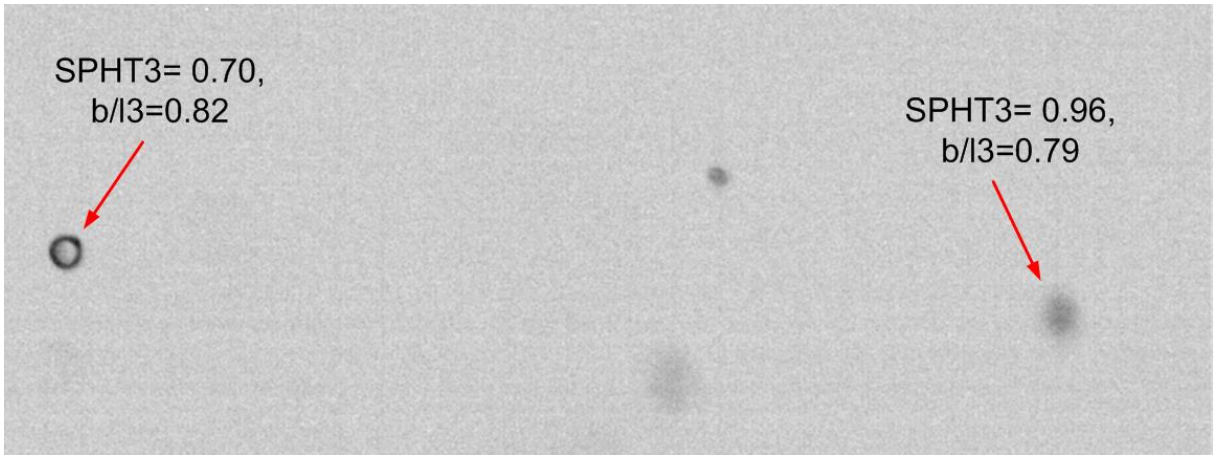

Figure 72 – Example of two analysed microspheres and the result of the software's analysis. SPHT3 = sphericity based on volume, b/l3 =particle aspect ratio based on volume.

The reason why no boron was detected in the SEM EDS analysis was expected since a rather short live time was used in conjunction with the spherical surfaces of the microspheres. For accurate and quantitative analysis of lighter elements, such as boron, a much longer live time, i.e. total time where the system counts incoming X-rays, should have been used. Thus, the software would then have a large enough sample size for statistically significant data for boron. Spherical surfaces furthermore complicate the analysis as the software expects the spectra coming from a flat surface. It is possible that both these factors affected the detection of boron. [68] The darker spots on the microspheres in the SEM images did not show any difference in composition. However, since gold was omitted in the analysis they were most likely caused by the gold layer detaching, revealing the lighter elements in the glass seen as a darker contrast. During the SEM analysis, more dark spots appeared with time suggesting that this was the case.

5.4 Oxide reduction and impact strength

5.4.1 Tool steel

From the microstructural investigation of the top of the reference capsule by SEM EDS it could be determined that the inclusions that were lined in sequence were surface oxides. These oxides had similar composition as the bulk material and were thus from the oxidation of the surface. The same was true for the center of TS1MS were inclusions lined in sequence were also found. Figures 54 and 58 thus show the prior particle boundaries, PPB.

No contamination of microspheres could be found in TS1MS. The microspheres that were detected in the low-alloy steel were mostly larger than 1 µm and more irregular compared to the normal inclusions. They also contained boron which further infers them to be microspheres. No inclusions agreeing with these characteristics could be found in the tool steel which thus was not contaminated by microspheres. Closer to the capsule walls, no clear PPB could be distinguished. Oxides also had a composition more resembling deoxidation products or slag inclusions from the steelmaking process, i.e. endogenous/exogenous inclusions containing Al, Si, Mg and Ca as in figures 55 and 59. Since the PPBs were not as distinguishable closer to the capsule wall for TS1MS, a reduction might have occurred leaving the more stable endo/exogenous inclusions. Surface oxides have good contact with the hydrogen during the reduction step and thus have a higher likelihood of being reduced. Endo/exogenous inclusions are instead randomly dispersed inside the powder particles and

have longer average distance to the reducing gas. Moreover, they are often more stable compared to the surface oxides, for instance SiO_2 in the stability diagram at different H_2/H_2O ratios in Figure 3. That is probably why larger SiAlMg-oxides remained even when PPB were absent.

From the SEM images of TS1AB it is clear that ammonia borane had leaked into the material. The composition of the contaminated area, see Figure 56, in the center of the capsule especially infer that the ammonia borane had fallen through the stainless steel mesh because of the high nitrogen and boron contents. Further from the fill pipe, less contamination was observed. While the ammonia borane in the center was found as a more or less continuous network surrounding the metal particles, only individual pores was found closer to the capsule wall. They are most likely remnants of where ammonia borane particles were located. The fact that no boron and little nitrogen in addition to increased carbon content indicates that the isolated ammonia borane particles were ripped out during sample preparation. Then, during polishing the diamond paste infiltrated these areas causing the increase in carbon content. It was not expected beforehand that such an excessive leakage would occur. In hindsight, the particle size distribution should have been measured or an extended preventive measure, such as the oxide wool, could have prevented contamination of the powder.

Both TS1AB and TS1MS generally contained larger inclusions compared to TS1R as shown by the cumulative size distribution in Figure 60. In the case of TS1AB, large pores, i.e. remnants of ammonia borane, were excluded from the measurements. However, smaller inclusions/pores could still have been caused by ammonia borane, thus influencing the results by increasing the average size. A more accurate measurement of the inclusions was perhaps done for TS1MS since no microspheres were detected. Therefore, the measurements were likely only performed on the oxides of interest. One source of error is the manual adjustment of the threshold in the image analysis software deciding which particles to measure. Another is the different magnifications causing some particles to be pixilated in one image while not in another influencing the measurements of the diameters. For a better result, stitched images of a larger area with better resolution should have been analysed.

Oxygen content was increased in the top of TS1AB and TS1MS compared to the reference. The contaminated area in the center of TS1AB, i.e. with continuous ammonia borane inclusions, had an almost tenfold increase in nitrogen content compared to the virgin powder and also tripled oxygen content. The two other samples, located outside this area, were comparable to the measurements in TS1MS. The standard deviation was thus greater for TS1AB than TS1MS. In hindsight, the dwell temperature where reduction was supposed to take place should have been increased. After the HIP of TS1AB, samples were analysed from the bottom which showed no significant reduction had occurred. It was therefore determined that the dwell temperature for the low-alloy steel should be increased to 600 °C, since it had more complex reduction behaviour in the PAS measurements. For consistency, the same reduction temperature was used for TS1R and TS1MS. Instead, calculation of the reduction rate should have been performed to better estimate dwell time and temperature. In the end, the compromise between minimal hydrogen loss and enhanced reduction rates were probably weighted too much against minimizing the hydrogen loss.

Even though no microspheres were detected in TS1MS, an increase in oxygen content was observed at the top. Microspheres, which oxygen content was measured to be 47 wt% in the SEM EDS analysis, were perhaps present in the material after all. Especially since oxygen content was reduced compared to the reference in the bottom where contamination is less likely. Ammonia borane also reduced the oxygen content in the bottom while still having increased nitrogen content compared to the other two capsules. As oxygen seems to follow the extent of ammonia borane contamination, any contamination would also yield higher oxygen content than what was measured in the bottom. Therefore, there was probably no contamination in the bottom of TS1AB and oxide reduction is then measured with better accuracy. Why there was still higher nitrogen content is likely because of nitrogen containing decomposition products. The deviation is much smaller than the top pointing to a homogenous increase in nitrogen content. This corresponds better with a homogenous spread of gaseous species between the powder particles instead of isolated ammonia borane particles randomly distributed throughout the material. To confirm that no contamination had occurred, a microstructural investigation should also be performed in the bottom of the capsules. After all, a drastically increased inclusion size was not observed which could be a problem if for example longer treatment times were used.

5.4.2 Low-alloy steel

No clear PPB was visible in LAS2R and the analysed inclusions' composition indicate that they originate from the steelmaking process, i.e. containing Al, Si, Mg and Ca as in Figure 50. Surface oxides with a composition closer matching the bulk composition were found as smaller inclusions in all capsules, see for example Figure 52. In contrast to TS1MS, microspheres had leaked into LAS2MS resulting in larger individual inclusions as well as large clusters of microspheres. This consequently decreased the impact toughness as seen by Figure 62. The few large clusters could explain the larger spread in impact toughness for the top of LAS2MS. A cluster located in the crack path would drastically enhance the crack propagation. For LAS2R, the impact toughness was stable indicating a lack of gradient in for example oxygen content and microstructure.

Due to the large amount of micron sized microspheres, it was not possible to characterize every inclusion and exclude the ones that were microspheres from the size measurements. Obvious microspheres, which had been analysed with SEM EDS, were excluded but several smaller inclusions caused by microspheres were most likely still included in the measurements. Therefore, an increased size distribution compared to the reference was observed for LAS2MS. Furthermore, boron was detected in the contaminants which was not observed during the analysis of the virgin microspheres. This is most likely caused by microspheres in the HIP'd material being crushed at the high temperature and pressure resulting in a larger amount of glass in the analysed area. Instead of a 1 micron thick, spherical shell in the virgin microspheres, the analysed area is a polished surface with several microspheres crushed together. Therefore, the detection of boron was easier.

Similar isolated pores were found in LAS2AB as in TS1AB and the origin is likely the same. During sample preparation, ammonia borane was ripped out and polishing agent was then accumulated in these areas causing the increase in carbon content. Otherwise, stable oxides caused by the steelmaking process were also found in LAS2AB. Since it was simpler to distinguish the inclusions from the pores caused by ammonia borane, a better analysis of the inclusion size could be performed compared to TS1AB. Still, the size distribution was larger

compared to the reference. It is possible that smaller ammonia borane inclusions were still included or that the released gaseous species, such as diborane or borazine, caused additional inclusions to be formed or already present inclusions to coarsen.

Because of the large ammonia borane contaminants, impact toughness was lower compared to both LAS2R and LAS2MS. Thus, ammonia borane contamination had a larger influence on impact toughness than microsphere contaminants. This is likely because of the size difference with an average larger size of around 10 µm for LAS2AB compared to around 1 µm (excluding the few clusters) in LAS2MS. Both LAS2MS and LAS2AB had higher impact toughness in the three bottom impact testing bars likely because of an increased distance to the source of the contaminants, i.e. the hydrogen carriers in the fill pipe.

LAS2AB had slightly increased impact toughness in the bottom but not as large of an increase as the bottom of LAS2MS. Even though more than ten times the amount of H_2 was released, oxygen content was reduced to similar levels for both materials, except for the contaminated areas. However, the reduction of the tool steel seems to not be obstructed since the oxygen content in TS1AB was reduced even more than TS1MS in the bottom. Perhaps the difference in composition between the tool steel and the low-alloy steel enables a higher solubility of nitrogen into the metal decreasing the obstruction of reduction reactions. The tool steel has higher Cr, Mo and V content which all increase the nitrogen solubility. [69] The difference in nitrogen content in the bottom was higher for the two treated tool steel capsules compared to the two low-alloy steel capsules strengthening this hypothesis, assuming no ammonia borane contamination occurred in the bottom. The low-alloy steel could thus not dissolve enough nitrogen to keep the confidential method active. The second possible explanation for LAS2AB not increasing impact toughness in the bottom as much as LAS2MS could be an increase of harmful nitrides due to the increased nitrogen content. However, no nitrides were found in the SEM EDS analysis.

One aspect that could have caused microspheres to contaminate the material even though excessive preventive measures was done is the absent of fill powder in the fill pipe. The fill pipe was loaded with as much microspheres as possible to maximize the amount of added hydrogen. Therefore, fill powder was not used resulting in major deformation of the fill pipe during HIP. The oxide wool and stainless steel mesh could therefore have shifted their position, leaving a free path down into the metal power. In the case of ammonia borane, which has a much larger volumetric storage density of hydrogen, fill powder could be used resulting in a much less deformed fill pipe. By using pure hydrogen gas during the fill procedure and increasing the storage density, fill powder could also have been used together with the microspheres. There is then a larger chance that the protective mesh and oxide wool would prevent leakage, perhaps even without using a foil shaped into a cup.

One interesting aspect of the chemical analysis was that even with confirmed leakage of microspheres into the material, oxygen content decreased compared to the reference. Again, microspheres contain 47 wt% oxygen and the decrease in oxygen content therefore suggests that the reduction of oxides fully compensated the contamination. Implying that without contamination, even further oxide reduction and improvement in impact toughness can be achieved. However, oxygen was not reduced in the bottom positions. One possible explanation is an insufficient amount of H_2 reaching the bottom not fulfilling the reduction

condition. Another explanation is that the great amount of fines, with larger specific surface and thus higher oxygen content, gathered in the bottom. [66, 67] This theory is further strengthen by the fact that except for one of three measurements, oxygen content in the bottom of LAS2R was higher which was not the case for the sieved tool steel.

In summary, even though ammonia borane releases a lot of hydrogen, other decomposition species can possibly limit its reduction ability. Microspheres which instead only release hydrogen showed overall better reduction ability even though it releases less hydrogen compared to ammonia borane. It shows a clear decrease in oxygen content in the low-alloy steel for the top and middle as well as two out of three measurements in the bottom. In the tool steel, oxygen content is also reduced at the bottom but not at the top due to contamination.

6 Conclusions

- Ammonia borane mostly decomposes into species agreeing with previous studies with deviations explained by the experimental setup. Hydrogen is during heating released below 200 °C.
- Microspheres successfully separate out H_2 from an Ar/H_2 gas mixture releasing only H_2 when heated. Almost all of the microspheres withstood 675 bar of isostatic pressure from the gas mixture at 300 °C resulting in a hydrogen storage capacity of 0.16 wt%, 84 % of the theoretical storage capacity at these conditions. The theoretical storage capacity was not reached due to equipment limitations. H_2 is released in a wider interval compared to ammonia borane, between approximately 200 – 500 °C.
- Ammonia borane leaked into the capsules in both cases, contaminating the material resulting in decreased impact toughness compared to the reference. More contaminants and lower impact toughness was observed closer to where ammonia borane was placed, i.e. the top of the capsules. Even though similar oxygen levels as the capsule with microspheres were obtained impact toughness was not improved as much. Ammonia borane's decomposition products likely obstruct the oxide reduction or introduce new inclusions lowering the impact toughness.
- Even though further protective measures were taken to prohibit microspheres leaking in to the capsule, confirmed leakage occurred in one of two cases. Inclusions caused by the microspheres were generally larger than surface and exo/endogenous oxides. The impact toughness in the contaminated area at the top was therefore decreased compared to the reference.
- The bottom of the capsules containing hydrogen carriers were less contaminated and had reduced oxygen content and improved impact toughness.

Ultimately, hydrogen filled microspheres could theoretically reduce oxides by incorporating them into sealed HIP-capsules. Furthermore, the risk of contamination could be decreased if microspheres were filled at the same pressure with pure hydrogen gas. Because, a higher storage density makes it possible to also use fill powder thus limiting the deformation of the fill pipe during HIP. The preventive measures, i.e. oxide wool and steel mesh, would then remain in place, stopping microspheres from contaminating the metal powder.

7 Recommendations for future work

- Fill microspheres in a high pressure autoclave using pure H_2 for a reduced risk of contamination and better reduction conditions inside the sealed HIP-capsule.
- Use thermogravimetric analysis (TGA) to better determine the storage capacity of the microspheres.
- Investigate whether the reduction step is necessary or if the temperature and dwell time should be increased by calculating the reduction rate. It could then be determined if a normal HIP-cycle could reduce oxides without an additional step.

8 Acknowledgments

The Åforsk foundation is acknowledged for financial support of the research work regarding H_2 filling of hollow glass microspheres and in-situ reduction of PM HIP material. Carpenter Powder Products AB, Uddeholms AB and Quintus Technologies AB are acknowledged for their assistance throughout the project. 3M is acknowledged for providing samples of hollow glass microspheres. The authors are grateful towards all above mentioned organizations for the opportunity to carry out this research.

9 References

[1] H. Danninger and C. Gierl-Mayer, “7 – Advanced powder metallurgy steel alloys,” in *Advances in Powder Metallurgy*, Cambridge, Woodhead Publishing Limited, 2013, pp. 149-201.

[2] Sandvik AB, “Metal powder in low-alloy steel - Sandvik Materials Technology,” 2018. [Online]. Available: https://www.materials.sandvik/en/products/metal-powder/list-of-materials/low-alloy-steels/. [Accessed 23 05 2018].

[3] D. W. Gandy, “energy.gov,” 10 2016. [Online]. Available: https://www.energy.gov/sites/prod/files/2016/10/f34/05%20-%20Innovative%20Manufacturing%20Process%20for%20Nuclear%20Power%20Plant%20Components%20via%20Powder%20Metallurgy%20and%20Hot%20Isostatic%20Processing%20Methods_0.pdf. [Accessed 23 05 2018].

[4] J. Tallmadge, “Powder Production by Gas and Water Atomization of Liquid Metals,” in *Powder Metallurgy Processing: The Techniques and Analyses*, New York, Academic Press, Inc., 1978, pp. 1-32.

[5] O. Grinder, “Surface Oxidation of Steel Powder,” *Steel Research International,* vol. 81, no. 10, pp. 908-913, 2010.

[6] L. Tan, G. He, F. Liu, Y. Li and L. Jiang, “Effects of Temperature and Pressure of Hot Isostatic Pressing on the Grain Structure of Powder Metallurgy Superalloy,” *Materials,* vol. 11, no. 2, 2018.

[7] D. Francois, A. Pineau and A. Zaoui, Mechanical Behaviour of Materials, New York: Springer Dordrecht Heidelberg, 2013.

[8] R. M. German, Powder Metallurgy and Particulate Materials Processing, Princeton: Metal Powder Industries Foundation, 2005.

[9] European Powder Metallurgy Association, “epma.com,” 2018. [Online]. Available: https://www.epma.com/hot-isostatic-pressing. [Accessed 21 02 2018].

[10] F. THÜMMLER and R.OBERACKER, An In troduction to Powder Metallurgy, London: The Institute of Materials, 1993.

[11] C. Broeckmann, “Hot isostatic pressing of near net shape components – process fundamentals and future challenges,” *Powder Metallurgy,* vol. 55, no. 3, pp. 176-179, 2012.

[12] K. Kim and Y. Jeon, “DENSIFICATION BEHAVIOR AND GRAIN GROWTH OF TOOL STEEL POWDER UNDER HIGH TEMPERATURE,” *Acta Metallurgica,* vol. 46, no. 16, pp. 5745-5754, 1998.

[13] S. Irukuvarghula, H. Hassanin, C. Cayron, M. Attallah, D. Stewart and M. Preuss, “Evolution of grain boundary network topology in 316L austenitic stainless steel during powder hot isostatic pressing,” *Acta Materialia,* vol. 133, pp. 269-281, 2017.

[14] P. Antona and C.Mapelli, “Hot isostatic pressing (HIP): The state of the art & improvement on two steels,” *Metallurgical Science and Technology,* pp. 1-7, 2013.

[15] A. Cooper, N. Cooper, J. Dhers and A. Sherry, “Effect of Oxygen Content Upon the Microstructural and Mechanical Properties of Type 316L Austenitic Stainless Steel

Manufactured by Hot Isostatic Pressing," *Metallurgical and Materials Transactions A,* vol. 47, no. 9, pp. 4467-4475, 2016.

[16] M. Norell, L. Nyborg and M. Friesel, "Segregants at Prior Particle Boundaries in Powder," *Powder Metallurgy,* vol. 41, no. 1, pp. 31-39, 1998.

[17] P. A. Howell, "Glass bubbles of increased collapse strength". United States of America Patent 4,391,646, 05 07 1983.

[18] 3M Center, "multimedia.3m.com," 2013. [Online]. Available: http://multimedia.3m.com/mws/media/91049O/3m-glass-bubbles-k-s-and-im-series.pdf. [Accessed 05 02 2018].

[19] L. Pilon, "Hydrogen Storage in Hollow Microspheres," in *Handbook of Hydrogen Energy,* Boca Raton, Taylor & Francis Group, LLC, 2014, pp. 763-809.

[20] W. R. Beck and D. L. O'brien, "Glass bubbles prepared by reheating solid glass particles". United States of America Patent 3,365,315, 23 01 1968.

[21] J. Shelby and B. Kenyon, "Glass Membrane for Controlled Diffusion of Gases". United States of America Patent US 6,231,642 B1, 15 05 2001.

[22] Merck KGaA, "sigmaaldrich.com," 2018. [Online]. Available: https://www.sigmaaldrich.com/catalog/product/aldrich/682098?lang=en&region=SE. [Accessed 19 01 2018].

[23] Sigma-Aldrich, *Hydrogen Storage Materials,* vol. 2, Aldrich Chemical Co., Inc, 2007.

[24] F. Baitalow, J. Baumann, G. Wolf, K. Jaenicke-Rößler and G. Leitner, "Thermal decomposition of B–N–H compounds investigated by using combined thermoanalytical methods," *Thermochimica Acta,* vol. 391, no. 1-2, pp. 159-168, 2002.

[25] S. Frueh, R. Kellett, C. Mallery, T. Molter, W. S. Willis, C. King'ondu and S. L. Suib, "Pyrolytic Decomposition of Ammonia Borane to Boron Nitride," *Inorganic Chemistry,* vol. 50, no. 3, pp. 783-792, 2011.

[26] V. Babenko, G. Lane, A. A. Koos, A. T. Murdock, K. So, J. Britton, S. S. Meysami, J. Moffat and N. Grobert, "Time dependent decomposition of ammonia borane for the controlled production of 2D hexagonal boron nitride," Macmillan Publishers Limited, 2017.

[27] D. Wagner, O. Devisme, F. Patisson and D. Ablitzer, "A LABORATORY STUDY OF THE REDUCTION OF IRON OXIDES BY HYDROGEN," in *Sohn International Symposium* , San Diego, 2006.

[28] H. Karlsson, S. Berg and Y. Yang, "Surface product formation on chromium alloyed steel powder particle," in *Euro PM2001 Proceedings*, Nice, 2001.

[29] E. Hryha, C. Gierl, L. Nyborg, H. Danninger and E. Dudrova, "Surface composition of the steel powders pre-alloyed with manganese," *Applied Surface Science,* vol. 256, no. 12, pp. 3946-3961, 2010.

[30] I. Arvanitidis, C. Artin, P. Claesson, H. Jacobsson, P. Johansso, J. Rassmus and D. Swartling, "Study of the kinetics of reduction of iron chromate by hydrogen," *Scandinavian Journal of Metallurgy,* vol. 25, no. 4, pp. 141-147, 1996.

[31] W. F. Chu and A. Rahmel, "The Kinetics of the Reduction of Chromium Oxide by Hydrogen," *METALLURGICAL TRANSACTIONS B,* vol. 10B, pp. 401-407, 1979.

[32] B. Jankovic, B. Adnadevic and S. Mentus, “The kinetic study of temperature-programmed reduction of nickel oxide in hydrogen atmosphere,” *Chemical Engineering Science,* vol. 63, no. 3, pp. 567-575, 2008.

[33] National Institute of Standards and Technology, NIST-JANAF Thermochemical Tables, Fourth Edition, Woodbury: American Institute of Physics & American Chemical Society, 1998.

[34] A. Lind, J. Sundström and A. Peacock, “The effect of reduced oxygen content powder on the impact toughness of 316 steel powder joined to 316 steel by low temperature HIP,” *Fusion Engineering and Design,* Vols. 75-79, pp. 979-983, 2005.

[35] J. Shelby, M. Hall, M. Snyder and P. Wachtel, “A Radically New Method for Hydrogen Storage in Hollow Glass Microspheres,” Alfred University, Alfred, NY, 2009.

[36] M. Tajmar and A. Reissner, “Development of Innovative Hydrogen and Micro Energy Solutions at the Austrian Research Centers,” in *6th International Energy Conversion Engineering Conference (IECEC),* Cleveland, 2008.

[37] G. Schmid, J. Bauer, A. Eder and C. Eisenmenger-Sittner, “A hybrid hydrolytic hydrogen storage system based on catalyst-coated hollow glass microspheres,” *International Journal of Energy Research,* vol. 41, no. 2, pp. 297-314, 2017.

[38] P. Mellin, *Personal conversation,* Stockholm, 2018-02-15.

[39] J. Shelby, “Final Report: Separation and Purification of Hydrogen From Mixed Gas Streams Using Hollow Glass Microspheres,” United States Enviromental Protection Agency, Alfred, 2008.

[40] J. Shelby, Handbook of Gas Diffusion in Solids and Melts, Materials Park: ASM International, 1996.

[41] G. Rambach and C. Hendricks, “Hydrogen Transport and Storage in Engineered Glass Microspheres,” in *U.S. DOE Hydrogen Program Review,* Golden, CO, 1996.

[42] P. C. Souers, Hydrogen Properties for Fusion Energy, Berkeley: University of California Press, Ltd., 1986.

[43] B. Duret and A. Saudin, “MICROSPHERES FOR ON-BOARD HYDROGEN STORAGE,” *International Journal of Hydrogen Energy,* vol. 19, no. 9, pp. 757-764, 1994.

[44] W. M. Haynes, CRC Handbook of Chemistry and Physics, Boca Raton: Taylor & Francis Group, 2012.

[45] Boron Specialties , “boron.com,” 2018. [Online]. Available: http://www.boron.com/ammonia_borane.html. [Accessed 04 04 2018].

[46] D. S. Wilkinson, Mass Transport in Solids and Fluids, Cambridge: Cambridge University Press, 2000.

[47] C. San Marchi and B. Somerday, “Technical Reference for Hydrogen Compatibility of Materials,” Sandia National Laboratories, Albuquerque, 2012.

[48] L. Zhigilei, “University of Virginia,” [Online]. Available: http://people.virginia.edu/~lz2n/mse305/notes/DiffEq-solution.pdf. [Accessed 18 01 2018].

[49] Horiba Scientific, “horiba.com,” 2018. [Online]. Available: http://www.horiba.com/us/en/scientific/products/elemental-analyzers/oxygennitrogenhydrogen/details/emga-920-528/. [Accessed 27 02 2018].

[50] Retsch Technology GmbH, “www.retsch.dk,” 2012. [Online]. Available: http://www.retsch.dk/pdf/pdf_camsizer/CamsizerXT_en.pdf. [Accessed 15 02 2018].

[51] Retsch Technology GmbH, *CAMSIZER Characteristics,* Haan: Retsch Technology GmbH, 2009.

[52] Horiba Scientific, *A Guidebook to Particle Size Analysis,* Irvine: Horiba Instrument, INC., 2017.

[53] V. Barwick, J. Langley, T. Mallet, B. Stein and K. Webb, “BEST PRACTICE GUIDE FOR GENERATING MASS SPECTRA,” LGC Limited, Teddington, 2006.

[54] National Institute of Standards and Technology, “Molecular Weight Search,” 2017. [Online]. Available: http://webbook.nist.gov/chemistry/mw-ser/#. [Accessed 26 01 2018].

[55] SIGMA-ALDRICH, “sigmaaldrich.com,” 2018. [Online]. Available: https://www.sigmaaldrich.com/catalog/product/vetec/v001298?lang=en&region=SE. [Accessed 27 02 2018].

[56] D. Hughes-Hallett, W. G. McCallum, A. M. Gleason, E. Connally, D. E. Flath and e. al., Calculus: Single Variable, John & Wiley and Sons, 2005.

[57] K. Frisk, A. Markström, C. Eggertson, J. Gårdstam and S. Caddéo, “Modelling of the HDH (Hydrogen Dehydrogenisation) method for reduced oxygen content in powder materials,” Swerea KIMAB, Stockholm, 2008.

[58] S. S. Institute, Metallic materials – Charpy pendulum impact test – Part 1: Test method (ISO 148-1:2016), Stockholm: SIS Förlag AB, 2016.

[59] Pfeiffer Vacuum GmbH, “Mass spectrometer catalog,” Pfeiffer Vacuum GmbH, Asslar, 2005.

[60] C. Leygraf, I. Odnevall Wallinder, J. Tidblad and T. Graedel, Atmospheric Corrosion, Hoboken: John Wiley & Sons, Inc., 2016.

[61] North Carolina Climate Office, “Composition of the Atmosphere,” 2018. [Online]. Available: https://climate.ncsu.edu/edu/Composition. [Accessed 22 03 2018].

[62] J. Campbell, J. Grens and J. Poco, “Preparation and Properties of Hollow Glass Microspheres for Use in Laser Fusion Experiments,” LAWRENCE LIVERMORE NATIONAL LABORATORY , Livermore, 1983.

[63] SCHOTT AG, *Technical Glasses,* Mainz: SCHOTT AG, 2014.

[64] National Center for Biotechnology Information, “PubChem Compound Database,” 2018. [Online]. Available: https://pubchem.ncbi.nlm.nih.gov/compound/Boric_oxide#section=Top. [Accessed 18 04 2018].

[65] C. Marchi, B. Somerday and S. Robinson, “Permeability, solubility and diffusivity of hydrogen isotopes in stainless steels at high gas pressures,” *International Journal of Hydrogen Energy,* vol. 32, no. 1, pp. 100-116, 2007.

[66] F. Persson, A. Eliasson and P. Jönsson, “Oxidation of Water Atomized Powders,” *Steel Research International,* vol. 85, no. 12, pp. 1629-1638, 2014.

[67] J. Meyer, “Advanced gas atomization production of oxide dispersion strengthened (ODS) Ni-base superalloys through process and solidification control,” Iowa State University, Ames, 2013.

[68] I. Heikkilä, *Personal conversation,* Stockholm, 2018-04-11.

[69] G. Stein and I. Hucklenbroich, “Manufacturing and Applications of High Nitrogen Steels,” *Materials and Manufacturing Processes,* vol. 19, no. 1, pp. 7-17, 2004.

swerea | KIMAB
Box 7047, 164 07 Kista, Sweden
Visiting Isafjordsgatan 28 A, 164 40 Kista, Sweden
+46 8 440 48 00, kimab@swerea.se, www.swereakimab.se